

**Quantum dynamics on complex quantum
networks and its simulation using
periodically driven systems**

(複雑量子ネットワークにおける量子ダイナミクスと
周期駆動系によるシミュレーション)

A Thesis Presented to
Graduate School of Science
Tokyo University of Science

In Particular Fulfillment
of the Requirements for the Degree of
Doctor of Science

by

Tomo Osada

March 2020

Abstract

This thesis defines closed finite-dimensional quantum systems that contain complex transitions between states as complex quantum networks, and theoretically investigates quantum dynamics on those systems, as well as presenting a method to experimentally simulate such quantum dynamics using systems under a periodic drive. First, from the perspective of quantum computation, whether complex quantum networks are useful to implement quantum spatial search algorithms is investigated. Specifically, the continuous-time spatial search algorithm using a tight-binding Hamiltonian is analyzed, where the correlation between the structural characteristics of the Hamiltonian and the time evolution of the search algorithm is investigated. In addition, to experimentally simulate the time evolution generated by the tight-binding Hamiltonian holding complex network structure, a method using an array of optical waveguides or a many-body quantum spins system is proposed. In particular, the thesis shows that complex quantum networks appear in the effective Floquet Hamiltonian of periodically driven systems. The following paragraphs are the outline of each Chapter of the thesis.

In Chapter 1, namely the Introduction, the background of the research and the significance of the thesis are described. Recent developments in the technology of quantum engineering and control have made it possible to manipulate single qubits such as single atoms, ions, and superconducting qubits with high precision, as well as allowing to control interactions between individual qubits to create artificial many-body systems. Such technology is indispensable for the realization of quantum computers or quantum simulators, and thus the method to engineer a high-dimensional quantum many-body system while controlling it with high fidelity has become an important issue. Thanks to these technologies, there is a growing interest on engineering and investigating quantum systems that are beyond simple lattice or regular structures, such as structures with randomness and long-range interactions. Such systems are called *complex quantum networks*, and some research areas to explore novel physical phenomena in these systems or exploring the application of these systems to quantum information processing tasks have

opened up. On this background, this thesis analyzes the usefulness of complex quantum networks for the quantum search algorithm, which is one of the most fundamental and important quantum information processing tasks. The quantum search algorithm is an algorithm intended to run on quantum processors, that detects a marked state among N states by time-evolving a single particle on the N dimensional Hilbert space. This thesis analyzes the time evolution of the quantum search algorithm on two specific models of complex networks and derives the time complexity of the algorithm. The analysis leads to providing new perspective to understand quantum dynamics on complex structures. In addition, the thesis proposes a method to experimentally simulate the dynamics on complex quantum networks with current technologies available in the labs. By using a coupled optical waveguide system or a many-body spin system subject to periodic drive (constraint by a time-periodic Hamiltonian), the thesis shows that an effective Floquet Hamiltonian having complex network structure can be derived.

Chapter 2 summarizes the preliminaries on quantum mechanics and graph theory, which will be necessary to explain the analysis and results in this thesis. A closed, finite-dimensional quantum systems are featured, where some Hamiltonian systems including the tight-binding Hamiltonian, many-body spin Hamiltonians, and time-periodic Hamiltonians are introduced. Graph theory and complex network science are outlined in the later part of the chapter, with descriptions of general methods of analyzing complex networks. Finally, the introduced quantum systems and network science are combined, which makes the discussion of this thesis unique.

Chapter 3 puts together the main results of the thesis. This chapter investigates the quantum spatial search algorithm on complex quantum networks. First, an introduction on the unstructured search problem and the Grover's algorithm that solves such problem is provided. Next the spatial search algorithm is introduced, which uses a tight-binding Hamiltonian for the construction of the algorithm. The tight-binding Hamiltonian is a type of Hamiltonian that generates a continuous-time evolution where a single particle hops between the states on the Hilbert space. The specific Hamiltonians treated in this thesis are conditioned to satisfy the small-world property or the scale-free property defined in the context of complex network science. When the matrix representation of the Hamiltonian contains a large number non-zero off-diagonal entries, this corresponds to the small-world property. When the sum of each row of the Hamiltonian matrix satisfies a power law distribution, this corresponds to the scale-free property. To derive the time

complexity of the search algorithm using such Hamiltonians, the eigenstates and eigenvalues of the matrices are mainly analyzed using numerical calculation. The correlation between the time evolution of the search algorithm and the structure of the Hamiltonian can be investigated from this analysis. The obtained results tells us that in the case of the Hamiltonian holding the small-world property, when the amount of non-zero off-diagonal matrix elements exceeds a threshold, the efficiency where the particle diffuses and interfere with itself significantly increases, leading to the availability of a fast search algorithm. From the other case where the Hamiltonian holds the scale-free property, it was discovered that the time complexity of the search algorithm has a strong correlation with the closeness centrality of the underlying scale-free network. These results suggest that complex quantum networks holding the small-world property are particularly useful for quantum search algorithms. In addition, the analysis using the scale-free complex quantum networks revealed a new property of the quantum search algorithm.

Chapter 4 proposes and theoretically investigates a method to simulate quantum dynamics in complex quantum networks using time-periodic Floquet systems. First a system where optical waveguides are evanescently coupled to each other in a linear chain, with a single photon or two-photon state input is considered. The optical waveguides are periodically modulated with respect to the propagation direction, such that the coupling constant between the waveguides changes periodically during the propagation of the photons. The Floquet theory is used to derive the effective time-independent Hamiltonian of the single period of the modulation. The obtained effective Hamiltonian matrix contains non-zero off-diagonal entries which matches with the properties of random graphs. Additionally, towards the actual experimental implementation, a photonic system that generates single-photon and two-photon states with high-efficiency is proposed. As the second type of physical system, a many-body spin system under the time-crystalline phase is considered. Here, the time-crystalline phase refers to a non-equilibrium steady state where the spin-1/2 many-body localized Ising chain is time-periodically subject to a transversal magnetic field. After properly adjusting the strength of the transversal magnetic field, the effective Hamiltonian is derived using the Floquet theory, which results to a Hamiltonian matrix satisfying the scale-free property. These analysis shows that quantum dynamics on complex quantum networks can be simulated using quantum systems under time-periodic drives.

Chapter 5 is the summary and conclusions of the thesis.

Acknowledgements

I would like to first thank my supervisor Associate Professor Kaoru Sanaka, who has supported me for six years, starting from my undergraduate course. Prof. Sanaka has always encouraged me to pursue my own research interest, and provided the best environment for me to proceed my study. I thank him with all my heart for the continuous help and discussions, as well as giving me a lot of opportunities to explore different things during the Ph.D course. I could definitely not complete this work without Prof. Sanaka's support.

I thank Prof. Kae Nemoto at National Institute of Informatics (NII) with all my heart. Prof. Nemoto has gave me all the support she could provide during my Ph.D course. Although I was not officially belonged to NII, Kae has always treated me as her true student and protected me, allowed me to visit the NII QIST group anytime, and always gave me critical and encouraging advice on my study. I also thank Dr. William J. Munro, group leader at NTT Basic Research Laboratories (BRL) with all my heart. Bill has provided me a lot of help during all of the time of my Ph.D course, and he has drove the motivation on my study. Bill has always marked my paper drafts with clear advice, and even allowed me to use the server in his group for my study. Without Kae and Bill's support, I could never continue my research this far. Kae and Bill are the best people I've ever met in my life and I genuinely respect them.

I thank Prof. Yasser Omar and Dr. Bruno Coutinho at Instituto de Telecomunicações, Lisbon. We have met in a Winter School at Austria in 2017, and from then we have started our collaboration. Yasser and Bruno has constantly gave me the opportunities to discuss and provided great advice on our work, even though we were living far away from Lisbon to Tokyo. Yasser has also invited me to stay in his lab for two weeks, during my first year of my Ph.D. The experience I had during the stay was one of the most valuable experience in my life, and I cannot thank him enough for his support.

I thank all of the members of Sanaka lab at Tokyo University of Science. The time with my colleagues was such a precious time. I especially thank Tsubakiyama Takaho, Satoshi Kobayashi, Ryo Nozaki, Haruka Terashima, Satoshi Kubo, and Yoshiro Sato for their support, and for their continuous effort to conduct the experiment in the lab. The actual experimental of the two-photon state generation scheme described in the thesis

was conducted by these colleagues. The author of this thesis has only contributed on the theoretical part of the work. The work could never been completed without their effort and patience on conducting the experiment. Especially, Haruka Terashima has obtained the experimental results showed in the published journal article, and Yoshiro Sato has conducted the experiment in the published video of the article. I also thank again to Tsubakiyama Takaho, Kei Yasuno and Satoshi Kobayashi who gave me a lot of support and an enjoyable time during my study.

I thank all of the members of the NII QIST Kae Nemoto group. I would like to thank Shojun Nakayama, Emi Yukawa, Shane Dooley, Li Yu, Michael Hanks, Jaeha Lee, Zeliang Xiang, Fumiaki Matsuoka, Katsuya Furusho, Yusuke Hama, Nicolo Piparo, Marta P. Estarellas, Claude Gravel and Akitada Sakurai for a lot of interesting discussions and advice to my work. I also thank Yukiko Sanaka, secretary in the QIST group for her help. I thank Victor Bastidas in NTT BRL for the helpful and fun discussions on our study. The way he explains things were always super clear and interesting, which stimulated my motivation. I also thank Benjamin Renoust for the great support on the complex network science side of our work. I would never been so intrigued by the depth of complex network science without the discussions with him. I thank again to Marta P. Estarellas for the discussions on our time crystal work. Her passion on the scientific research has also drove my research motivation. Having a lot of discussions and beer with these great researches has broaden my sight and stimulated me so much. Especially, our work on the simulation of complex quantum networks using time crystals were completed by the great contribution from Marta, Victor, and Benjamin.

I thank Prof. Tetsuro Nikuni, Prof. Eiji Tokunaga, Prof. Jaw-Shen Tsai, Prof. Noboru Watanabe, Prof. Kae Nemoto, and Prof. Kaoru Sanaka for reviewing my thesis. They have spent a lot of time and effort to accurately understand and review my work, which I thank with all my heart.

Finally, I thank my parents with all my heart for the understanding on the path I took, and allowing me to pursue to the direction that I wanted to go. Definitely I could never come this far without their understanding and support.

Contents

1	Introduction	1
1.1	Introduction	1
2	From Quantum mechanics to complex networks	6
2.1	Quantum systems, quantum states and linear operators	6
2.2	Observables and measurements	8
2.3	Hamiltonian and the time evolution operator	9
2.4	Time-periodic Hamiltonians and effective Hamiltonians	11
2.5	Qubit system	13
2.6	Examples of Hamiltonian systems	19
2.6.1	The tight-binding Hamiltonian	19
2.6.2	The spin chain Hamiltonian	20
2.7	Introduction to graph theory and complex network science	23
2.8	Essential concepts of complex networks	31
2.9	Writing arbitrary Hamiltonians as tight-binding models and their interpretation as networks	40
3	Quantum spatial search on complex networks	48
3.1	Formalization of unstructured search problem	48
3.2	Quantum algorithm to solve the unstructured search problem	49
3.3	Introduction and literature review of the spatial search algorithms	55
3.4	What this thesis tackles in the field of spatial search	62
3.5	Preliminaries of the spatial search algorithm	64
3.5.1	Definitions of the spatial search algorithm by continuous-time quantum walk	64

CONTENTS

3.5.2	Spatial search on the complete graph: analytical approach	67
3.5.3	Spatial search on a general graph	69
3.5.4	Numerical method to analyze spatial search	72
3.6	Spatial search on the long-range percolation model	77
3.6.1	Defining the LRP model	77
3.6.2	Time complexity of the spatial search on the LRP model	78
3.6.3	Average degree of the LRP model at the critical connectivity	81
3.7	Spatial search on the Scale-free network	86
3.7.1	Definition of the Bollobás scale-free network	87
3.7.2	The distribution and the scaling of the search time	89
3.7.3	Correlations with network measures	94
3.7.4	Limitation of the search algorithm on complex networks and trans- lation to a state transfer protocol	98
3.8	Conclusions and discussions	101
4	Simulation of complex quantum networks using driven quantum sys- tems	104
4.1	Simulating complex network structures with effective Floquet Hamiltonians	104
4.2	Simulating random networks with periodically modulated optical waveguides	105
4.2.1	Single or two-photon state propagating through an coupled waveg- uide array	106
4.2.2	Periodically modulated waveguide array and it's effective Hamiltonian	109
4.2.3	Preparation of the two photon source as the input state of the waveguide array	115
4.3	Simulating scale-free networks with time crystals	118
4.3.1	Discrete time crystals in spin systems	119
4.3.2	Appearance of scale-free networks in the time crystalline system with a small error	120
4.4	Conclusions	123
5	Conclusions	124

List of Figures

2.1	The schematic picture of periodic drive and Floquet theory.	11
2.2	The Bloch sphere.	15
2.3	The schematic picture of the tight-binding Hamiltonian.	19
2.4	Illustration of an spin chain model.	21
2.5	Example of an graph.	24
2.6	Degree and degree distribution of a graph.	26
2.7	Shortest path of a graph.	28
2.8	Diameter of a graph.	28
2.9	Clustering coefficient of a node.	29
2.10	Process of generating a Erdős-Rényi random graph.	32
2.11	The semicircle law and the leading eigenvector of the ER graph.	33
2.12	Visualization of a scale-free network.	36
2.13	Comparison of power law and binomial distribution.	36
2.14	Spectral distribution of the Bollobás scale-free network.	39
2.15	Approach to interpret quantum Hamiltonians as graphs.	41
2.16	Hamiltonian matrix of the TFI model and its graph representation.	43
2.17	The resonance rule.	45
2.18	Resonance rule in a two level system.	46
2.19	The Resonance rule applied adjacency matrix and its graph.	47
3.1	Problem setting of classical and quantum search.	50
3.2	Grover's iteration.	53
3.3	State transformation in the Grover's algorithm.	54
3.4	Grover's algorithm with physical restrictions.	55
3.5	Illustration of the Benioff's problem.	56

LIST OF FIGURES

3.6	Correspondence between the Grover's algorithm and the spatial search algorithm.	65
3.7	Search on the complete graph.	69
3.8	Optimizing γ at the minimum energy gap.	74
3.9	Flowchart of the numerical calculation of the search time.	76
3.10	The long-range percolation model.	78
3.11	Optimal measurement time versus α of the LRP model.	79
3.12	Normalized energy gap and success probability versus α ($d = 2$).	80
3.13	Performance of the search versus α at $N = 1024$	82
3.14	Normalized energy gap and success probability versus α ($d = 2$).	83
3.15	Clustering coefficient of the LRP model and the ER graph.	86
3.16	Measured degree distribution of the Bollobás model.	88
3.17	The leading eigenvector of the Bollobás model.	90
3.18	Distribution of the search time on the Bollobás model.	91
3.19	Scaling of the search time on the Bollobás model.	93
3.20	Correlation between the search time and network centrality measures.	95
3.21	Distribution of the success probability.	98
3.22	Measuring the state at harmonic times.	99
3.23	Dependence of the search time on the minimum degree of the network.	100
4.1	Graphical representation of the waveguide array Hamiltonian with one or two-photon input.	108
4.2	Illustration of the periodically modulated optical waveguides.	110
4.3	Effective Hamiltonian and adjacency matrix of the driven waveguide array.	111
4.4	The graph visualization of the driven waveguide array.	112
4.5	The degree distribution of the graph corresponding to the driven waveguide array.	113
4.6	The quasi energies and driving effect of the Hamiltonian.	114
4.7	Experimental scheme to generate the two-photon state.	117
4.8	The time crystalline system.	120
4.9	Effective Hamiltonian and adjacency matrix of the time crystalline system.	121
4.10	The graph visualization of the time crystalline system.	122
4.11	The degree distribution of the graph corresponding to the time crystalline system.	122

List of published and referenced papers

Published papers

1. Spatial search on a two-dimensional lattice with long-range interactions
Tomo Osada, Kaoru Sanaka, William John Munro, and Kae Nemoto,
Physical Review A 97, 062319 (2018).
© 2018 American Physical Society.
→ Corresponds to Chapter 3. Sections 3.4, 3.5, 3.6
2. A Photonic System for Generating Unconditional Polarization-Entangled Photons
Based on Multiple Quantum Interference
Haruka Terashima, Yoshiro Sato, Satoshi Kobayashi, Takaho Tsubakiyama, Ryo
Nozaki, Satoshi Kubo, Tomo Osada, and Kaoru Sanaka,
Journal of Visualized Experiments (151), e59705 (2019).
→ Corresponds to Chapter 4. Sections 4.1, 4.2

Referenced papers

3. Continuous-time quantum walk spatial search on the Bollobás scale-free network
Tomo Osada, Bruno Coutinho, Yasser Omar, Kaoru Sanaka, William John Munro,
and Kae Nemoto,
Accepted for publication in Physical Review A (2020), arXiv:1912.11243.
© 2020 American Physical Society.
→ Corresponds to Chapter 3. Sections 3.4, 3.5, 3.7, 3.8
4. Simulating complex quantum networks with time crystals
Marta Pascual Estarellas, Tomo Osada, Victor Manuel Bastidas, Benjamin Renoust,
Kaoru Sanaka, William John Munro, and Kae Nemoto,
arXiv:1907.13146.
→ Corresponds to Chapter 4. Sections 4.1, 4.3

Chapter 1

Introduction

1.1 Introduction

The technology to engineer and manipulate quantum systems is progressing rapidly. In 2019, Google has announced an achievement of quantum supremacy by developing a 54-qubit (53 of them functioning) quantum processor using superconducting circuits [1]. This means that they can control 53 quantum bits (i.e. 53 artificially created two level systems) individually, create interactions among them, and read out their states with high precision. This is a surprisingly high level of technological achievement, and represents the current level of quantum technology modern humanity can access. Considering the fragile nature of quantum systems and the unwanted crosstalk between individual qubits [2], it is not hard to imagine how much the experimentalists have struggled to achieve the result.

Historically, control of quantum systems were done on collective, ensemble systems. A typical experiment is the observation of nuclear magnetic resonance (NMR) [3]. NMR is a phenomena where nuclei of an atom or molecule responds to the magnetic field applied on the system. Early experiments were conducted using liquid state molecules [4, 5], where thousands of molecules are contained in the system. Collective phenomena is observed from such ensemble system, and the ability to control the interaction between the nuclei is limited. A better degree of control on the individual nuclei is possible in solid state systems such as the nitrogen vacancy center [6], since the atoms are fixed in certain positions up to phononic vibrations. However, if one is aiming to use these systems as quantum computational purposes, the limitation on the controllability of the interaction as well as the decoherence effect due to the collective phenomena is the bottleneck.

1.1. INTRODUCTION

A quantum system promising for quantum simulation and computation purposes were developed thanks to the invention of methods to trap charged molecules in space using electric fields. Such systems are called as ion trapped systems, and the quadrupole trapping method known as the Paul trap [7] is one of the most commonly used method in the current quantum simulation platform. Ions can be isolated in space, which allows one to read out the spin state of a single ion. The ability is not limited to merely isolation, but the dipole interactions between ions can be controlled as well, and the time evolution of the spin states can be precisely driven by the external magnetic field [8]. The great stability and controllability led to intriguing quantum simulation experiments [9].

We can say that now the quantum technology has entered the era where one can control single qubits and many-body system composed of tens of qubits with a very high precision. The ultimate goal is to scale up the number of qubits up to order of millions or billions. Such level of technology is necessary in order to build a fault-tolerant quantum computer. Additionally, one is getting more freedom on how to interact the qubits, which can be beyond nearest neighbour or lattice structures. This includes distance dependent long-range interaction [9], or coupling several qubits non-trivially by placing them in a random manner [10]. With such examples, we are able to create a *network* of qubits.

However, why would creating a quantum matter beyond regular structures be interesting? Since quantum error correction and quantum computation can be in principle achieved with an isolated two-dimensional lattice structure of qubits [11], why do we even need to care about network structures?

The motivation to think about networks can be stimulated by looking at various classical systems around us. For example, consider the power grid, which is an interconnected system to deliver electricity from the power plants to consumers. After the electricity is produced at the power plant, it goes through a series of stations and finally gets down to houses. This is one type of network, when we think of the power plants, stations and houses as elements, and treat the transmission lines as the links (interaction) between the elements. The structure of the network is not a lattice-like structure, and it must be in a pretty complex, cascading structure where the power plants are in the center of the network while the houses are at the endpoints. Such complex structured network is built in this way since the delivery can be efficient [12], as well as robust to certain failure of stations or transmission lines [13].

The power grid is just one example of complex networks. There are numerous com-

1.1. INTRODUCTION

plex structured networks around us, including social, technological or biological systems. Some instances are the Internet, World Wide Web, transportation system such as airline networks, protein-protein interaction network, etc. A well established field that map these real-world systems as networks to analyze their structural properties is known as *complex network science*. A seminal paper in this field discovered that many instances of these real-world network share a common property called as the scale-free property. The scale-free property is defined by the degree distribution of the network (i.e. distribution of the number of neighbours of each node) following the power law function $P(k) \propto k^{-\beta}$, $\beta > 0$. This means that few *hub* nodes have large number of neighbours, while most other nodes have small number of neighbours. The power stations corresponds to the hub nodes in the previous example. Complex network science has been also successful on analyzing different types of dynamics on networks, such as random walks, spreading of disease or spreading of information [14–17].

Now one may ask whether there are any complex *quantum* networks. We shall define a *quantum network* as a quantum system (either open or closed) which consists of a set of discrete elements defined in a quantum regime (e.g. qubits, basis states, quantum repeaters, or any subspace of the system) and a set of relations between the elements (e.g. qubit-qubit interaction, transition between states, communication channels, or any relation between the subspaces). A *complex quantum network* is a quantum network whose relation between elements are beyond regular structures, such as containing randomness or scale-free property, and so on. Can we find in the nature, or engineer any kind of complex quantum network? If we engineer a quantum system in a complex network structure, is it robust to failures? Can quantum information efficiently be delivered on a complex network?

So far, to the best of our knowledge, a large scale complex quantum network has not been found in the nature, or at least no natural quantum system has been treated as a large-scale complex network. Although, there is a growing interest in engineering complex quantum networks or discovering ideas to utilize them for quantum information processing tasks, both theoretically and experimentally. Some example of the theoretical work involved constructing computational algorithms such as a community detection algorithm [18] or a quantum version of the PageRank algorithm [19]. Closed quantum dynamics are also explored on certain types of complex networks [20, 21], as well as entanglement routing problem on complex networks [22]. Research in the direction of

1.1. INTRODUCTION

engineering complex quantum networks includes systems using photonic waveguides [23], coupled nitrogen vacancy centers [10], and periodically driven systems [24]. Another interesting observation is the high efficiency energy transport happening in photosynthetic systems [25]. This system is a small network composed of 14 chlorophylls where each of them can be treated as a two level system. The chlorophylls are interacting to each other, allowing transfer of excitation created from the energy absorbed from the incident photon. Although the system typically lives at room temperature, it has been shown that quantum nature is responsible for the energy transfer due to the high energy scale of photons. An even more surprising observation is that the energy transfer is enhanced by the existence of phononic environmental noise.

This thesis aims to contribute to understand coherent dynamics on complex quantum networks, as well as discussing some methods to simulate such dynamics on quantum systems that are accessible with current technology. Specifically, we consider single particle quantum walks and quantum spatial search algorithm on two examples of complex network models. Quantum walks, known as the quantum analog of random walks, is essentially a time evolution of quantum particles hopping around the nodes of a network. As quantum particles are allowed to form superposition states, quantum walks have been often used to construct quantum algorithms. One application of quantum walk is the spatial search algorithm, where one aims to search for a marked node in the network [26]. We especially consider the spatial search algorithm which uses the continuous-time evolution obeying the Schrödinger's equation, constrained by a tight-binding Hamiltonian where a network structure is imprinted in it. We examine this spatial search algorithm on network models known as the long-range percolation model and the Bollobás scale-free network. The former has a small-world property while the latter has a scale-free property, which are both crucially important features that appear in real-world complex networks. To the best of our knowledge, the spatial search algorithm has been never analyzed on these class of complex networks. The thesis provides a novel insight whether complex quantum networks are useful for spatial search algorithm, by investigating the correlation between the network's property and the time complexity of the spatial search algorithm.

The thesis also proposes and investigates a method to simulate the closed quantum dynamics on complex quantum networks, using periodically driven systems available with current experimental technologies. Instead of considering to create complex interactions between qubits, we rather focus on the transitions between basis states spanning the

1.1. INTRODUCTION

Hilbert space. We introduce a simple idea to view arbitrary finite-dimensional Hamiltonians as adjacency matrices of networks. Based on this idea, first we consider a system consists of an array of coupled optical waveguides. We show that although the waveguides are nearest-neighbour coupled spatially in a one-dimensional line, when the coupling constants are periodically modulated one can obtain an effective time-independent Hamiltonian showing a random graph-like complex network structure. Secondly we consider a many body spin system in a time-crystalline phase. We show that the transitions between the many body states satisfies the scale-free property when a small imperfection is introduced in the system.

This thesis contributes towards exploration of quantum dynamics and quantum algorithmic application of complex structured quantum systems, as well as presenting a method to simulate those dynamics effectively using periodically driven systems.

The rest of the thesis is structured as follows. Chapter 2 summarizes the preliminaries of quantum mechanics and graph (network) theory which will be necessary to explain the results presented in the later chapters. The idea of interpreting arbitrary finite-dimensional Hamiltonians as networks is also introduced here. Chapter 3 puts together the analysis of the quantum walk and spatial search algorithm on complex networks. We start by reviewing the literature of spatial search algorithms, clarify the aim of the thesis, and present the results. Chapter 4 discusses the method to simulate quantum dynamics on complex quantum networks using periodically driven systems. Chapter 5 is the overall summary of the thesis.

Chapter 2

From Quantum mechanics to complex networks

2.1 Quantum systems, quantum states and linear operators

A quantum system is a space or set of objects which obey the laws of quantum mechanics. Basic examples can be electron systems, atomic systems, or photonic systems. Typically, a quantum system is not defined on the object itself, but rather defined on certain degrees of freedom of the object; e.g. position and momentum of an electron, spin degrees of freedom of a bound electron, energy levels (orbits of electrons) of an atom, number and frequency of photons, etc. One usually focuses on certain degrees of freedom of the object to restrict the space where to consider its dynamics or property, which allows the problem to be tractable. This restriction defines the property of the space where the quantum system is defined.

The space defining the quantum system is a complete, complex inner product space, which is known as the Hilbert space. This is a complex vector space, where any complex vector defined on such space corresponds to a state of the quantum system. A state represents the values of the degrees of freedom of the quantum system in the form of complex state vector.

From now on, let us introduce a mathematical formulation of quantum systems. Here we consider a N -dimensional (finite dimensional) Hilbert space \mathcal{H} . This is a complex vector space \mathbb{C}^N , which means that the space is spanned by N mutually orthogonal

2.1. QUANTUM SYSTEMS, QUANTUM STATES AND LINEAR OPERATORS

vectors, and the linear combination of the vectors is written using complex, continuous value coefficients. Specifically we write the state, or the vector defined on \mathcal{H} , using the Dirac notation such as $|\psi\rangle$. This is the ket vector

$$|\psi\rangle = (a_1, a_2, \dots, a_N)^T \quad (2.1)$$

where each component $a_i \in \mathbb{C}$ is the complex, continuous value coefficient of each degrees of freedom. A bra vector is defined as

$$\langle\phi| = (b_1, b_2, \dots, b_N), \quad (2.2)$$

and the inner product of two vectors $|\psi\rangle$ and $|\phi\rangle$ can be written using the bra and ket vector such as¹

$$\langle\phi|\psi\rangle = \sum_i^N a_i b_i. \quad (2.3)$$

The complex conjugate of a ket vector $|\psi\rangle$ can be represented by a bra vector as

$$\langle\psi| = (a_1^*, a_2^*, \dots, a_N^*), \quad (2.4)$$

and the norm of $|\psi\rangle$ is defined as

$$\|\psi\| = \sqrt{\langle\psi|\psi\rangle} = \sqrt{\sum_i^N |a_i|^2}. \quad (2.5)$$

The normalization condition of a vector is $\sum_i^N |a_i|^2 = 1$.

In Eq. (2.1), we have defined the state vector as a $N \times 1$ matrix form. However, the state vector can be also written as follows using set of orthonormal basis states, such as

$$|\psi\rangle = \sum_{i=1}^N a_i |i\rangle. \quad (2.6)$$

As the Hilbert space is defined as a vector space, the entire space can be spanned by choosing a certain set of N basis states $\{|1\rangle, \dots, |i\rangle, \dots, |N\rangle\}$. They are mutually orthogonal and normalized such that $\langle i|j\rangle = \delta_{ij}$. This gives the $N \times 1$ matrix form of the basis

¹We represent the complex conjugate of a complex number using the superscript $*$, such that when $z = x + iy$, its complex conjugate is $z^* = x - iy$.

2.2. OBSERVABLES AND MEASUREMENTS

state $|i\rangle$ to be

$$|i\rangle = (0, \dots, 1, \dots, 0)^T, \quad (2.7)$$

where the entries are all zero except for the i -th entry. Eq. (2.6) means that the vector $|\psi\rangle$ is written as the linear combination or the superposition of the basis states. Such representation is useful to clarify which set of basis states one is using to write down the state.

A linear operator on the Hilbert space can be represented using two vectors $|\psi\rangle, |\phi\rangle \in \mathcal{H}$, as $|\phi\rangle\langle\psi|$. The linear operator is defined as the transformation acting on an arbitrary state $|\chi\rangle \in \mathcal{H}$,

$$|\phi\rangle\langle\psi||\chi\rangle = \langle\psi|\chi\rangle|\phi\rangle \in \mathcal{H}. \quad (2.8)$$

$|\phi\rangle\langle\psi|$ maps a state $|\chi\rangle$ to another state which is a vector $|\phi\rangle$ multiplied by the inner product $\langle\psi|\chi\rangle$. The matrix form of $|\phi\rangle\langle\psi|$ is

$$|\phi\rangle\langle\psi| = \begin{pmatrix} b_1 a_1^* & \dots & b_1 a_N^* \\ \vdots & \ddots & \vdots \\ b_N a_1^* & \dots & b_N a_N^* \end{pmatrix}. \quad (2.9)$$

As further introduction will follow in the later sections, physical quantities (observables), unitary operators or projectors will be represented by such linear operators.

2.2 Observables and measurements

In the previous section we have defined how a quantum system and its states are represented, as well as introducing a basic notation of the transformation of the states. While states mathematically describes how the physical object exists, in order for us to learn something from the system, we need to make a measurement on an observable of the quantum system. An observable $A \in \mathcal{H}$ is defined as an Hermitian operator on \mathcal{H} . An Hermitian operator is an operator satisfying $A = A^\dagger$. The measurement outcome of the observable A is given by its eigenvalues λ . The Hermite property of A gives the condition that all eigenvalues λ are real, which is an important assumption for the observable to be physically achievable. When the dimension of A is N , there will be $N - l$ possible outcomes where l is the number of degeneracy in the eigenvalues. The outcome will be determined by the Born rule, such that when the observable A is measured while the state

2.3. HAMILTONIAN AND THE TIME EVOLUTION OPERATOR

of the system is $|\psi\rangle$, the probability that the outcome x being λ is given by

$$\Pr(x = \lambda \mid |\psi\rangle) = \langle\psi|P_\lambda|\psi\rangle. \quad (2.10)$$

Here, P_λ is the projector (projection operator) to eigenvalue λ of A . The projector has the property $P_\lambda = P_\lambda^\dagger = P_\lambda^2$ and the completeness $\sum_{\lambda \in \sigma(A)} P_\lambda = 1$.

When the eigenvalue λ of A has degeneracy of l , the corresponding eigenspace has dimension l . Therefore, one can take l orthonormal eigenbasis $\{|\lambda_i\rangle\}_{i=1}^l$ and write the projection on this eigenspace as $P_\lambda = \sum_{i=1}^l |\lambda_i\rangle\langle\lambda_i|$. Using this, Eq. (2.10) will be

$$\Pr(x = \lambda \mid |\psi\rangle) = \sum_{i=1}^l |\langle\lambda_i|\psi\rangle|^2. \quad (2.11)$$

When λ has no degeneracy, Eq. (2.10) will be reduced to

$$\Pr(x = \lambda \mid |\psi\rangle) = \langle\psi|\lambda_i\rangle\langle\lambda_i|\psi\rangle = |\langle\lambda_i|\psi\rangle|^2, \quad (2.12)$$

which is the basis measurement, in the basis of the eigenspace of observable A . The eigenvalue decomposition of A is given by

$$A = \sum_{i=1}^N \lambda_i |\lambda_i\rangle\langle\lambda_i|. \quad (2.13)$$

2.3 Hamiltonian and the time evolution operator

Now we consider a specific type of transformation on \mathcal{H} , which is the time evolution. A continuous time evolution is generated by the Hamiltonian $H \in \mathcal{H}$ defined on the quantum system. H is an Hermitian operator which constrains the energy of the system, and is an observable whose outcome is the energy of the quantum system. The eigenvalue decomposition can be written as

$$H = \sum_{i=1}^N E_i |E_i\rangle\langle E_i|, \quad (2.14)$$

where the eigenvalues E_i are especially called as the energy, and $|E_i\rangle$ are especially called as the energy eigenstate. Some examples of Hamiltonian systems will be introduced in

2.3. HAMILTONIAN AND THE TIME EVOLUTION OPERATOR

the latter section.

A closed quantum system² time-evolves according to the Schrödinger's equation

$$i\hbar \frac{d}{dt} |\psi(t)\rangle = H |\psi(t)\rangle, \quad (2.15)$$

where $|\psi(t)\rangle$ is the state at time t , H is the Hamiltonian and \hbar is the Planck constant. $\hbar \approx 6.626 \times 10^{-34} / 2\pi [J \cdot s]$ is a tiny quantity compared to the scale we care about in our daily life, though is an important quantity that determines the typical scale where the quantum effects appear. When H is time-independent (i.e. does not change its form or parameters in time), one can solve the Schrödinger's equation to obtain

$$|\psi(t)\rangle = \exp(-iHt/\hbar) |\psi(0)\rangle, \quad (2.16)$$

and define the time evolution operator

$$U(t; 0) \equiv \exp(-iHt/\hbar). \quad (2.17)$$

The time evolution of the state from time 0 to time t can be simply written as $|\psi(t)\rangle = U(t; 0) |\psi(0)\rangle$. This is an unitary transformation of the state vector and $U(t; 0)$ is an unitary operator, where the length of the vector is preserved at all times, $\langle \psi(t) | \psi(t) \rangle = 1$.

An operator U is unitary when $U^\dagger U = U U^\dagger = I_{\mathcal{H}}$ is satisfied. Applying an unitary operator on a set of orthonormal basis states $\{|\phi_i\rangle\}_{i=1}^N$ defines a new set of orthonormal basis states $\{U|\phi_i\rangle\}_{i=1}^N$. The orthonormality of $\{U|\phi_i\rangle\}_{i=1}^N$ can be straightforwardly shown as $\langle \phi_i | U^\dagger U | \phi_j \rangle = \langle \phi_i | \phi_j \rangle = \delta_{ij}$, given that U is unitary.

It is important to know that $U(t; 0)$ and H share the same set of eigenvectors $\{|E_i\rangle\}_{i=1}^N$ such that

$$U(t; 0) = \exp(-iHt/\hbar) = \exp\left(-it/\hbar \sum_{i=1}^N E_i |E_i\rangle \langle E_i|\right) \quad (2.18)$$

$$= \sum_{i=1}^N \exp(-iE_i t/\hbar) |E_i\rangle \langle E_i|. \quad (2.19)$$

We could bring $\sum_{i=1}^N |E_i\rangle \langle E_i|$ off the shoulder of the matrix exponential since it is a

²We defined a closed system as a quantum system whose Hamiltonian H_s describes the full dynamics, and assume there exists no (or omit) interaction with a bath, which can be described by a bath Hamiltonian H_b .

2.4. TIME-PERIODIC HAMILTONIANS AND EFFECTIVE HAMILTONIANS

diagonal matrix. The eigenvalues of U , which is $\lambda_i = \exp(-iE_i t/\hbar)$ lies on the unit cycle in the complex plane.

2.4 Time-periodic Hamiltonians and effective Hamiltonians

Solving the Schrödinger's equation when the Hamiltonian H was time-independent was straightforward in the previous section. Now we consider the case of a time-dependent Hamiltonian $H(t)$. We will especially focus on an instance where $H(t)$ is time-periodic with a period of $T = 2\pi/\omega$, such that $H(t+T) = H(t)$. For example, imagine a parameter in the Hamiltonian is a time-periodic function $f(t)$, illustrated in the left side of Figure 2.1. Such time-periodic systems are sometimes called as driven systems. There are different techniques to solve the Schrödinger's equation in such situation for specific systems, such as the rotating wave approximation for atom-light interaction systems, but here we focus on a general approach using Floquet theory.

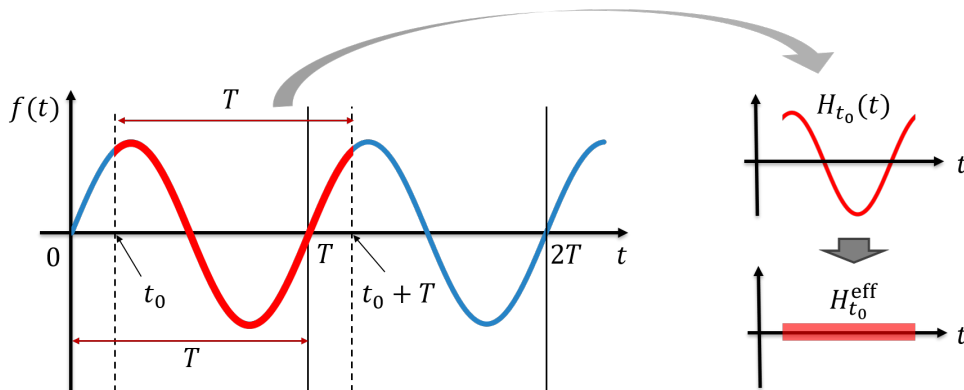


Figure 2.1: The schematic picture of periodic drive and Floquet theory. $f(t)$ represents the time-periodic parameter in a Hamiltonian, whose periodicity is $f(t+T) = f(t)$. Here we use Floquet theory in the context of integrating the time-dependent Hamiltonian of the single period of the drive $H_{t_0}(t)$, and obtaining the effective time-independent Hamiltonian $H_{t_0}^{\text{eff}}$.

The essence of the Floquet theory is to view the time-dependent systems at periodic times so that the time evolution becomes effectively a time evolution generated by a time-independent Hamiltonian. The core lies in the definition of the Floquet operator,

$$\mathcal{F} = U(T; 0) = \mathcal{T} \exp \left(-i \int_0^T H(\tau) d\tau / \hbar \right). \quad (2.20)$$

2.4. TIME-PERIODIC HAMILTONIANS AND EFFECTIVE HAMILTONIANS

This is the unitary time evolution operator $U(T;0)$ with a duration of one period, from time $t = 0$ to $t = T$. The symbol \mathcal{T} is the time ordering operator. Such time ordering is necessary when the Hamiltonian at each time do not commute, such as $[H(t_1), H(t_2)] = H(t_1)H(t_2) - H(t_2)H(t_1) \neq 0$. Importantly, once we obtain $U(T;0)$, the time evolved state at periodic times nT , where $n = 0, 1, 2, \dots$, can be obtained from n multiplication of $U(T;0)$ such as

$$|\psi(nT)\rangle = U(nT;0)|\psi(0)\rangle = [U(T;0)]^n|\psi(0)\rangle. \quad (2.21)$$

In the process of obtaining $U(T;0)$, we integrated the action of $H(t)$ within one period which averaged the detail of the action within the period. Also, one can straightforwardly shift the time duration (i.e. phase) of the integral by $t_0 < T$ and get

$$U(t_0 + T; t_0) = \mathcal{T} \exp\left(-i \int_{t_0}^{t_0+T} H(\tau) d\tau / \hbar\right). \quad (2.22)$$

Note that $U(t_0 + T; t_0)$ and $U(T;0)$ will have different values in their matrix entries when the Hamiltonians at two times do not commute, $[H(0), H(t_0)] \neq 0$. Although, the Floquet operators at different phases can be related by

$$U(t_0 + T; t_0) = U(t_0; 0)U(T; 0)U^\dagger(t_0, 0), \quad (2.23)$$

which is equivalent to rotating the basis to write the unitary operator of one period. To express the time evolved state at arbitrary time t , we need to explicitly include the dynamics contributing from the time duration within the period, such as

$$|\psi(t)\rangle = U(t - t_0 - nT; t_0 + nT)[U(t_0 + T; t_0)]^n U(t_0; 0)|\psi(0)\rangle. \quad (2.24)$$

The operators on both sides of $[U(t_0 + T; t_0)]^n$ is called as the micromotion or the kick operator.

The Floquet operator \mathcal{F} can be diagonalized and we can define a set of effective energy eigenvalues and eigenstates. We write the eigenvalue decomposition as

$$\mathcal{F} = \sum_{i=1}^N \exp(-i\lambda_i T / \hbar) |\lambda_i\rangle \langle \lambda_i|, \quad (2.25)$$

2.5. QUBIT SYSTEM

where in this case $|\lambda_i\rangle$ is commonly called as Floquet states and λ_i is called as quasi energies. The term *quasi* emphasizes that these eigenvalues are not actual physical energies, since the energy of the time-depending Hamiltonian may be not fixed at each instantaneous times. The quasi energies are bounded by $-\hbar\omega/2 \leq \lambda_i \leq \hbar\omega/2$, and the quasi energies does not change with respect to the phase shift by t_0 defined in Eq. (2.22).

An effective Hamiltonian H^{eff} of one period (or n periods) can be defined as a Hermitian operator satisfying the following equation,

$$\mathcal{F} = U(T; 0) = \exp(-iH^{\text{eff}}T/\hbar). \quad (2.26)$$

This is an interpretation of the Floquet operator that the time evolution over one period T is generated by an effective time-independent Hamiltonian (see the right side of Figure 2.1). \mathcal{F} and H^{eff} share the same Floquet states $|\lambda_i\rangle$ as the eigenstates, the quasi energies λ_i are the eigenvalues of H^{eff} . From Eq. (2.23), we can get a phase shifted effective Hamiltonian by,

$$H_{t_0}^{\text{eff}} = U(t_0; 0)H_0^{\text{eff}}U^\dagger(t_0, 0), \quad (2.27)$$

The effective Hamiltonian can be conventionally obtained by taking the matrix logarithm of the Floquet operator,

$$H^{\text{eff}} = \frac{i\hbar}{T} \log(\mathcal{F}). \quad (2.28)$$

Although the perspective of the effective Hamiltonian only tells us the dynamics or properties of the system at stroboscopic times of $T, 2T, 3T, \dots$, the effective Hamiltonian and it's eigenvalue decomposition tells us important and intuitive understanding of the system in many cases. A comprehensive review on periodically driven systems and Floquet theory can be found in [27].

2.5 Qubit system

Here we introduce the qubit system and its time evolution. A qubit system (or qubit) is a quantum system defined on a two-dimensional Hilbert space, \mathcal{H}^2 . This is a two-dimensional complex vector space \mathbb{C}^2 . We define the orthonormal basis of a qubit as

$$|0\rangle = \begin{pmatrix} 1 \\ 0 \end{pmatrix}, |1\rangle = \begin{pmatrix} 0 \\ 1 \end{pmatrix} \quad (2.29)$$

2.5. QUBIT SYSTEM

and write the state of the qubit system as

$$|\psi\rangle = \alpha|0\rangle + \beta|1\rangle, \quad |\alpha|^2 + |\beta|^2 = 1. \quad (2.30)$$

The basis states $|0\rangle, |1\rangle$ are often called as the computational basis. As a physical example, a spin up and spin down states of a spin-1/2 particle $\{|\uparrow\rangle, |\downarrow\rangle\}$ can form a computational basis of the qubit. Another example is the polarization state of a single photon $|H\rangle, |V\rangle$, where H and V stands for horizontal and vertical polarization. The measurement of the qubit $|\psi\rangle$ in the basis $\{|0\rangle, |1\rangle\}$ gives the output 0 with probability $|\alpha|^2$, and 1 with probability $|\beta|^2$. The equally balanced superposition states of the computational basis

$$|\psi\rangle = \frac{1}{\sqrt{2}} (|0\rangle + e^{i\phi}|1\rangle) \quad (2.31)$$

with relative phases $\phi = 0$ or $\phi = \pi$ are often defined as the plus and minus states

$$|+\rangle = \frac{1}{\sqrt{2}} (|0\rangle + |1\rangle) = \frac{1}{\sqrt{2}} \begin{pmatrix} 1 \\ 1 \end{pmatrix}, \quad (2.32)$$

$$|-\rangle = \frac{1}{\sqrt{2}} (|0\rangle - |1\rangle) = \frac{1}{\sqrt{2}} \begin{pmatrix} 1 \\ -1 \end{pmatrix}, \quad (2.33)$$

for convenience.

A state of a qubit can be geometrically and intuitively represented using the Bloch vector. Any qubit state can be represented using two real parameters $0 \leq \theta \leq \pi$ and $0 \leq \phi < 2\pi$ as

$$|\psi\rangle = \cos(\theta/2)|0\rangle + e^{i\phi} \sin(\theta/2)|1\rangle. \quad (2.34)$$

Such Bloch vector can be visualized as a vector pointing on the surface of a three dimensional unit sphere. In the polar coordinates, an arbitrary point on the surface of the unit sphere can be represented using the parameters θ, ϕ as in Figure 2.2 The unit sphere in this context is called as the Bloch sphere.

As we have defined the representation of the state vector of a qubit, we shall consider its unitary time evolution and some especially important unitary transformations on the system. We define four unitary operators including the identity and the three Pauli x, y

2.5. QUBIT SYSTEM

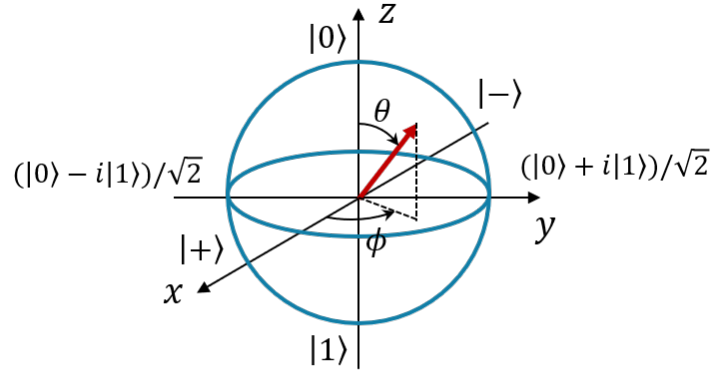


Figure 2.2: The Bloch sphere and Bloch vector representation of a qubit.

and z operators (or matrices) $\sigma^x, \sigma^y, \sigma^z$.

$$\mathbb{I} = \begin{pmatrix} 1 & 0 \\ 0 & 1 \end{pmatrix}, \quad (2.35)$$

$$\sigma^x = \begin{pmatrix} 0 & 1 \\ 1 & 0 \end{pmatrix}, \quad (2.36)$$

$$\sigma^y = \begin{pmatrix} 0 & -i \\ i & 0 \end{pmatrix}, \quad (2.37)$$

$$\sigma^z = \begin{pmatrix} 1 & 0 \\ 0 & -1 \end{pmatrix}. \quad (2.38)$$

The three Pauli operators satisfy $\sigma^x \sigma^x = \sigma^y \sigma^y = \sigma^z \sigma^z = \mathbb{I}$, and the commutation relation $[\sigma^x, \sigma^y] = 2i\sigma^z$, $[\sigma^y, \sigma^z] = 2i\sigma^x$, $[\sigma^z, \sigma^x] = 2i\sigma^y$. The computational basis $\{|0\rangle, |1\rangle\}$ are the two eigenstates of σ^z with eigenvalues ± 1 , and the plus and minus states $\{|+\rangle, |-\rangle\}$ are the two eigenstates of σ^x with eigenvalues ± 1 .

Let us consider the unitary time evolution operator generated by the Pauli matrices. Assume that the Hamiltonian of the system is described as $H = \hbar\omega\sigma^k/2$, where $k = x, y, z$.

2.5. QUBIT SYSTEM

The time evolution operator can be written as,

$$U = e^{-itH/\hbar} = e^{-i\omega t\sigma^k/2} \quad (2.39)$$

$$= \mathbb{I} + \left(-\frac{i\omega t}{2}\sigma^k\right) + \frac{1}{2!}\left(-\frac{i\omega t}{2}\sigma^k\right)^2 + \frac{1}{3!}\left(-\frac{i\omega t}{2}\sigma^k\right)^3 + \dots \quad (2.40)$$

$$= \mathbb{I} + \left(-\frac{i\omega t}{2}\right)\sigma^k + \frac{1}{2!}\left(-\frac{i\omega t}{2}\right)^2\mathbb{I} + \frac{1}{3!}\left(-\frac{i\omega t}{2}\right)^3\sigma^k + \dots \quad (2.41)$$

$$= \cos(\omega t/2)\mathbb{I} - i\sin(\omega t/2)\sigma^k. \quad (2.42)$$

Here we used that the Pauli matrices are unitary $(\sigma^k)^2 = \mathbb{I}$, and the series expansion of sine and cosine functions. The above transformation corresponds to the rotation of the Bloch vector around the axis k with an angle of ωt . Note that any Hamiltonian of a qubit system can be written, and thus any rotation of the Bloch vector can be generated, in the form $H = a\mathbb{I} + b\sigma^x + c\sigma^y + d\sigma^z$.

Another important unitary operator in the context of quantum computation is the Hadamard operator,

$$U_H = \frac{1}{\sqrt{2}}(\sigma^x + \sigma^z) = \frac{1}{\sqrt{2}} \begin{pmatrix} 1 & 1 \\ 1 & -1 \end{pmatrix}. \quad (2.43)$$

When the Hadamard operator is applied on the computational basis states, an equally balanced superposition state,

$$U_H|0\rangle = \frac{1}{\sqrt{2}}(|0\rangle + |1\rangle), \quad U_H|1\rangle = \frac{1}{\sqrt{2}}(|0\rangle - |1\rangle) \quad (2.44)$$

is generated. Such states are often used as the initial state of quantum algorithms.

As the final part of this section, we define a composite system of qubits. When the quantum system is composed of n qubits which are labeled as $r = 1, 2, \dots, n$, the whole Hilbert space is constructed by the tensor product of individual qubits, such as $\mathbb{C}_1^2 \otimes \mathbb{C}_2^2 \otimes \dots \otimes \mathbb{C}_n^2 = \mathbb{C}^{2^n}$. The dimension of the whole Hilbert space is 2^n . The orthonormal basis state are constructed from the tensor product of the computational basis states, such as $\{|b_1\rangle \otimes |b_2\rangle \otimes \dots \otimes |b_n\rangle\}_{b_1, \dots, b_n=0,1}$. Note that the dimension of the system explodes exponentially as the number of qubits increases. This limits us the ability to simulate full quantum dynamics (i.e. follow the dynamics of all 2^n complex amplitudes) using a classical computer. The full information of the system, or the unitary matrices cannot be

2.5. QUBIT SYSTEM

even fully stored in the computational memory as the system gets larger.

Let us consider the case of a two qubit system to show some examples. The system is spanned by $2^2 = 4$ basis states,

$$|0_1\rangle|0_2\rangle = \begin{pmatrix} 1 \\ 0 \\ 0 \\ 0 \end{pmatrix}, \quad |0_1\rangle|1_2\rangle = \begin{pmatrix} 0 \\ 1 \\ 0 \\ 0 \end{pmatrix}, \quad |1_1\rangle|0_2\rangle = \begin{pmatrix} 0 \\ 0 \\ 1 \\ 0 \end{pmatrix}, \quad |1_1\rangle|1_2\rangle = \begin{pmatrix} 0 \\ 0 \\ 0 \\ 1 \end{pmatrix}. \quad (2.45)$$

Hereafter we omit to explicitly write the tensor product operation \otimes . Operators on such system has to be a $2^2 \times 2^2$ matrix, which can be for example created from the tensor product of Pauli matrices,

$$\sigma_1^x \sigma_2^x = \begin{pmatrix} 0 & 1 \\ 1 & 0 \end{pmatrix} \otimes \begin{pmatrix} 0 & 1 \\ 1 & 0 \end{pmatrix} = \begin{pmatrix} 0 & 0 & 0 & 1 \\ 0 & 0 & 1 & 0 \\ 0 & 1 & 0 & 0 \\ 1 & 0 & 0 & 0 \end{pmatrix}. \quad (2.46)$$

This means both qubits 1 and 2 are flipped around the x axis. For example, $\sigma_1^x \sigma_2^x |0_1\rangle|0_2\rangle = |1_1\rangle|1_2\rangle$. This is a two qubit operation. When we want to flip only one spin (i.e. non-trivially transform the subsystem), the untouched spin also has to be applied by the identity operator. The resulting operator is a tensor product $\sigma_1^x \mathbb{I}_2$, though in most cases we will omit to write the identity operator such as

$$\sigma_1^x \mathbb{I}_2 = \sigma_1^x = \begin{pmatrix} 0 & 1 \\ 1 & 0 \end{pmatrix} \otimes \begin{pmatrix} 1 & 0 \\ 0 & 1 \end{pmatrix} = \begin{pmatrix} 0 & 0 & 1 & 0 \\ 0 & 0 & 0 & 1 \\ 1 & 0 & 0 & 0 \\ 0 & 1 & 0 & 0 \end{pmatrix}. \quad (2.47)$$

With this operation, only the first spin is flipped such as $\sigma_1^x |0_1\rangle|0_2\rangle = |1_1\rangle|0_2\rangle$. This is a single qubit operation.

When the Hilbert space is composed of two or more qubits, and important concept called as the entanglement comes in³. Entanglement is defined on states of the system.

³Although the comprehensive discussion of entanglement has to be done using density matrices of quantum states, here we only consider entanglement of pure states for a brief discussion.

2.5. QUBIT SYSTEM

A quantum state is described to be *entangled* when the state cannot be decomposed into tensor products of single qubit states. When the state can be otherwise decomposed, such state is described as separable states. For example, the two qubit Bell state as follows is an entangled state.

$$|\psi\rangle = \frac{1}{\sqrt{2}}(|0_1\rangle|0_2\rangle + |1_1\rangle|1_2\rangle), \quad (2.48)$$

while a state as follows is an example of separable state.

$$|\psi\rangle = \frac{1}{2}(|0_1\rangle|0_2\rangle + |0_1\rangle|1_2\rangle + |1_1\rangle|0_2\rangle + |1_1\rangle|1_2\rangle) = \frac{1}{\sqrt{2}}(|0_1\rangle + |1_1\rangle) \otimes \frac{1}{\sqrt{2}}(|0_2\rangle + |1_2\rangle). \quad (2.49)$$

Entanglement, which can be quantitatively evaluated using measures such as von Neumann entropy, is a result of interactions between two subsystems. The interactions that generates entanglement between qubits can be only induced from operators that are not separable into single qubit operators (if the states are initially separable). For example, unitary operations in Eq. (2.46) or (2.47) cannot entangle a two qubit state, as they are tensor products of single qubit operations. An non-separable unitary operator such as the Controlled-NOT gate,

$$C_{\text{NOT}} = \begin{pmatrix} 1 & 0 & 0 & 0 \\ 0 & 1 & 0 & 0 \\ 0 & 0 & 0 & 1 \\ 0 & 0 & 1 & 0 \end{pmatrix}. \quad (2.50)$$

can generate entanglement between qubits. This is a fundamental and important two qubit operator for quantum computation, which induces interaction between qubits. Indicated from its name, this operator applies a NOT operation (i.e. bit flip) on the second qubit, controlled by the state of the first qubit. The second qubit is flipped only if the first qubit is in the $|1_1\rangle$ state. We can show that the Controlled-NOT gate creates a entangled state from a simple example:

$$C_{\text{NOT}}(U_{H1}|0_1\rangle|0_2\rangle) = C_{\text{NOT}}\left(\frac{1}{\sqrt{2}}(|0_1\rangle + |1_1\rangle)|0_2\rangle\right) = \frac{1}{\sqrt{2}}(|0_1\rangle|0_2\rangle + |1_1\rangle|1_2\rangle). \quad (2.51)$$

The sequence of operations $C_{\text{NOT}}U_{H1}$ is sometimes referred as the two qubit entangling gate.

2.6 Examples of Hamiltonian systems

In this section, some examples of quantum systems governed by Hamiltonians are introduced, which includes the tight-binding model and spin chain models.

2.6.1 The tight-binding Hamiltonian

The tight-binding Hamiltonian describes the quantum system as a single particle hopping between discrete sites. The physics behind this Hamiltonian is the tight-binding approximation, which is typically a model to describe the state of an electron bound by the periodic potential of a crystal, aiming to compute the band diagram of the system [28]. The state of the electron (particle) $|\psi\rangle$ is written as the superposition of basis states $|i\rangle$, where $|i\rangle$ describes the electron (particle) localized at the position of the atom (site) i . The tight-binding Hamiltonian of the system with N sites can be written as

$$H_{tb} = \sum_{i \neq j}^N (K_{ij}|i\rangle\langle j| + K_{ji}|j\rangle\langle i|) + \sum_{i=1}^N \mathcal{E}_i|i\rangle\langle i|. \quad (2.52)$$

Here, K_{ij} is the transition (hopping) energy between sites i and j , and \mathcal{E}_i is the on-site energy of site i . Usually one has the condition $K_{ji} = K_{ij}^*$, where the star (*) represents the complex conjugate, so that H_{tb} is Hermitian. See Figure 2.3 for an intuitive illustration describing the Hamiltonian.

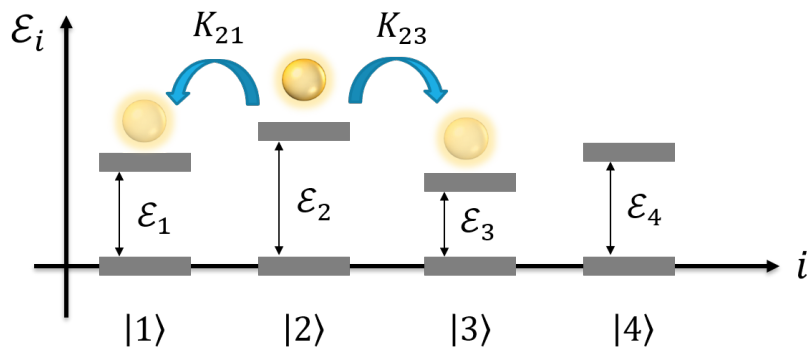


Figure 2.3: The schematic picture of the tight-binding Hamiltonian defined in Eq. (2.52). Here a system of $N = 4$ sites is illustrated. \mathcal{E}_i represents the on-site energy of site i , while K_{ij} is the transition (hopping) energy between sites i and j . The time evolution in this system can be interpreted as a single particle hopping between sites.

Recalling that each term $|i\rangle\langle j|$ is a tensor product, $|i\rangle \otimes \langle j| = (0, \dots, 1_i, \dots, 0)^T \otimes (0, \dots, 1_j, \dots, 0)$ is a $N \times N$ matrix where the (i, j) -th entry is 1, while all other entries are

2.6. EXAMPLES OF HAMILTONIAN SYSTEMS

0. Therefore, the matrix form of the tight-binding Hamiltonian can be straightforwardly written as

$$H_{tb} = \begin{pmatrix} \mathcal{E}_1 & K_{12} & \dots & K_{1N} \\ K_{21} & \mathcal{E}_2 & & \vdots \\ \vdots & & \ddots & \\ K_{N1} & \dots & & \mathcal{E}_N \end{pmatrix}. \quad (2.53)$$

Each rows and columns corresponds to the basis states $|i\rangle$ and $\langle j|$. Mathematically, the only requirement on the basis states is that they are orthonormal. Therefore, $|i\rangle$ can be an arbitrary basis state of the Hamiltonian, not limited to the situation where an electron or a particle is localized at discrete sites. As a general understanding of the tight-binding Hamiltonian, we can say that transitions (or flow of complex amplitudes) between states $|i\rangle$ and $|j\rangle$ occurs with a rate proportional to K_{ij} , while some fraction of the complex amplitudes stays on the state $|i\rangle$, only acquiring a global phase with a rate proportional to \mathcal{E}_i . The direct transition between states $|i\rangle, |j\rangle$ is only present when $K_{ij} \neq 0$. The balance between $|\mathcal{E}_i - \mathcal{E}_j|$ and K_{ij} determines the fraction of the complex amplitude that moves from $|i\rangle$ to $|j\rangle$.

The above matrix form and interpretation of the tight-binding Hamiltonian is simple but powerful, since in principle any Hamiltonian defined on a N -dimensional Hilbert space can be written in such $N \times N$ matrix form.

2.6.2 The spin chain Hamiltonian

A many-body spin system can be described by a Hamiltonian composed of Pauli matrices. Here we assume each particle of the many-body system only has the spin degrees of freedom, and their position are static. We assume we do not have more than one particle at each position, and the particles can only interact with each other via its spin degrees of freedom.

The Ising model The basic example of a spin chain Hamiltonian of n spin-1/2 particles is the Ising model, which can be written as

$$H_{Ising} = - \sum_{r \neq s}^n J_{rs}^z \sigma_r^z \sigma_s^z - \sum_{r=1}^n B_r^z \sigma_r^z. \quad (2.54)$$

2.6. EXAMPLES OF HAMILTONIAN SYSTEMS

σ_r^z is the 2×2 Pauli z matrix on spin r , J_{rs}^z is the strength of interaction between spins r and s , while B_r^z is the strength of the magnetic field applied along the z axis onto spin r . The term $\sigma_r^z \sigma_s^z$ denotes the tensor product of n matrices, formally written as $\prod_{k=1, \dots, r-1}^{\otimes} \mathbb{I}_k \otimes \sigma_r^z \otimes \prod_{l=r+1, \dots, s-1}^{\otimes} \mathbb{I}_l \otimes \sigma_s^z \otimes \prod_{m=s+1, \dots, n}^{\otimes} \mathbb{I}_m$. The terms representing the interaction between spins, $\sigma_r^z \sigma_s^z$, can be understood that the energy of the system will change depending on the correlation between pair of spins. Here we represent the $+1$ and -1 eigenstates of σ_r^z as $|\uparrow\rangle$ and $|\downarrow\rangle$, respectively. Figure 2.4 illustrates such system.

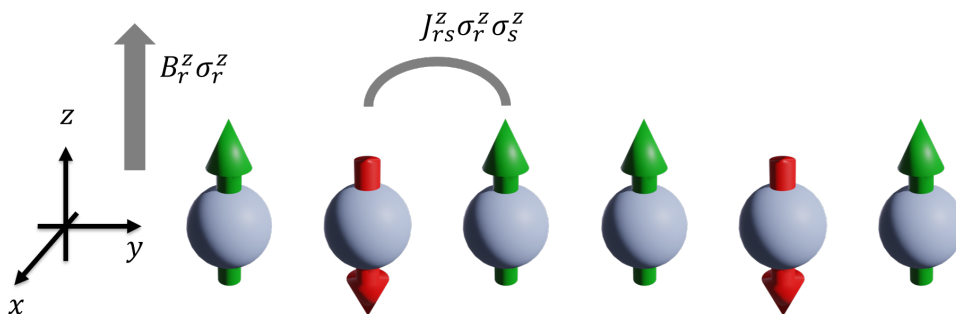


Figure 2.4: An illustration of an Ising spin chain model composed of 6 spins. The arrows going through the spheres represent the direction of the spin magnetic moment, namely the state of the spin $|\uparrow\rangle, |\downarrow\rangle$. $B_r^z \sigma_r^z$ corresponds to the situation where a magnetic field B_r^z in the z -axis direction is applied on each spin. $J_{rs}^z \sigma_r^z \sigma_s^z$ represents the situation where spins r and s are interacting with energy J_{rs}^z .

Consider the expectation value of the energy of a state $|\langle \psi | H | \psi \rangle|$. First, look at the second term of Eq. (2.54), $-\sum_{r=1}^n B_r^z \sigma_r^z$. By keeping in mind that $|\langle \psi | \sigma_r^z | \psi \rangle| \in [-1, 1]$, we can easily see that the energy is lower as more number of the spins are pointing the up direction $|\uparrow\rangle$, since $|\langle \uparrow | \sigma_r^z | \uparrow \rangle| = 1$. From the first term $-\sum_{r \neq s}^n J_{rs}^z \sigma_r^z \sigma_s^z$, we can see that the energy is also dependent on the number of pair of spins that are pointing the opposite direction, called as the domain walls. For example, $|\langle \uparrow_r \uparrow_s | \sigma_r^z \sigma_s^z | \uparrow_r \uparrow_s \rangle| = 1$, while $|\langle \uparrow_r \downarrow_s | \sigma_r^z \sigma_s^z | \uparrow_r \downarrow_s \rangle| = -1$. The Ising model is classified as ferromagnetic when $J_{rs}^z > 0$, and anti-ferromagnetic when $J_{rs}^z < 0$. The energy is lower as spins align to the same direction $|\uparrow \uparrow \uparrow \dots\rangle$ in the case of ferromagnetic, while spins pointing in the opposite direction $|\uparrow \downarrow \uparrow \dots\rangle$ leads to lower energy in the anti-ferromagnetic case. We can consider the structure of the interaction in terms of which pair of r and s having non-zero J_{rs}^z . Fundamental examples are nearest neighbour coupled or the d -dimensional lattice settings, but complex interaction structures can be also considered, which changes the energy landscape of the system.

Note that if we write the Ising Hamiltonian as a matrix form using the basis constructed by the product states of the eigenstates of σ_r^z , such as $\{|\uparrow \uparrow \uparrow \dots \uparrow\rangle, |\uparrow \uparrow \uparrow \dots \downarrow\rangle$

2.6. EXAMPLES OF HAMILTONIAN SYSTEMS

$\rangle, \dots, |\downarrow\downarrow\downarrow \dots \downarrow\rangle\}$, the matrix will be diagonal.

The tilted-field Ising model The Ising model with an additional transversal magnetic field g is often referred to as the tilted-field Ising model.

$$H_{TFI} = - \sum_{r \neq s}^n J_{rs}^z \sigma_r^z \sigma_s^z - \sum_{r=1}^n B_r^z \sigma_r^z - g \sum_{r=1}^n \sigma_r^x, \quad (2.55)$$

where g is the strength of the magnetic field applied along the x axis. In the Ising model, corresponding to $g = 0$, when the system is initialized in a state where all spins are parallel to the z axis, the state essentially does not evolve with time as it is an eigenstate of the Hamiltonian (which corresponds to the fact that the Hamiltonian is diagonal in this basis). In contrast, when $g > 0$, the spins will rotate around the x axis, as well as being effected by the σ^z terms. When the applied magnetic field $B_r^z > 0$ is disordered such that B_r^z is a random variable in $B_r^z \in [0, W]$, the system can be in a localized phase depending on W/g [29]. When the system is in the localized phase, the states will be frozen in it's initial state during the time evolution.

The XY model Another spin chain model that is well-studied in the literature is the XY model (or the XX model). The Hamiltonian of this model can be written as

$$H_{XY} = - \sum_{r \neq s}^n J_{rs}^{XY} (\sigma_r^x \sigma_s^x + \sigma_r^y \sigma_s^y) - \sum_{r=1}^n B_r^z \sigma_r^z. \quad (2.56)$$

As this Hamiltonian commute with σ^z , the number of excitations k (i.e. the number of spin ups k) is conserved during the time evolution. As no transition occur between each k -excitation subspaces, the Hamiltonian is block diagonal when it's written in the basis constructed by the product states of the eigenstates of σ_r^z . The k -th block in the matrix is a square matrix with dimension ${}_n C_k$.

When $k = 1$, where the corresponding subspace often referred to as the single excitation subspace, the XY model can be mapped to a tight-binding model using the Jordan-Wigner transformation. Such transformation can be done by defining two spin-ladder

2.7. INTRODUCTION TO GRAPH THEORY AND COMPLEX NETWORK SCIENCE

operators

$$\sigma_r^+ = (\sigma_r^x + i\sigma_r^y)/2 \quad (2.57)$$

$$\sigma_r^- = (\sigma_r^x - i\sigma_r^y)/2. \quad (2.58)$$

One can find that σ_r^z can be written in terms of the ladder operators as

$$\sigma_r^z = 2\sigma_r^+\sigma_r^- - 1. \quad (2.59)$$

Using these operators, the XY Hamiltonian in Eq. (2.56) can be written as

$$H_{XY} = -2 \sum_{r \neq s}^n J_{rs}^{XY} (\sigma_r^+\sigma_s^- + \sigma_r^-\sigma_s^+) - \sum_{r=1}^n B_r^z (2\sigma_r^+\sigma_r^- - 1). \quad (2.60)$$

From this we can interpret the interaction term (the first sum) as the hopping rate, since the term $\sigma_r^+\sigma_s^-$ annihilates one excitation from mode s and creates one excitation in mode r (i.e. flips the s -th spin $|\uparrow_s\rangle \rightarrow |\downarrow_s\rangle$ while flipping the r -th spin $|\downarrow_r\rangle \rightarrow |\uparrow_r\rangle$). The term $\sigma_r^+\sigma_r^-$ in the latter sum can be interpreted as the excitation number operator. As the dimension of the single excitation subspace is ${}_nC_1 = n$, Eq. (2.60) can be straight forwardly written as

$$H_{XY,k=1} = -2 \sum_{r \neq s}^n (J_{rs}^{XY} |r\rangle\langle s| + |s\rangle\langle r|) - \sum_{r=1}^n B_r^z (2|r\rangle\langle r| - 1). \quad (2.61)$$

$|r\rangle\langle s|$ projects the excitation from mode s to r , which corresponds to the transition between states $|s\rangle$ (spin s is pointing up while all others are pointing down) and $|r\rangle$.

2.7 Introduction to graph theory and complex network science

In this section, we introduce the concept of graph theory and complex network science. We define basic notations of graphs and networks, which will be followed by introductions to some measures and methods to analyze graphs and networks.

Graph theory is a field in mathematics that deals with the relationship between discrete elements. In this thesis, we use the term graph and network as mathematically equivalent

2.7. INTRODUCTION TO GRAPH THEORY AND COMPLEX NETWORK SCIENCE

objects. Although, the term graph is used to describe the object in a rather mathematical context, while the term network is used in a more general situation to indicate any object with some relationship or structure. A graphical example of a graph is shown in Figure 2.5. Generally the dots in the figure are called as nodes or vertices, while the lines connecting the nodes are called as edges or links. A graph is defined by the set of these nodes and edges, that is represented by $G(V, E)$. V is the set of nodes and E is the set of edges. Graph theory mainly deals with the mathematical aspects of such object $G(V, E)$. In contrast, network theory or complex network science is a field that applies graph theory to understand real-world systems. For example, consider the hyperlinks between the web pages in the World Wide Web (WWW). Bunch of websites exist on the WWW, and those websites are linked to each other so that the user can surf the web. If we take a subset of the web pages and the hyperlinks connecting the pages within the subset, we can map this as a network. The nodes are the web pages and the nodes are connected by an edge when one web page has a hyperlink to another. Complex network science is a field to analyze such networks mapped from the real-world systems. There are other examples of networks which includes social networks (e.g. follower network in Facebook or Twitter, transportation networks such as the flight between airports), technological networks (e.g. the Internet, the configuration of processing units in a computer), biological or chemical reaction networks (e.g. protein-protein interaction in living cells, connections of the neurons in a brain), just to name a few. In fact any discrete system that has some kind of interaction between each elements can be represented by a network, and graph theory is applied to analyze the properties of networks.

From now on, we define the basic notations and measures in graph theory to describe and analyze graphs.

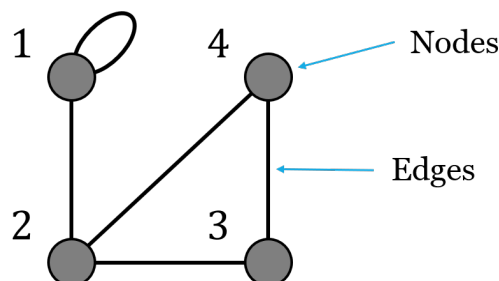


Figure 2.5: An example of an undirected, unweighted graph with 4 nodes.

2.7. INTRODUCTION TO GRAPH THEORY AND COMPLEX NETWORK SCIENCE

Adjacency matrix Assume a graph $G(V, E)$ consists of N nodes. A graph is uniquely determined by defining an adjacency matrix A_G . This is an $N \times N$ real matrix. The N nodes have to be labeled such as $\{1, 2, 3, \dots, i, \dots, N\} \in V$ to define the adjacency matrix. An entry of the adjacency matrix A_{ij} is,

$$A_{ij} = 1 \quad (2.62)$$

if nodes i and j are connected by an edge $e_{ij} \in E$, and

$$A_{ij} = 0 \quad (2.63)$$

if no edge directly connecting the nodes i and j exists. The adjacency matrix of the example graph in Figure 2.5 is expressed as,

$$A_G = \begin{pmatrix} 1 & 1 & 0 & 0 \\ 1 & 0 & 1 & 1 \\ 0 & 1 & 0 & 1 \\ 0 & 1 & 1 & 0 \end{pmatrix}. \quad (2.64)$$

The adjacency matrix completely describes which nodes are connected and which nodes are not. There are different classes of graphs that can be described in such matrix form. The above example is an *undirected, unweighted* graph. Undirected stands for the case where the edges do not have a direction, and the corresponding adjacency matrix is always a symmetric matrix. Unweighted stands for the case where all the non-zero entries of A_G representing the connected nodes are identical (usually taken as 1). In contrast, if the entries have different values, the graph is classified as weighted. In this thesis we will not consider any directed graph, but weighted graphs will appear in the later sections.

Degree, degree distribution A degree k_i is the number of edges that are connected to node i . For unweighted graphs, it also denotes the number of neighbours of node i . Using the adjacency matrix, degrees can be simply given by summing the rows or columns,

$$k_i = \sum_{j=1}^N A_{ij}. \quad (2.65)$$

2.7. INTRODUCTION TO GRAPH THEORY AND COMPLEX NETWORK SCIENCE

See the left side of Figure 2.6 for an graphical example. If the degrees are identical for all i , the graph is called as a regular graph, and otherwise a non-regular graph. Degrees are the simplest but very important quantity which you may want to compute from the adjacency matrix. The average degree $\langle k \rangle = \sum_i^N k_i/N$ is also commonly used to roughly know the connectivity the graph. For large-scale complex networks, taking the distribution of the degrees can capture the global property of the network. The degree distribution $\text{Pr}(k)$ is defined as the probability function to sample a degree k node from the network (see the right side of Figure 2.6).

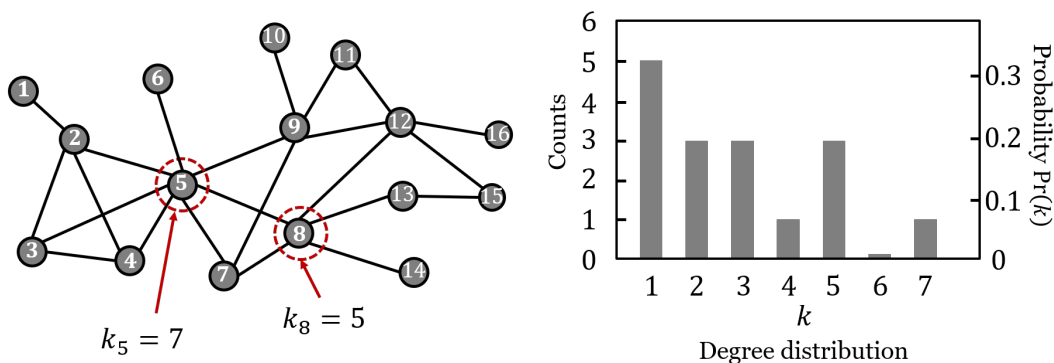


Figure 2.6: An example graph, its degree, and its degree distribution. k_5 or k_8 is the degree of node 5 or 8, which represents the number of neighbours (i.e. number of lines connected to that node). The degree distribution on the right is measured by taking the histogram of the degree of all nodes in the network, and normalizing it to make it as a probability distribution.

Graph spectrum The spectrum of the graph stands for the eigenvalues of the adjacency matrix A_G . Knowing the spectrum of a graph gives us a lot of information about the graph, especially associated to the structure or dynamical processes on the graph. For example, the gap between the largest and second largest eigenvalues of the adjacency matrix gives the mixing time of a random walk process on the corresponding graph. The eigenvectors of A_G can also tell us the properties of the graph. One example is that the eigenvector corresponding to the largest eigenvalue (i.e. leading eigenvector) is the stationary distribution of the corresponding Markov chain on the graph. The whole field to analyze graphs using the spectrum is called as the spectral graph theory.

Laplacian matrix A Laplacian matrix \mathcal{L}_G is defined as,

$$L_G = D_G - A_G. \quad (2.66)$$

2.7. INTRODUCTION TO GRAPH THEORY AND COMPLEX NETWORK SCIENCE

D_G is a diagonal matrix that contains the degree of each nodes as the diagonal entries, such as

$$D_{ii} = k_i. \quad (2.67)$$

The Laplacian matrix is especially helpful when analyzing some physical spreading dynamics on graphs. The eigenvalues of a Laplacian matrix is always 0 or positive. This is relevant for Hamiltonians describing quantum systems. The eigenstate with eigenvalue 0 can be viewed as the ground state. There are cases where the 0 eigenvalues can be degenerated. The multiplicity of 0 tells us the number of connected components. The connected component is a subset of nodes that can be reached from one to another using the edges.

Next, we introduce some important measures mainly used in the context of complex network science.

Shortest path length, average path length A shortest path length (shortest path distance) l_{ij} between a pair of nodes i, j is the minimum number of edges (steps) one needs to reach from node i to node j . For example, in the graph shown in Figure 2.7, the shortest path length from node 1 to 14 is $l_{1,14} = 4$. The average path length is the average of l_{ij} over all possible pair of nodes⁴

$$\langle l_{ij} \rangle = \frac{2}{N(N-1)} \sum_{i=1}^N \sum_{i < j} l_{ij}. \quad (2.69)$$

This quantity is often used to characterize how the network is compact compared to its total number of nodes. Especially, a network is called as *small-world* when the average path length scales about $O(\log N)$.

Diameter A diameter of a network is the maximum of the shortest path length, that is

$$l_{max} = \max_{i,j} (l_{ij}). \quad (2.70)$$

⁴The number of all possible pair of nodes can be given by

$$\binom{N}{2} = \frac{N!}{2!(N-2)!} = \frac{N(N-1)}{2}. \quad (2.68)$$

2.7. INTRODUCTION TO GRAPH THEORY AND COMPLEX NETWORK SCIENCE

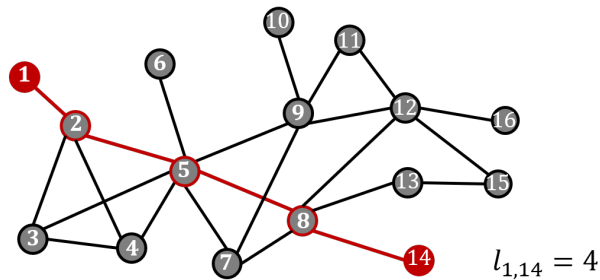


Figure 2.7: Shortest path of a graph. Here, the shortest path between nodes 1 and 14 is indicated as the red path. The shortest path length $l_{1,14}$ is measured by counting how many edges are contributing to the shortest path.

The diameter is $l_{max} = 5$ in the example of Figure 2.8 (note that there are more than one shortest paths where $l_{ij} = 5$). Compared to the average path length, the diameter rather describes the abstract size the network. For example, the diameter of a $\sqrt{N} \times \sqrt{N}$ two-dimensional square lattice is $2\sqrt{N}$ (measured with Manhattan distance). For d -dimensional lattice, it is $dN^{1/d}$. Even if the network is not periodic or symmetric as a lattice, if the diameter of a network scales as $\propto N^{1/d_e}$, one can say that the effective dimension of the network is d_e . This measure is also used to describe how small-world the network is.

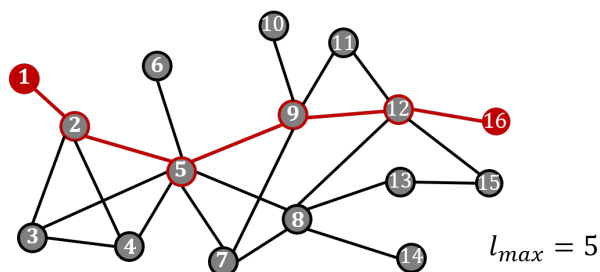


Figure 2.8: Diameter of a graph. We can find that the diameter of this graph is $l_{max} = 5$ by checking the shortest paths length between all pair of nodes, and finding the maxima. The red path $\{1, 2, 5, 9, 12, 16\}$ is just one instance of the path which has the maximum shortest path length; $\{1, 2, 5, 8, 13, 15\}$ also has the maximum shortest path length.

Clustering coefficient A (local) clustering coefficient Cl_i of a node i is defined as,

$$Cl_i = \frac{2T_i}{k_i(k_i - 1)}. \quad (2.71)$$

T_i is the number of triangles that includes node i as one of its vertex. A triangle means that three nodes i, j, k are mutually connected to each other by an edge. See Figure 2.9 where

2.7. INTRODUCTION TO GRAPH THEORY AND COMPLEX NETWORK SCIENCE

such triangle are indicated with colors. Cl_i is obtained by dividing T_i with the possible number of triangles that can be formed using node i and its k_i neighbours, $2/[k_i(k_i - 1)]$. This means that when $Cl_i = 1$, a local fully connected graph (called as a clique) of $k_i + 1$ nodes is created around node i . We can understand that Cl_i tells how much edges are clustered around node i . The average clustering coefficient $\langle Cl_i \rangle = \sum_{i=1}^N Cl_i/N$ is also commonly used to measure the global property of the graph.

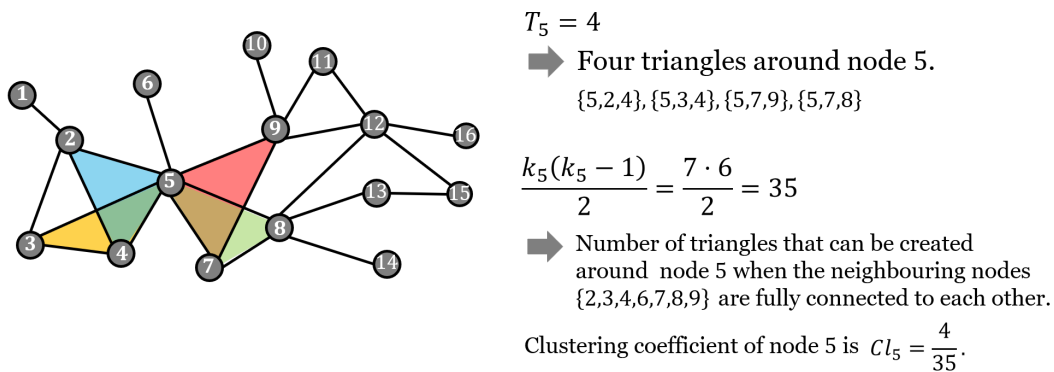


Figure 2.9: Clustering coefficient of a node. For example, the clustering coefficient of node 5 is computed by counting the number of triangles that includes node 5 as one of its vertex, and dividing that value with the number of possible triangles that can be created using node 5 when all its neighbours are fully connected to each other (forming a locally complete graph).

Centrality measures A centrality C_i of a node i measures how much central in the network the node i is. We can interpret this as how important the node i is for the whole network. There are several types of centrality measures, where each centrality measure represents the importance of a node from different aspects of the network structure or process.

- The **degree centrality** of node i is defined as

$$C_i^d = \frac{1}{N - 1} \sum_j^N A_{ij}. \quad (2.72)$$

This is simply the fraction of nodes which are connected to node i . A higher degree node has a higher degree centrality, and it can influence the network more than the lower degree nodes.

2.7. INTRODUCTION TO GRAPH THEORY AND COMPLEX NETWORK SCIENCE

- The **closeness centrality** of node i is defined as

$$C_i^c = \left(\frac{\sum_{j \neq i}^{N-1} l_{ij}}{N-1} \right)^{-1}, \quad (2.73)$$

where l_{ij} is the shortest path length between nodes i, j . As this quantity sums the shortest path lengths from node i to all other nodes, it represents how close the node i is to all other nodes. A node with higher closeness centrality can reach to other nodes in an average short number of steps, and thus it can give more influence to the dynamics on the network.

- The **betweenness centrality** of node i is defined as

$$C_i^b = \frac{\sum_{k \neq i \neq j} \sigma_{kj}(i)}{\sigma_{kj}}, \quad (2.74)$$

where σ_{ij} is the number of shortest paths from node i to j , and $\sigma_{ij}(w)$ is the number of shortest paths that goes through node w among them. This measures how often the node i can be visited while moving from nodes k to j using the shortest paths. This measures how importance a node is as a relay point, since one may need to re-route a lot of number of paths when a node with high betweenness centrality is deleted from the network.

- The **eigenvector centrality** of node i is defined as

$$C_i^e = v_i, \quad \text{where} \quad A_G |\lambda_k\rangle = \lambda_k |\lambda_k\rangle = \sum_i^N v_i |i\rangle. \quad (2.75)$$

This is simply the component on node i of the eigenvector of the graph adjacency matrix. λ_k is usually chosen to be the largest eigenvalue. Eigenvector centrality measures how many important nodes are connected to node i . In many cases the eigenvector centrality is measured using the leading eigenvector $|\lambda_1\rangle$, the eigenvector corresponding to the largest eigenvalue of the adjacency matrix.

- The **random walk closeness centrality** of node i is defined as

$$C_i^{rc} = \left(\frac{\sum_j H(j, i)}{N} \right)^{-1}, \quad (2.76)$$

2.8. ESSENTIAL CONCEPTS OF COMPLEX NETWORKS

where $H(j, i)$ is the first mean passage time from node i to node j . The first mean passage time is the average time of a random walker to reach node i for the first time, starting from node j . This is another closeness centrality measure, although the distance between nodes are measured as the time of a random walker to reach from one node to the other, instead of the shortest path distances. This is a centrality measure based on the random walk process on the network.

2.8 Essential concepts of complex networks

Here we introduce some important concepts and examples used in complex network science. The central aim of complex network science is to create mathematical models that can reproduce the properties or dynamics of real-world networks. Numerous models have been proposed and analyzed in the literature, although most of the models are based on the basic concepts that will be explained in this section. We will first explain the Erdős-Rényi random graph, which is the seminal network model that plays a role as the basic building block of complex network science. After that we explain two common concept in complex networks, which are the small-world property and the scale-free property.

Erdős-Rényi random graph The Erdős-Rényi random graph (ER graph) is a probabilistic model to generate a network whose connections between nodes are random. A ER graph consists of N nodes is defined as follows:

- An ER graph $G(N, p)$ is a graph where each pair of N labeled nodes are connected with probability p . [30]

To generate such graph, first we start with N disconnected nodes, and for each pair of nodes i, j , sample a random number x_{ij} from a uniform distribution. If $x_{ij} > p$, we draw an edge between that pair of nodes.

As an more intuitive explanation, assume a graph with 8 disconnected nodes (see left side of Figure 2.10). Choose any pair of node and flip a coin. If the result is heads, draw an edge between that pair of node, and do not draw an edge if the result is tails. This corresponds to the case of $p = 0.5$ in Figure 2.10. Repeat this coin toss for all possible pair of nodes. As the number of possible pairs is $8(8-1)/2 = 28$, you need to toss the coin 28 times. After this process is done, you obtain one instance of the ER graph, $G(8, 0.5)$ (right side of Figure 2.10).

2.8. ESSENTIAL CONCEPTS OF COMPLEX NETWORKS

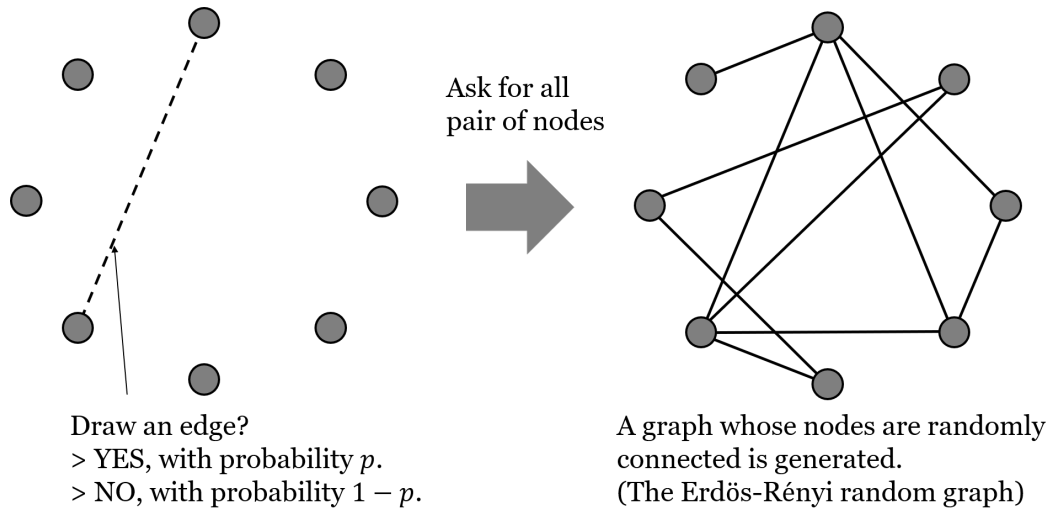


Figure 2.10: Schematic illustration of the process of generating an Erdős-Rényi random graph.

Let us list up some properties of the ER graph. First, the expectation value of the degree of node i is $\langle k_i \rangle = p(N - 1)$. The expected total number of edges in the network is $L = pN(N - 1)/2$. This is equal to multiplying p to the total number of edges in a complete graph, $N(N - 1)/2$. The degree distribution $P(k)$ of the ER graph is a binomial distribution, which can be derived by asking the probability that a node i has k edges. The probability where k of the node's edges are present is p^k . The probability where the remaining $N - 1 - k$ edges are missing is $(1 - p)^{N-1-k}$. Since there are

$$\binom{N - 1}{k} \quad (2.77)$$

possible ways to select k edges from the $N - 1$ potential edges, $P(k)$ is given by,

$$P(k) = \binom{N - 1}{k} p^k (1 - p)^{N-1-k}. \quad (2.78)$$

When $\langle k \rangle \ll N$, meaning that the network is sparse, the binomial distribution is well approximated by the Poisson distribution,

$$P(k) = e^{-\langle k \rangle} \frac{\langle k \rangle^k}{k!}. \quad (2.79)$$

The spectral properties of the ER graph is also interesting to investigate. The dis-

2.8. ESSENTIAL CONCEPTS OF COMPLEX NETWORKS

tribution of the eigenvalues λ_i of the adjacency matrix of a ER graph A_{ER} is known to follow the semi-circle law, as shown in Figure 2.11(a). This distribution (histogram) is computed by obtaining all eigenvalues λ_i satisfying $A_{ER}|\lambda_i\rangle = \lambda_i|\lambda_i\rangle$, and taking the distribution $P(\lambda_i = \lambda)$. The eigenvalues are distributed in a half-circular distribution, centered at 0 which resembles the name *semi-circle* law. We also see an isolated large eigenvalue apart from the semi-circle. The size of the gap between the semi-circle bulk and

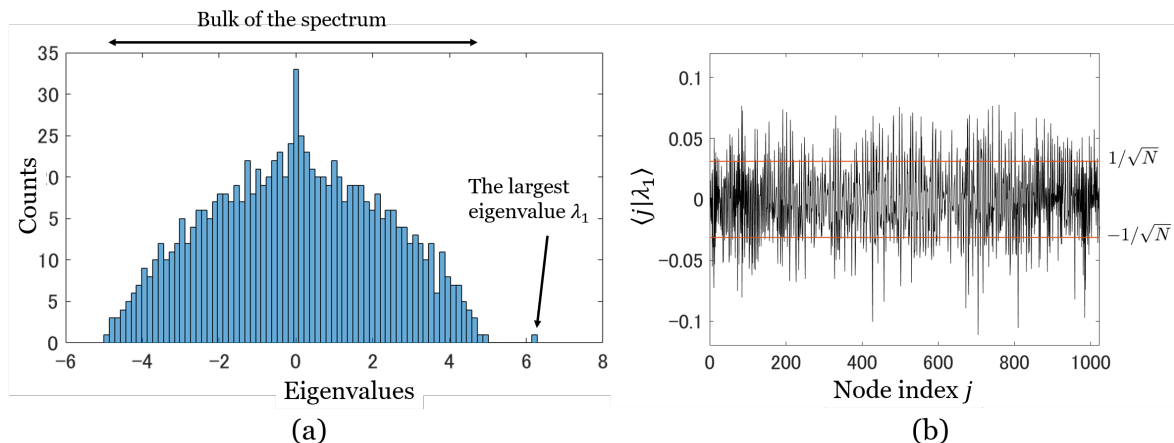


Figure 2.11: (a) The spectral distribution (histogram) of the ER graph. The distribution follows the semi-circle law, which means that the bulk of the spectrum is distributed in a shape of a half-circle. Note that there is one eigenvalue separated from the bulk, which is the largest eigenvalue. (b) Components of the leading eigenvector (i.e. eigenvector corresponding to the largest eigenvalue) $|\lambda_1\rangle$ of the ER graph. One can see that the components are taking random values, centered at 0, and the range of fluctuations is around $1/\sqrt{N}$, indicated with the red line. Both of the plots are obtained using a graph of $G(1024, 0.05)$.

the largest eigenvalue depends on the average degree, which indicates the connectivity of the graph. Additionally, the leading eigenvector of the adjacency matrix (the eigenvector corresponding to the largest eigenvalue of the matrix) has randomly distributed components around 0. See Figure 2.11(b), where the components c_j of the leading eigenvector $|\lambda_1\rangle = \sum_{j=1}^N c_j|j\rangle$ is plotted. These properties essentially tells that the ER graph has a pure random structure. The ER graph is generally used as a reference model to compare with different types of complex networks or real world networks. It is useful to consider how much the network of interest is different or similar to the ER graph. If the network has different properties from the ER graph, that indicates there are some special structure in the network (i.e. meaning that the network is not purely random).

Small-world property In many real-world complex networks, a property called as the small-world property is often observed. The small-world property is defined by the

2.8. ESSENTIAL CONCEPTS OF COMPLEX NETWORKS

diameter of the network satisfying a logarithmic growth according to the size of the network, $l_d \sim \log N$. Here N is the total number of nodes in the network. This means that the diameter of the network grows very slowly compared to the size of the network, and thus one can reach from one node to another in relatively short steps, when the shortest path is known.

We can analytically derive that the ER graph has the small-world property. Consider one node i in the graph and count the expected number of nodes that is within distance (step) l from the node i . Obviously the number of nodes corresponding to $l = 0$ is 1 (node i itself). The number of nodes corresponding to $l = 1$ is $\langle k \rangle$ in average, since node i has $\langle k \rangle$ neighbours in average. The number of nodes corresponding to $l = 2$ is $\langle k \rangle^2$ in average, since the $\langle k \rangle$ neighbours of node i have $\langle k \rangle$ neighbours in average. In this way, the sum of the number of nodes within distance l can be roughly calculated as

$$N(l) \approx 1 + \langle k \rangle + \langle k \rangle^2 + \dots + \langle k \rangle^l = \frac{\langle k \rangle^{l+1} - 1}{\langle k \rangle - 1}. \quad (2.80)$$

Here, as we assume the network has finite number of nodes, l must be upper bounded by the diameter of the network $l \leq l_{max}$. Additionally, $N(l)$ must not exceed N , since the total number of nodes in the network is N . Combining these two conditions, we can set that $N(l_{max}) \approx N$. Then from Eq. (2.80), we get

$$\frac{\langle k \rangle^{l_{max}+1} - 1}{\langle k \rangle - 1} \approx N. \quad (2.81)$$

Assuming that $\langle k \rangle \gg 1$,

$$\frac{\langle k \rangle^{l_{max}+1} - 1}{\langle k \rangle - 1} \approx \langle k \rangle^{l_{max}} \approx N. \quad (2.82)$$

Taking the logarithm, we get the expression of the diameter l_{max} of the ER graph as,

$$l_{max} \approx \frac{\log N}{\log \langle k \rangle}, \quad (2.83)$$

which satisfies the definition of the small-world property.

On the other hand, regular lattices are not small world as the diameter grows as $l_d \approx N^{1/d}$, where d is the dimension of the lattice. This can be easily understood by imagining a d -dimensional square lattice with the length of each sides being $N^{1/d}$. Importantly, lattices cannot satisfy the small-world property except the limit of infinite dimension,

2.8. ESSENTIAL CONCEPTS OF COMPLEX NETWORKS

$d \rightarrow \infty$. There are network models that explore the transition from non-small-world to small-world networks by adjusting the parameter to generate the network, such as the Watts-Strogatz model and the long-range percolation model. We will further introduce the latter model in the next Chapter, as we analyze the quantum search algorithm on that model.

Scale-free networks Another important property that appears in the real-world complex networks is the scale-free property. This property is defined as the network's degree distribution following a power law function of the form

$$P(k) \propto k^{-\beta}. \quad (2.84)$$

The exponent β is a real positive number, which determines the concentration of edges on certain nodes of the network. Figure 2.12 shows the visualization of an example of the scale-free network, while the power law degree distribution is plotted in Figure 2.13, together with a binomial distribution for comparison. Looking at the visualization of the network together with the degree distribution, the power law distribution can be interpreted intuitively as, (i) most of the nodes has small degree indicated from the small k side of the distribution, and (ii) there exists few nodes that has significantly large degree indicated from the long tail of the distribution. The largest degree node in the network is called as the hub, or sometimes call the set of large degree nodes as hubs. Scale-free networks are especially important class of networks in complex network science, since it has been discovered that the scale-free property is observed in many instances of real-world networks, such as the World-Wide-Web, airline network or the actor collaboration network [31], etc.

We shall look at the basic properties of scale-free networks, which can be derived from the degree distribution $P(k) \propto k^{-\beta}$. We set the total number of nodes in the network as N . Let us first estimate the size of the largest hub, namely the largest degree k_{max} of the network. This is also called as the natural cutoff of $P(k)$. In order to provide easier explanation of the calculation, first we consider a calculation using the exponential distribution,

$$P(k) = ce^{-\beta k}. \quad (2.85)$$

We set the minimum degree k_{min} (in principle this is $k_{min} \geq 1$ as we consider a connected

2.8. ESSENTIAL CONCEPTS OF COMPLEX NETWORKS

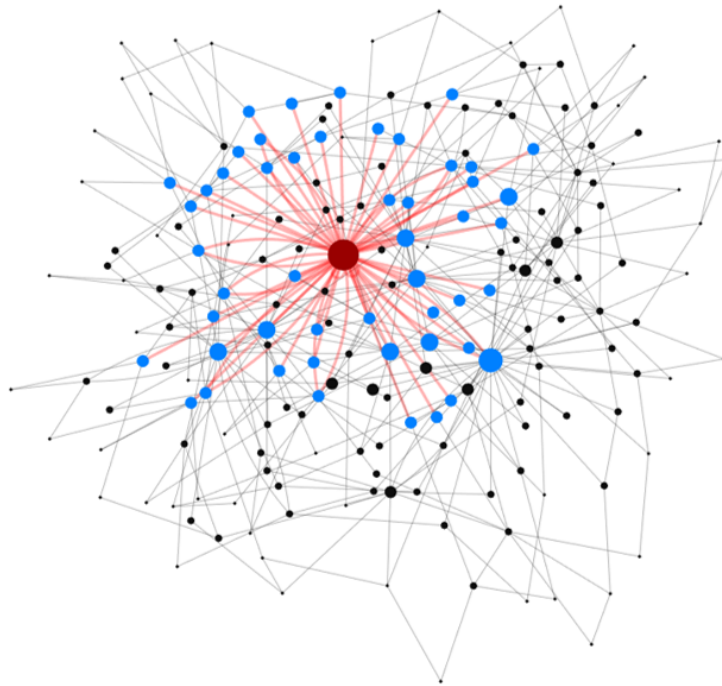


Figure 2.12: Visualization of a scale-free network. The network consists of $N = 200$ nodes, and the degree distribution follows $P(k) \propto k^{-3}$. A network generation model known as the Bollobás model (will be explained in Section 3.7) is used to generate the graph. The sizes of the nodes are proportional to its closeness centrality. The red node in the center has the largest degree in the network, which we call as the hub node. The edges connected to the hub node is draw in red, and the neighbours are the blue nodes. The common property of scale-free networks is the existence of the hub, while majority of the nodes have small degree (see the black nodes on the perimeter).

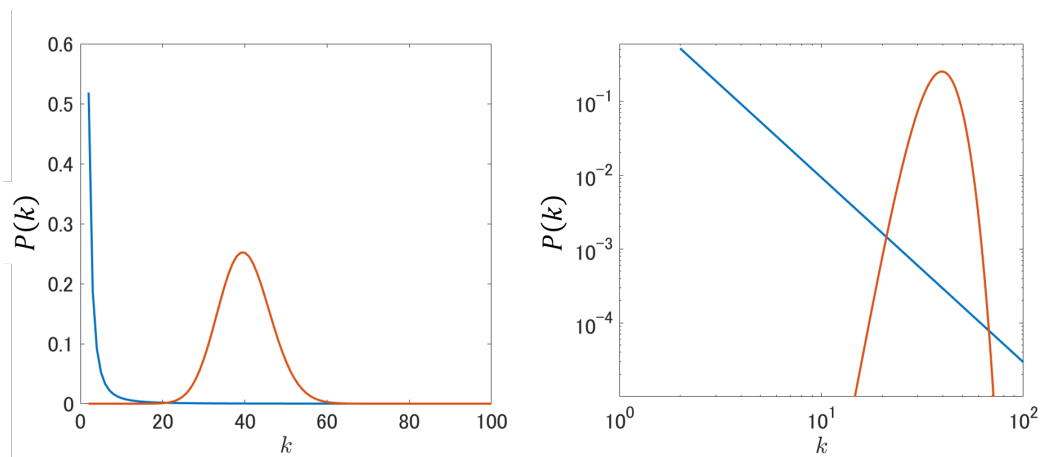


Figure 2.13: The Power law (blue) and binomial (red) distribution plotted together as a comparison, in linear scale (left) and logarithmic scale (right).

2.8. ESSENTIAL CONCEPTS OF COMPLEX NETWORKS

component⁵) and give the normalization condition

$$\int_{k_{min}}^{\infty} P(k)dk = 1 \quad (2.86)$$

$$[-ce^{-\beta k}/\beta]_{k_{min}}^{\infty} = 1 \quad (2.87)$$

$$ce^{-\beta k_{min}}/\beta = 1. \quad (2.88)$$

This gives $c = \beta e^{\beta k_{min}}$. To estimate k_{max} , we consider that the probability to find a node larger than k_{max} is $1/N$ (as small as maybe finding one node from the network), such as

$$\int_{k_{max}}^{\infty} P(k)dk = \frac{1}{N}. \quad (2.89)$$

This leads to the equation,

$$\beta e^{\beta k_{min}} \frac{e^{-\beta k_{max}}}{\beta} = \frac{1}{N} \quad (2.90)$$

$$e^{\beta(k_{min}-k_{max})} = \frac{1}{N} \quad (2.91)$$

$$k_{max} = k_{min} + \frac{\ln N}{\beta}. \quad (2.92)$$

This means that k_{max} is not greatly different from k_{min} since $\ln N$ is a slowly growing function of N . To apply the same calculation with a power law function

$$P(k) = ck^{-\beta}, \quad (2.93)$$

first consider the normalization condition

$$\int_{k_{min}}^{\infty} P(k)dk = 1 \quad (2.94)$$

which leads to

$$c = (\beta - 1)k_{min}^{\beta-1}. \quad (2.95)$$

Hence by substituting

$$P(k) = (\beta - 1)k_{min}^{\beta-1}k^{-\beta} \quad (2.96)$$

⁵A connected component is a subset of nodes that are connected by a path. If no path exists between two nodes, they belong to different connected components.

2.8. ESSENTIAL CONCEPTS OF COMPLEX NETWORKS

into Eq. (2.89), we get

$$k_{max} = k_{min} N^{\frac{1}{\beta-1}}. \quad (2.97)$$

This means that k_{max} of scale-free networks can be magnitudes of order larger than k_{min} , since the growth is polynomial to N . For example when $\beta = 3$, $k_{max} \sim \sqrt{N}$.

Next we will look at the n -th moment of the degree distribution, $\langle k^n \rangle$. $n = 1$ is the average, $n = 2$ is the variance and $n = 3$ corresponds to the skewness, which tells us how symmetric the distribution is around $\langle k \rangle$. The n -th moment of the power law distribution is

$$\langle k^n \rangle = \int_{k_{min}}^{k_{max}} k^n P(k) dk = \int_{k_{min}}^{k_{max}} c k^{n-\beta} dk = c \frac{k_{max}^{n-\beta+1} - k_{min}^{n-\beta+1}}{n - \beta + 1}. \quad (2.98)$$

We have seen from Eq. (2.97) that k_{max} increases polynomially with the network size, while k_{min} is usually fixed. Therefore in the large N limit, the behaviour of $\langle k^n \rangle$ is dominated by the behaviour of $k_{max}^{n-\beta+1}$. We can consider this by dividing into two cases.

- When $n - \beta + 1 \leq 0$, $k_{max}^{n-\beta+1}$ converges to zero as N increases. Therefore, the moments satisfying $n \leq \beta - 1$ are finite.
- When $n - \beta + 1 > 0$, $k_{max}^{n-\beta+1}$ goes to infinity as N increases. Therefore, the moments satisfying $n > \beta - 1$ diverge.

This result tells us that the distribution qualitatively changes at $\beta = 3$. When $\beta \geq 3$, moments of $n = 1$ and $n = 2$ are finite, but otherwise when $\beta < 3$, moments of $n = 2$ or greater diverge. The divergence of $\langle k^2 \rangle$, the variance, gives a strong implication that when a node is randomly chosen, one cannot identify the typical range of values the degree will take, since the variance goes to infinity. This is a critically different property compared to the ER graph which has the binomial degree distribution.

It is also known that scale-free networks have an *ultra-small-world* property. The average shortest path distances in a scale-free network has been shown to be [32],

$$\langle l \rangle \sim \begin{cases} const. & \beta = 2 \\ \ln(\ln N) & 2 < \beta < 3 \\ \frac{\ln N}{\ln(\ln N)} & \beta = 3 \\ \ln N & \beta > 3 \end{cases}. \quad (2.99)$$

As $\beta \rightarrow \infty$ corresponds to the Poisson distribution, scale-free networks satisfy the small-

2.8. ESSENTIAL CONCEPTS OF COMPLEX NETWORKS

world property at any β .

Finally we shall look at the spectral properties of scale-free networks. Figure 2.14 shows the distribution of the eigenvalues of the adjacency matrix of a scale-free network. To compute the eigenvalues numerically, we used a network generation model known as the Bollobás model and generated the adjacency matrix. We will dig in to detail of the Bollobás model in Section 3.7 of Chapter 3, and at this point we just mention that this model is one of the commonly used mathematical network model that generates a scale-free network with adjustable value of β . The distribution of the scale-free network displays a heavy tailed distribution, tailed on both positive and negative λ . This is very different from the ER graph which obeyed the semi-circle law. The spectral distribution for the scale-free network follows a power law distribution excluding the λ in the vicinity of zero.

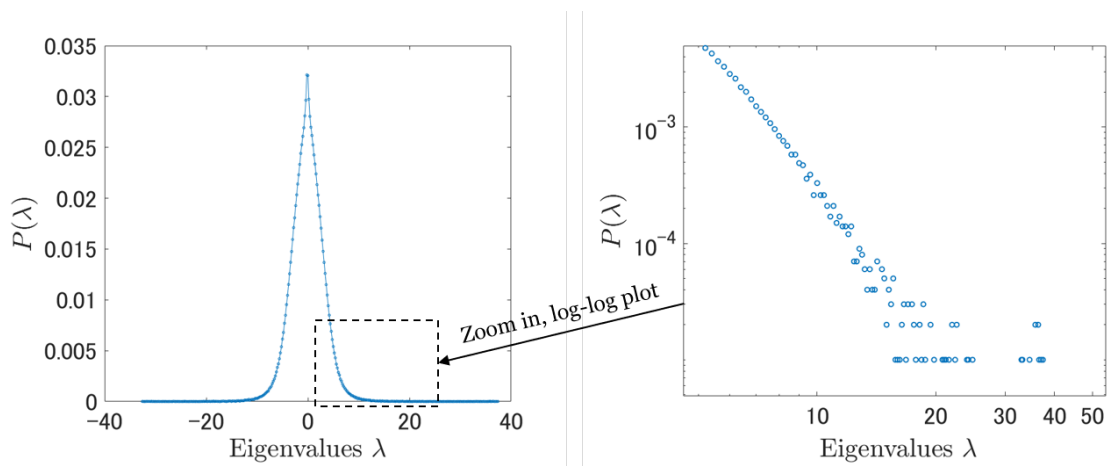


Figure 2.14: Spectral distribution of the Bollobás scale-free network. All of the eigenvalues of the adjacency matrix of a network with size $N = 5000$ and degree distribution exponent $\beta = 3$ is computed to obtain the distribution. The spectral distribution follows a power law function in the region excluding the eigenvalues close to zero.

2.9 Writing arbitrary Hamiltonians as tight-binding models and their interpretation as networks

In this final section of the current chapter, we introduce the core idea used in this thesis. The idea can be summarized into three components:

1. Take an arbitrary Hamiltonian defined on a N -dimensional Hilbert space. Choose a certain basis set $\{|i\rangle\}$ and write the Hamiltonian as a $N \times N$ matrix.
2. Interpret the matrix as an adjacency matrix of a weighted, undirected graph of N nodes.
3. Once the Hamiltonian is interpreted as a graph, the quantum system can be analyzed using the language from graph theory and complex network science. Moreover, one can work in the other way around and use a complex network as a tight-binding Hamiltonian, discussing its properties as a quantum system.

Figure 2.15 shows the diagrammatic explanation of this approach.

This idea is motivated by the work by Bastidas *et al.* [24] and Roy *et al.* [29] where they considered certain types of quantum systems and analyzed those systems using some concepts from graph theory and network science. Specifically, Bastidas *et al.* [24] discussed the properties of ergodic and localized quantum systems using the connectivity and degree distribution of graphs. Roy *et al.* [29] discussed localized-to-thermal transition of quantum spin systems using percolation of graphs. In this thesis, the idea is extended to especially bring the concepts of complex network science into quantum physics. Using the rest of this section, we will show the detailed explanation of the above idea with some examples.

Let us explain the first step to write . As introduced in Section 2.6.1, tight-binding Hamiltonians are matrices displaying transitions between all states of the Hilbert space. One can for example write a spin Hamiltonian in a tight-binding form by choosing a certain set of orthonormal basis states $\{|i\rangle\}$. By doing this, we are essentially translating the *interactions* between the spins into *transitions* between states. The selection of the set of basis states $\{|i\rangle\}$ is very important as it changes the form of the matrix and thus the structure of the transitions between states. For example, the energy eigenstate can be one choice to represent the spin Hamiltonian as a tight-binding matrix form. Trivially, the matrix will be diagonal and we cannot see transitions between states. However, this is

2.9. WRITING ARBITRARY HAMILTONIANS AS TIGHT-BINDING MODELS AND THEIR INTERPRETATION AS NETWORKS

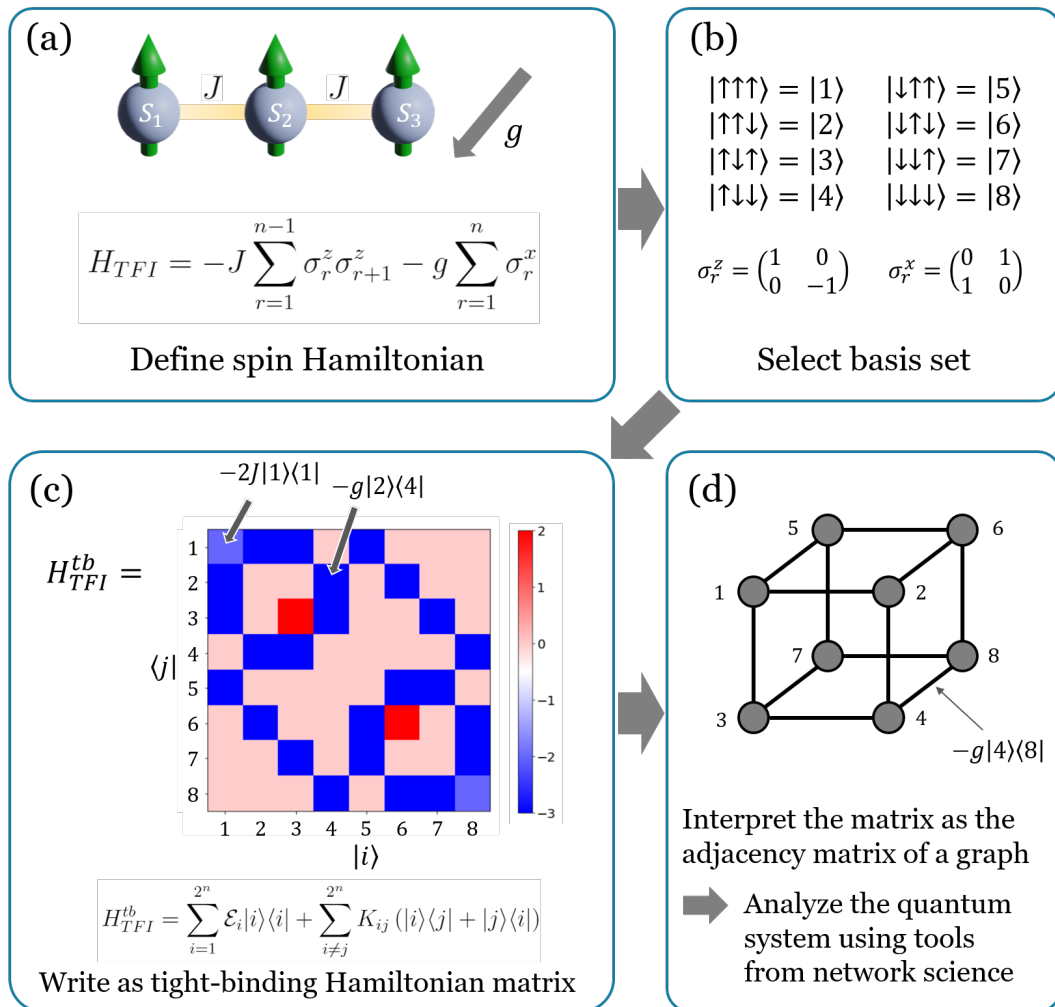


Figure 2.15: The approach to interpret and analyze Hamiltonian systems as graphs. (a) Assume we have a spin Hamiltonian we would like to analyze. (b) Select a certain set of basis set. (c) Once the basis set is fixed, the spin Hamiltonian can be written in a matrix form, which is the form of tight-binding Hamiltonians. (d) We can use the matrix form of the matrix as the adjacency matrix of a graph. By interpreting the quantum system as a graph is such way, we can use tools from graph theory and network science to analyze the system.

still an important basis to choose in some cases, such as applying additional perturbation to the system.

Let's take the tilted-field Ising model without the magnetic field in the z -direction as an example, where the spin Hamiltonian is

$$H_{TFI} = -J \sum_{r=1}^{n-1} \sigma_r^z \sigma_{r+1}^z - g \sum_{r=1}^n \sigma_r^x. \quad (2.100)$$

2.9. WRITING ARBITRARY HAMILTONIANS AS TIGHT-BINDING MODELS AND THEIR INTERPRETATION AS NETWORKS

Here σ_r^z and σ_r^x are the Pauli operators on the r -th spin, J is the strength of the Ising interaction, and g is the strength of the external magnetic field in the x -direction. We assume nearest-neighbour one-dimensional interaction of n spins. Now let us write this spin Hamiltonian in the tight-binding Hamiltonian matrix form. A non-trivial and interesting choice of basis in this case will be the product states of the eigenstates of σ_r^z . We denote the eigenstates as $\sigma_r^z|\uparrow\rangle = (+1)|\uparrow\rangle$ and $\sigma_r^z|\downarrow\rangle = (-1)|\downarrow\rangle$. The set of $N = 2^n$ basis states can be written as $\{|S_1\rangle \otimes |S_2\rangle \otimes \dots \otimes |S_n\rangle\}_{S_1, \dots, S_n = \uparrow, \downarrow}$. As these are n -bit binary numbers $|\uparrow \dots \uparrow \uparrow\rangle, |\uparrow \dots \uparrow \uparrow \downarrow\rangle, |\uparrow \dots \uparrow \downarrow \uparrow\rangle, \dots, |\downarrow \dots \downarrow \downarrow \downarrow\rangle$, we label these states with the decimal numbers as $|1\rangle, |2\rangle, \dots, |i\rangle, \dots, |N-1\rangle, |N\rangle$ in the ascending order. Using the matrix form of Pauli operators and their tensor product operations defined in Section 2.5, we can write H_{TFI} as the tight-binding Hamiltonian matrix,

$$H_{TFI}^{tb} = \sum_{i=1}^N \mathcal{E}_i |i\rangle \langle i| + \sum_{i \neq j}^N K_{ij} (|i\rangle \langle j| + |j\rangle \langle i|) = \begin{pmatrix} \mathcal{E}_1 & K_{12} & \dots & K_{1N} \\ K_{21} & \mathcal{E}_2 & & \vdots \\ \vdots & & \ddots & \\ K_{N1} & \dots & & \mathcal{E}_N \end{pmatrix}. \quad (2.101)$$

In the left side of Figure 2.16, we have shown the matrix elements of H_{TFI} as a color map, with $n = 5$ spins, $J = 1.0$, and $g = 3$. This is a $2^5 \times 2^5 = 32 \times 32$ matrix. The terms $-J\sigma_r^z\sigma_{r+1}^z$ in Eq. (2.100) contribute to the diagonal elements \mathcal{E}_i , while the terms $-g\sigma_r^x$ in Eq. (2.100) contribute to the off-diagonal elements K_{ij} . This perspective clearly shows that the matrix is diagonal when $g = 0$, and when $g > 0$ certain entries of the off-diagonals becomes non-zero. The non-zero g can be viewed as a perturbation applied to the system.

Now let us interpret the matrix as the adjacency matrix of a undirected, weighted graph. At this point, we only focus at the off-diagonal elements K_{ij} and omit the diagonal elements \mathcal{E}_i . We take the absolute value of the elements, $|K_{ij}|$, in the case when the entries are complex numbers. This will be good enough to see what kind of transitions the perturbation is generating. The graph corresponding to the matrix is shown on the right side of Figure 2.16. The nodes are each basis states $\{|S_1 S_2 \dots S_n\rangle\}_{S_1, \dots, S_n = \uparrow, \downarrow}$, and the edges between nodes are drawn if $K_{ij} \neq 0$. Therefore, the existence of the edge between pair of nodes means that transitions occur between the two states. As we have placed the nodes in specific positions in Figure 2.16, we can see that the graph has the structure of a 5-dimensional hypercube. In a hypercube, nodes that are apart by Hamming distance

2.9. WRITING ARBITRARY HAMILTONIANS AS TIGHT-BINDING MODELS AND THEIR INTERPRETATION AS NETWORKS

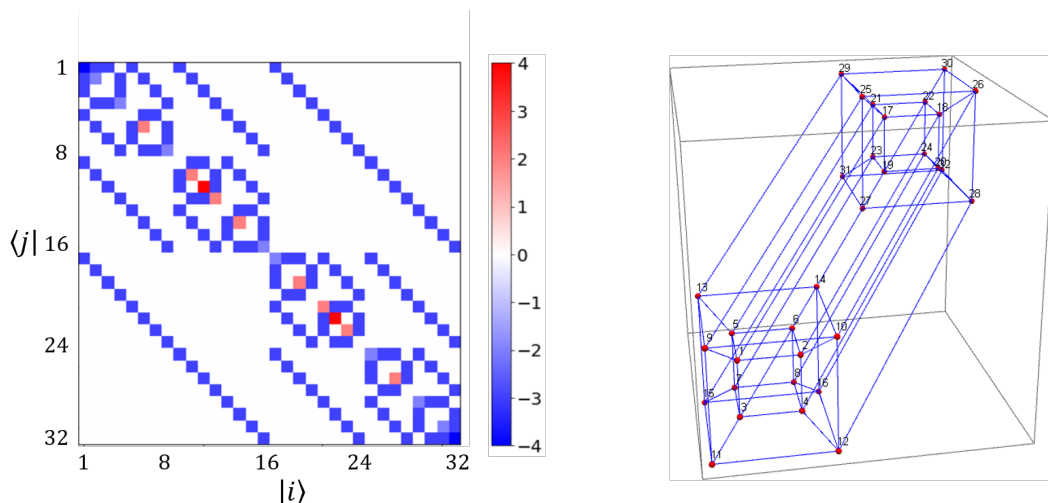


Figure 2.16: Hamiltonian matrix of the TFI model of Eq. (2.100) with $n = 5$ spins (left), and its graph representation (right). The entries $(H_{TFI}^{tb})_{ij}$ of the matrix is represented by the colormap. The graph on the right is drawn by assigning the nodes to each basis states $|i\rangle$ and taking the non-zero off-diagonal entries $(H_{TFI}^{tb})_{ij}$ as the edge connecting the nodes i and j .

one⁶ are connected to each other. This corresponds to the physical perspective that the term $g \sum_{r=1}^n \sigma_r^x$ can only flip one spin at a time, as this is a sum of local spin flips. Although this is a simple example, the graph viewpoint gives us insight of the structure and dynamics of the system in a graphical way.

We shall consider a slightly more complicated example to see the power of this graph interpretation of Hamiltonians. We consider the tilted-filed Ising model with a disordered magnetic field in the z -direction. The Hamiltonian takes the same form

$$H_{TFI} = -J \sum_{r=1}^{n-1} \sigma_r^z \sigma_{r+1}^z - \sum_{r=1}^n B_r \sigma_r^z - g \sum_{r=1}^n \sigma_r^x, \quad (2.102)$$

where B_r is a random variable within the interval $B_r \in [0, W]$. When the strength of the disorder of the magnetic field W is large enough, the system will be in a localized phase. In the localized phase, all of the eigenstates of the Hamiltonian are exponentially localized at certain configuration state $|S_1 S_2 \dots S_n\rangle$. Therefore, almost no transition can occur between the states and the initial state is almost frozen during the time evolution. It has been shown that when $W > 2J + g/2$, the Hamiltonian Eq. (2.102) will be in such localized phase [29]. Here we aim to see this localized phase from the graph interpretation

⁶Hamming distance is the necessary number of bit (spin) flips to change a bit string to another. For example, the Hamming distance between states $|\uparrow\uparrow\uparrow\uparrow\rangle$ and $|\downarrow\uparrow\downarrow\uparrow\rangle$ is 2 as you need to flip the first and third spins.

2.9. WRITING ARBITRARY HAMILTONIANS AS TIGHT-BINDING MODELS AND THEIR INTERPRETATION AS NETWORKS

of the Hamiltonian.

Let's consider writing the above spin Hamiltonian in the tight-binding Hamiltonian matrix form. By choosing the same basis set from the first example $\{|S_1 \dots S_n\rangle\}_{S_1, \dots, S_n = \uparrow, \downarrow}$, we can soon find out that the difference compared to the first example is only in the diagonal entries of the matrix. This is because the new term $\sum_{r=1}^n B_r \sigma_r^z$ only contributes to the diagonal entries, \mathcal{E}_i . If we directly interpret the matrix as an adjacency matrix, the graph will look exactly the same as the one in Figure 2.16. However, the key to understand the localized phase lies in the balance between the strength of the diagonal disorder W and the off-diagonal transitions g . To see the signature of the localized phase from the graph, we must take the diagonal entries into account in some way when representing the Hamiltonian as a graph.

The resonance rule To this end, we introduce the *resonance rule*, which is originally introduced by Roy *et al.* [29], in order to make use of the diagonal entries in the graph. We define a following rule when drawing the graph from the tight-binding Hamiltonian matrix:

- For all pair of nodes $|i\rangle$ and $|j\rangle$, draw an unweighted edge with only if $|\mathcal{E}_j - \mathcal{E}_i| < |K_{ij}|$ is satisfied. Otherwise, do not draw an edge between nodes $|i\rangle$ and $|j\rangle$.

Specifically, we initially prepare a $N \times N$ adjacency matrix A , with all of its entries being 0. For each matrix element A_{ij} , we refer to the tight-binding Hamiltonian matrix and calculate if $|\mathcal{E}_j - \mathcal{E}_i| < |K_{ij}|$ is satisfied. If the inequality is satisfied, we put $A_{ij} = 1$ in the adjacency matrix. If the inequality is not satisfied, we keep the entry as $A_{ij} = 0$. We do this for all pairs of i and j , except for the diagonals A_{ii} and we keep them as $A_{ii} = 0$. As a result we get an unweighted adjacency matrix and the corresponding unweighted graph. See Figure 2.17 for the illustrative explanation.

Let us give the physical intuition of this resonance rule by considering a simple two-level system. We define the two level Hamiltonian (2×2 matrix) as,

$$H_{2L} = \mathcal{E}_1|1\rangle\langle 1| + \mathcal{E}_2|2\rangle\langle 2| + K(|1\rangle\langle 2| + |2\rangle\langle 1|). \quad (2.103)$$

We can compute the eigenvalues of this system as $E_{\pm} = \{\mathcal{E}_1 + \mathcal{E}_2 \pm \sqrt{(\mathcal{E}_1 - \mathcal{E}_2)^2 + 4K^2}\}/2$. Define the energy gap of the avoided crossing $\Delta \equiv E_+ - E_- = \sqrt{(\mathcal{E}_1 - \mathcal{E}_2)^2 + 4K^2}$. When we initialize the system in one of the levels, the probability to find the system in the other

2.9. WRITING ARBITRARY HAMILTONIANS AS TIGHT-BINDING MODELS AND THEIR INTERPRETATION AS NETWORKS

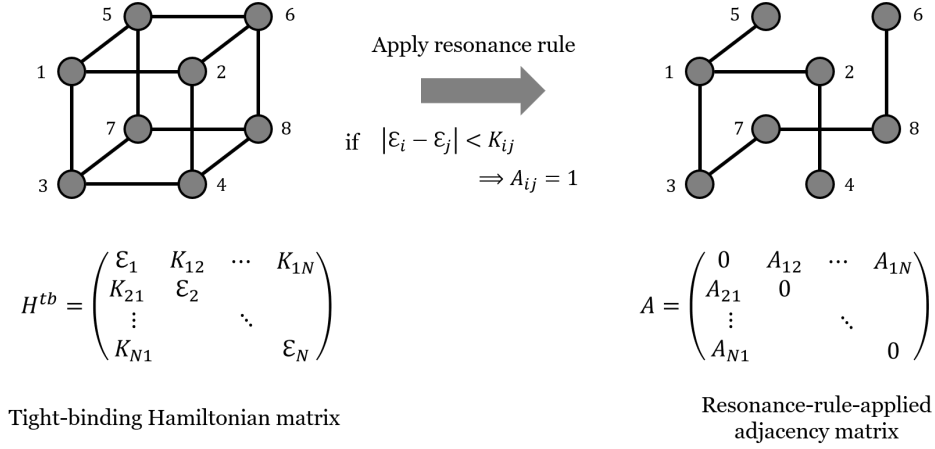


Figure 2.17: Applying the resonance rule on the tight-binding Hamiltonian to obtain the adjacency matrix of a graph. Given a Hamiltonian matrix H^{tb} , one asks if the condition $|\mathcal{E}_j - \mathcal{E}_i| < |K_{ij}|$ is satisfied for all pair of states, and if true draw an edge between the nodes i and j (set $A_{ij} = 1$).

level is

$$P(t) = \frac{4K^2}{\Delta^2} \sin^2\left(\frac{\Delta t}{2}\right) = \frac{1}{1 + \left(\frac{\varepsilon_1 - \varepsilon_2}{2K}\right)^2} \sin^2\left(\frac{\Delta t}{2}\right). \quad (2.104)$$

From the above equation, we can see that $|\mathcal{E}_1 - \mathcal{E}_2|$ is acting as a potential barrier. When $|\mathcal{E}_1 - \mathcal{E}_2| \ll 1$, the complex amplitude fully bounce back and forth between the states. As $|\mathcal{E}_1 - \mathcal{E}_2|$ increases, the greater fraction of the complex amplitudes stays on its initial state, which is the sign of localization. The resonance rule asks the relation between $|\mathcal{E}_1 - \mathcal{E}_2|$ and K , and picks up the transitions in the system where sufficiently large fraction of the complex amplitudes that moves from one site to the other (for this two level system, the fraction greater than $4/5$). See Figure 2.18 which illustrates the two cases, $|\mathcal{E}_1 - \mathcal{E}_2| < K$ and $|\mathcal{E}_1 - \mathcal{E}_2| \geq K$. The resonance rule cuts out the transitions in the condition of $|\mathcal{E}_1 - \mathcal{E}_2| \geq K$ when drawing the graph representation of the system.

As the resonance rule filters out the major transitions in the system and eliminates the narrow bandwidth transitions, the resulting graph we get after applying the rule will depict the abstract dynamics of the system. This allows us to understand the system intuitively. We now go back to Eq. (2.102) and apply the resonance rule on the disordered tilted-filed Ising Hamiltonian matrix. To show an example, we set the parameters as $J = 1$, $g = 2.1$ and $W = 4.6$, which satisfies $W > 2J + g/2$ where the system is in the localized phase. After the resonance rule on the Hamiltonian matrix with these parameters is applied, the unweighted adjacency matrix A_{TFI} and the corresponding graph is plotted in Figure 2.19. We see a sparse graph, which means there are not many major transitions in the system

2.9. WRITING ARBITRARY HAMILTONIANS AS TIGHT-BINDING MODELS AND THEIR INTERPRETATION AS NETWORKS

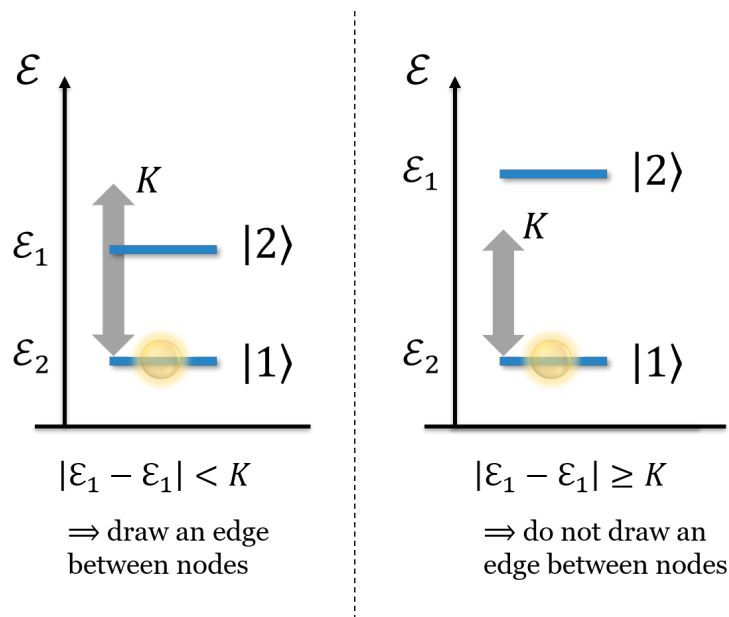


Figure 2.18: The resonance rule illustrated for a two level system.

compared to the no-disorder case. This is a sign of the localization, visualized as a graph. The complex amplitudes will tend to stay on its initial site or mostly travel around inside a small subspaces of the system (for example, see that nodes 12, 10, 26 is forming a small connected component, as well as node 32 being isolated).

As we have seen using two examples, the Hamiltonian matrix and graph interpretation of the system gives us intuitive insight about the dynamics of the system. Now we are interested in examples where the Hamiltonian matrix or the graph has the structure of complex networks, such as small-world or scale-free properties. The tilted-field Ising model without disorder showed a hypercube which is a regular, highly symmetric structure. When the disorder was present, randomness came in, chopping out some transitions from the hypercube graph. Can we find a complex structures that are beyond regular or purely random? In this thesis we name such complex structures as *complex quantum networks*, and aim to explore dynamics on such systems, as well as exploring the possibility to realize them experimentally using current technologies available in the labs.

We can naturally think of two directions. Take a Hamiltonian of a physically realizable quantum system, write it in the tight-binding form, interpret it as a graph, and ask if we can find complex network structure. The other direction is the other way around. Take an adjacency matrix of a complex network, interpret it as a tight-binding Hamiltonian, analyze the quantum dynamics on that quantum system, and ask if we can see interesting

2.9. WRITING ARBITRARY HAMILTONIANS AS TIGHT-BINDING MODELS AND THEIR INTERPRETATION AS NETWORKS

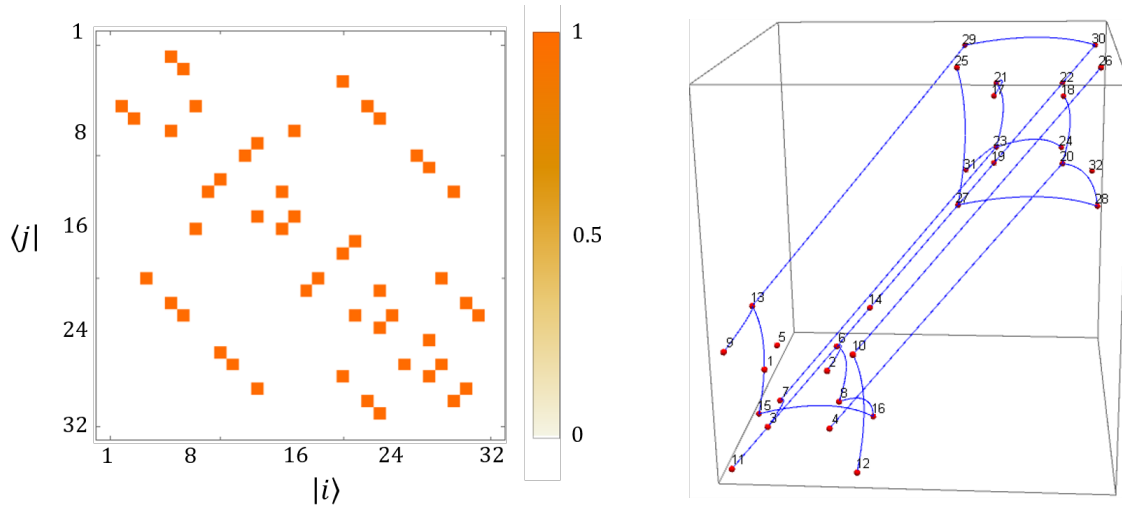


Figure 2.19: Resonance rule applied adjacency matrix A_{TFI} (left) and the corresponding graph (right) of the disordered TFI model. The matrix entries of the adjacency matrix $(A_{TFI})_{ij}$ is shown as the colormap in the left side. Note that here the adjacency matrix is unweighted; the entries are either 1 or 0. When the graph is visualized (right) from $(A_{TFI})_{ij}$, we can see that the connections are sparse compared to the no-disorder case, Figure 2.16, which is the sign of localization of states.

physics from it. We explore both directions in this thesis. We will start by exploring the latter direction in the next chapter.

Chapter 3

Quantum spatial search on complex networks

In this chapter, the problem known as the spatial search is explored. Spatial search is a problem to find a (k) marked node(s) among N nodes of the network using quantum dynamics. This is a good candidate to explore quantum dynamics on quantum systems holding complex network structures. Let us define and describe the problem with more detail, starting from the following section.

3.1 Formalization of unstructured search problem

Searching is one of the most fundamental computational problem. Search problem is a task to find one (or multiple) marked element(s) among N elements in the database as fast as possible. One can imagine a situation that you have a phone book where set of names and their phone numbers of N people are listed. You are given a piece of paper with a phone number written on it, and asked to find the name of the person corresponding to that number. Here we assume the database (list) is unstructured; e.g. the phone numbers are not correlated or ordered according to any rule. This means that when you refer to one number, you cannot gain any additional information about the other numbers¹. The best you can do in this situation will be the brute-force search. The solver has to scan the list one by one from the top to bottom until one hits the target phone number. If you are lucky, you may find the target at the top, but in the worst case, you may find it

¹As an example if the list is ordered, which is one type of data structure, one can know that the answer is in the upper or lower side of the observed number. One can perform binary search in this case

3.2. QUANTUM ALGORITHM TO SOLVE THE UNSTRUCTURED SEARCH PROBLEM

at the bottom, which is purely random at each trial. By defining the time consumed to scan one phone number as 1, the average time to find the target will be $N/2$.

A mathematically formal definition of such search problem is the evaluation of a black box function. Assume a function $f(x) : \{1, 2, \dots, N\} \rightarrow \{0, 1\}$ satisfying

$$f(x) = \begin{cases} 1, & \text{if } x = w \\ 0, & \text{if } x \neq w \end{cases}. \quad (3.1)$$

This function returns 1 if only one specific integer w is the input, while 0 is returned for any other integer. The solver's task is to identify the integer w which returns 1. The solver can input one integer x and obtain an output 0 or 1 at each time step. As the average time to obtain the output 1 and identify the integer w is $N/2$, the time complexity (or more precisely the query complexity) is $O(N)^2$.

3.2 Quantum algorithm to solve the unstructured search problem

We now consider solving the unstructured search problem using a quantum system. First we must translate the unstructured search problem to the quantum setting. See Figure 3.1 which shows the correspondence between the setting of classical and quantum search. In the classical search, a black box function is given, and the solver input an integer (or a bit string) $x \in \{1, 2, \dots, w, \dots, N\}$ to get an outcome value 0 or 1. In the quantum search, a black box unitary operator is given instead of the black box function. More precisely, the function $f(x)$ is used to construct the black box unitary operator (this will be defined later in this Section). The solver input a quantum state into the unitary operator instead of an integer x . When the size of the database is N , the quantum state will be a N -dimensional vector, and the unitary operator is a $N \times N$ matrix. The quantum state is written as the linear combination of N basis states $|x\rangle \in \{|1\rangle, |2\rangle, \dots, |w\rangle, \dots, |N\rangle\}$. The state is input to the black box and the unitary operator is applied on the state, transformed to a final state. The solver has to conduct a measurement on the state in the $\{|x\rangle\}$ basis to obtain the outcome. The time complexity of the quantum search will be evaluated by how many

²In computational complexity theory, one is usually interested in the order or scaling of the leading term of the time to solve the problem. The constant factor is omitted, and the dependence on the problem size N is represented using the big-O notation, $O(f(N))$.

3.2. QUANTUM ALGORITHM TO SOLVE THE UNSTRUCTURED SEARCH PROBLEM

times, or how much long the black box unitary has to be used in order to identify w from the outcome measurement.

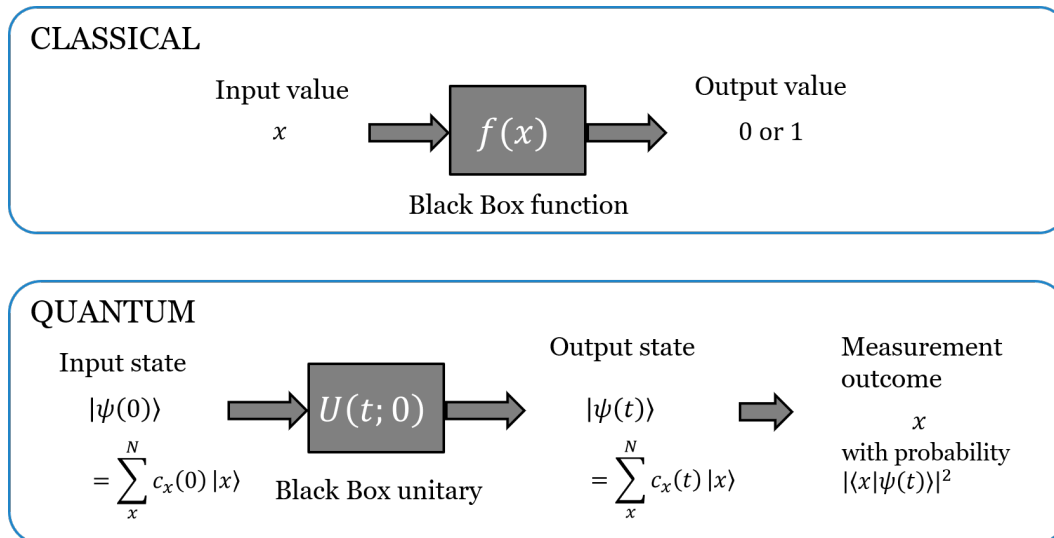


Figure 3.1: The problem definition of the classical and quantum search. In the classical case, the solver inputs a scalar value among N possible values into a black box function, which outputs a scalar value 0 or 1. Correspondingly, in the quantum case the solver inputs a N -dimensional quantum state (vector) into a black box where a unitary transformation is applied on the state. The solver has to measure the resulting state to obtain a single scalar value. For both classical and quantum, the solver aims to evaluate the black box function or unitary with the minimal use of the black box.

The first quantum algorithm that achieve to solve the unstructured problem with a time complexity of $O(\sqrt{N})$ was the Grover's algorithm [33]. Such time complexity is a quadratic improvement over the classical brute-force searching, $O(N)$. This quantum algorithm utilizes the nature of the superposition and interference of quantum states to solve the unstructured search problem.

Let us construct the Grover's algorithm. Define the dimension of the search space (i.e. size of the database) to be N . We encode the search space in a n qubit system, such that $N := 2^n$, and define a set of N basis states $\{|x\rangle\} = \{|a_1 a_2 \dots a_n\rangle\}_{a_1, \dots, a_n=0,1} = \{|0 \dots 000\rangle, |0 \dots 001\rangle, \dots, |w\rangle, \dots, |1 \dots 11\rangle\}$. The state $|w\rangle$ corresponds to the state encoding the target integer w . We call this state as the marked state, or the target state hereafter. As in the previous section, assume that the problem is to identify the integer w satisfying the function $f(x) : \{0, 1\}^n \rightarrow \{0, 1\}$ defined in Eq. (3.1). Here the variable x is represented in the binary form $\{0, 1\}^n$. The algorithm is defined by the following protocol:

3.2. QUANTUM ALGORITHM TO SOLVE THE UNSTRUCTURED SEARCH PROBLEM

1. Prepare a $n + 1$ qubit state $|0\rangle^{\otimes n}|1\rangle$, where the first part $|0\rangle^{\otimes n}$ corresponds to the search space $\{|x\rangle\}$, and the latter qubit $|0\rangle$ is an ancilla.
2. Apply the Hadamard operator $U_H^{\otimes n+1}$ on $n + 1$ qubits, where

$$U_H^{\otimes n+1} = \frac{1}{\sqrt{2}} \begin{pmatrix} 1 & 1 \\ 1 & -1 \end{pmatrix}^{\otimes n+1}. \quad (3.2)$$

3. Apply the oracle operator U_f on $n + 1$ qubits. U_f is defined as

$$U_f|x\rangle|b\rangle = |x\rangle|b \oplus f(x)\rangle. \quad (3.3)$$

This operator corresponds to the black box unitary operator.

4. Apply the Grover's diffusion operator D_f on the first n qubits, where D_f is defined as

$$D_f = -\mathbb{I} + 2U_H^{\otimes n}|0^n\rangle\langle 0^n|U_H^{\otimes n} = \begin{pmatrix} -1 + \frac{2}{N} & \frac{2}{N} & \dots & \frac{2}{N} \\ \frac{2}{N} & -1 + \frac{2}{N} & & \vdots \\ \vdots & & \ddots & \frac{2}{N} \\ \frac{2}{N} & \dots & \frac{2}{N} & -1 + \frac{2}{N} \end{pmatrix}. \quad (3.4)$$

5. Repeat 3. and 4. for $\lfloor (\pi/4)\sqrt{N} \rfloor$ times.
6. Measure the first n qubits in the computational basis and examine the n bit string outcome x_m .

Grover showed that after this protocol the probability of x_m being the integer w is $P_w \geq 1 - 1/N$. As the probability of the measurement outcome being w is almost unity after calling the black-box function $f(x)$ for $O(\sqrt{N})$ times, one can identify w with almost unity probability, which corresponds to the succession of the search algorithm.

We shall consider the analysis of the protocol and the meaning of each operators U_f and D_f in order to understand how the algorithm works. We focus on the unitary evolution of the $n + 1$ qubit state. The initial state of the system is defined in the Step

³The symbol \oplus represents the *exclusive or* operation on a binary number. Therefore, the qubit $|b\rangle$ is flipped only if $f(x) = 1$, such that $|0 \oplus 0\rangle = |0\rangle$, $|1 \oplus 0\rangle = |1\rangle$, $|0 \oplus 1\rangle = |1\rangle$ and $|1 \oplus 1\rangle = |0\rangle$.

3.2. QUANTUM ALGORITHM TO SOLVE THE UNSTRUCTURED SEARCH PROBLEM

1 of the protocol described in the previous paragraph as $|\phi_1\rangle = |0\rangle^{\otimes n}|1\rangle$. This is a state with n qubits in the 0 state, with an additional qubit in the 1 state is attached. First consider the state of the qubits after Step 2, which can be calculated as

$$|\phi_2\rangle = U_H^{\otimes n+1}|0\rangle^{\otimes n}|1\rangle = \frac{1}{\sqrt{N}} \sum_{x \in \{0,1\}^n} |x\rangle \otimes \frac{1}{\sqrt{2}}(|0\rangle - |1\rangle) \quad (3.5)$$

$$= \left(\frac{1}{\sqrt{N}}|w\rangle + \sqrt{\frac{N-1}{N}}|w_\perp\rangle \right) \otimes \frac{1}{\sqrt{2}}(|0\rangle - |1\rangle). \quad (3.6)$$

In the first line, the Hadamard operator created the uniform superposition state of all qubits. In the second line, the n qubit state is separated using the marked state $|w\rangle$ and $|w_\perp\rangle = \sum_{x \neq w} |x\rangle / \sqrt{N-1}$ which is the state spanning the subspace excluding the marked state. Now consider the state after the Step 3,

$$|\phi_3\rangle = U_f|\phi_2\rangle = \left(\frac{1}{\sqrt{N}}|w\rangle + \sqrt{\frac{N-1}{N}}|w_\perp\rangle \right) \otimes \frac{1}{\sqrt{2}}(|0 \oplus f(x)\rangle - |1 \oplus f(x)\rangle) \quad (3.7)$$

$$= \frac{1}{\sqrt{N}}|w\rangle \otimes \frac{1}{\sqrt{2}}(|1\rangle - |0\rangle) + \sqrt{\frac{N-1}{N}}|w_\perp\rangle \otimes \frac{1}{\sqrt{2}}(|0\rangle - |1\rangle) \quad (3.8)$$

$$= \left(-\frac{1}{\sqrt{N}}|w\rangle + \sqrt{\frac{N-1}{N}}|w_\perp\rangle \right) \otimes \frac{1}{\sqrt{2}}(|0\rangle - |1\rangle). \quad (3.9)$$

In the first line, we can see that the operator U_f is only acting on the ancilla qubit. Since $f(x)$ takes the value 1 only if the attached n -qubit state is $|w\rangle$, and takes the value 0 otherwise, the ancilla qubit is flipped only when $x = w$ (second line). From the third line, notice that finally the action of operator U_f is to flip the phase factor in front of the marked state. If we view the search space consisting of n spins as a two dimensional space spanned by the states $|w\rangle$ and $|w_\perp\rangle$, the transformation by U_f can be illustrated as in panel (b) of Figure 3.2. Next we consider the state after Step 4. Noting that the Grover's diffusion operator can be written as $D_f = -\mathbb{I} + 2|\phi_2\rangle\langle\phi_2|$, we get

$$|\phi_4\rangle = D_f|\phi_3\rangle = (-\mathbb{I} + 2|\phi_2\rangle\langle\phi_2|)|\phi_3\rangle \otimes \frac{1}{\sqrt{2}}(|0\rangle - |1\rangle) \quad (3.10)$$

$$= -|\phi_3\rangle + 2\langle\phi_2|\phi_3\rangle|\phi_2\rangle \otimes \frac{1}{\sqrt{2}}(|0\rangle - |1\rangle). \quad (3.11)$$

The transformation by D_f can be illustrated as in panel (c) of Figure 3.2. The vector

3.2. QUANTUM ALGORITHM TO SOLVE THE UNSTRUCTURED SEARCH PROBLEM

$|\phi_3\rangle$ is reflected against the vector $|\phi_2\rangle$. Now we see that the resulting vector $|\phi_4\rangle$ is closer to the marked state $|w\rangle$. The operator D_f can be also interpreted as an operator to mix amplitudes between all pair of computational basis states, which can be understood from the matrix representation in Eq. (3.4).

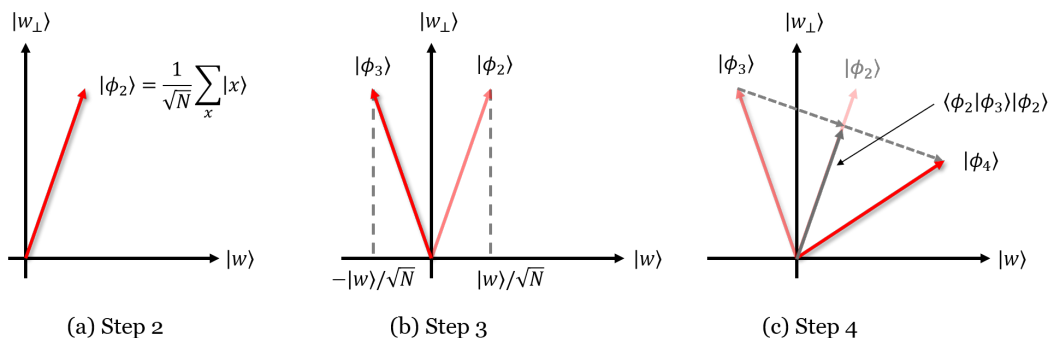


Figure 3.2: Each step of the Grover's algorithm (defined in main text) illustrated as a vector rotation in a two-dimensional space spanned by $|w\rangle$ and $|w_\perp\rangle$. $|w\rangle$ is the marked state and $|w_\perp\rangle = \sum_{x \neq w} |x\rangle / \sqrt{N-1}$ spans the rest of the space. The red vector $|\phi_k\rangle$ is the state of the n qubits after step k . (a) The uniform superposition state of $N = 2^n$ basis states. (b) After the oracle operator U_f is applied, the vector is reflected against the axis $|w_\perp\rangle$. (c) After the diffusion operator is applied, the vector is reflected against the vector $|\phi_2\rangle$ in the previous Step 2.

The sequential application of the operators U_f and D_f to the state is the single iteration of the Grover's algorithm. This iteration is repeated to gradually rotate the state towards the marked state $|w\rangle$. Defining the inner product $\langle \phi_2 | w^\perp \rangle \equiv \cos \theta = \sqrt{N-1}/N$, the angle between the states $|w^\perp\rangle$ and $|\phi_2\rangle$ is θ . After applying the operators U_f and D_f to the state $|\phi_2\rangle$, now the angle between the resulting state $|\phi_4\rangle$ and $|w^\perp\rangle$ is increased to 3θ . We can see that the angle is increased by 2θ at each iteration. Therefore, the state of the system after k iterations can be represented as

$$|\phi\rangle = \sin((2k+1)\theta)|w\rangle + \cos((2k+1)\theta)|w^\perp\rangle. \quad (3.12)$$

The key of the Grover's algorithm is to measure the state $|\phi\rangle$ in the computational basis when the probability $P_w = |\langle w | \phi \rangle|^2 = \sin^2((2k+1)\theta)$ is maximized (i.e. when the probability that the outcome of the measurement being w is maximized). This is achieved when $\sin^2(\pi/2) = 1$, which gives the optimal number of iterations $k = \pi/4\theta - 1/2$. One note is that k has to be an integer, and thus we write $k = \pi/4\theta - \delta$, where $0 \leq \delta < 1$.

3.2. QUANTUM ALGORITHM TO SOLVE THE UNSTRUCTURED SEARCH PROBLEM

Substituting this into $P_w = \sin^2((2k + 1)\theta)$, we get

$$P_w = \sin^2((\pi/2) + (-2\delta + 1)\theta) \quad (3.13)$$

$$= \cos^2((-2\delta + 1)\theta) \quad (3.14)$$

$$\geq \cos^2 \theta = (N - 1)/N = 1 - 1/N. \quad (3.15)$$

This proves the probability of the success of the Grover's algorithm, $P_w \geq 1 - 1/N$. If we consider $N \gg 1$ such that $\theta \approx \sin \theta = 1/\sqrt{N}$, the optimal number of iteration is $k = \lfloor (\pi/4)\sqrt{N} \rfloor$, as provided in the step 5 of the protocol.

An intuitive understanding of the Grover's algorithm is that, (i) the quantum state of the system is initialized as a uniform superposition state, (ii) the state is transformed to a state that is localized on the marked state $|w\rangle$ after using the black box unitary for $O(\sqrt{N})$ times, (iii) and the measurement conducted on such localized state identifies the number w with almost probability 1. See Figure 3.3 which illustrates such transformation of the state. Unlike the classical search, we can view that the integers x is processed in parallel as a quantum superposition state. However as we can only obtain one information (outcome) from the measurement of the state, the unitary transformation amplifies the probability of measuring the outcome we are aiming to get.

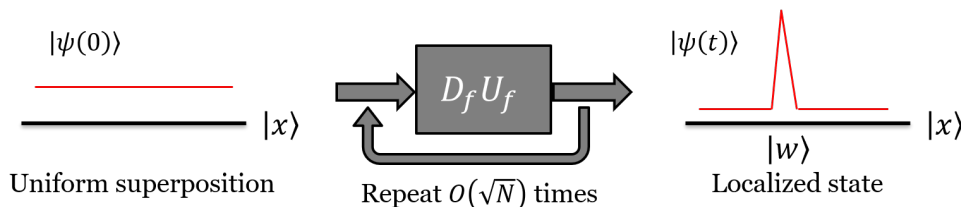


Figure 3.3: Illustration of the state transformation in the Grover's algorithm. Repetitively applying the black box unitary operator for $O(\sqrt{N})$ times on the uniformly superposed initial state, the state is transformed to a localized state on the marked state $|w\rangle$. By measuring the final state in the $\{|x\rangle\}$ basis, the solver can identify the index of the marked state with probability approximately equal to 1.

Importantly, the Grover's algorithm is not the only construction of the algorithm to solve the unstructured search problem. An alternative construction of the algorithm is known as the spatial search algorithm, which will be introduced in the following sections.

3.3 Introduction and literature review of the spatial search algorithms

Origin of the spatial search problem The spatial search problem is an alternative description of the unstructured search problem, which adds a restriction to the unstructured search (see Figure 3.4). The restriction added to the problem is the *spatial configuration of the database*, which gives constraint on how one can explore the search space. In the Grover’s algorithm, the unitary operator D_f applied on the states was just constructed mathematically as an operator to rotate the state towards the marked state. However, is this operator physically realizable when the database is embedded in some physical space? If one considers some motion in a physical space, the space has certain constraints in the degrees of freedom. This can be imprinted as the locality of the unitary operator, for example a situation where a particle is moving on a *spatial* space such as a d -dimensional grid. Here the particle is constrained to move locally between nearest-neighbouring sites at each step.

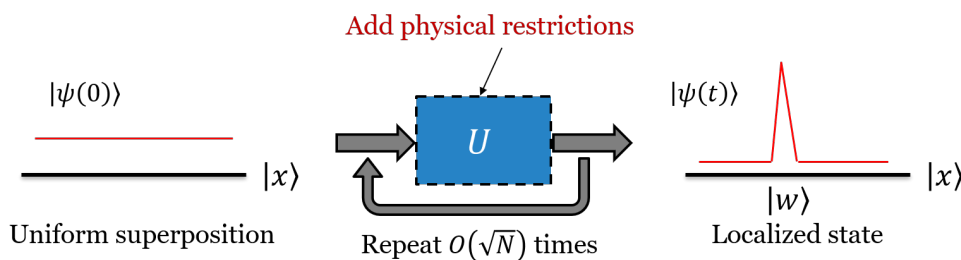


Figure 3.4: Spatial search is originally formalized as the variation of Grover’s algorithm where some physical restrictions are considered during the unitary transformation. An example of such restriction can be the locality of the unitary operation, or equivalently the spatial configuration of the data.

To give a concrete example, imagine a two-dimensional square lattice of size $\sqrt{N} \times \sqrt{N}$ and hence there are N lattice points in total. Assume each of these lattice points holds one piece of data. Formally, we label the lattice points with the basis states $\{|i\rangle\} = \{1, 2, \dots, N\}$. We again assume we have a black-box function $f(x) : \{1, 2, \dots, N\} \rightarrow \{0, 1\}$ satisfying Eq. (3.1), and consider the task to identify the integer w . Assume we place one particle on one of the lattice points. The particle has the freedom to move to the neighbouring lattice points (up, down, left, or right) at each time step, and allowed to call the black-box function which flips the phase of the coefficient on $|w\rangle$ [see Eq. (3.1)]. In this situation, the way the particle can explore the search space will be restricted by

3.3. INTRODUCTION AND LITERATURE REVIEW OF THE SPATIAL SEARCH ALGORITHMS

the lattice structure, as illustrated in Figure 3.5. In the unitary operator perspective, the Grover's diffusion operator D_f defined in Eq. (3.4) has to be replaced to another unitary operator allowing only local hopping. This is because D_f allows the particle to hop to every single site with equal weight in a single time step (which can be seen from the fact that all off-diagonal entries of Eq. (3.4) is non-zero). Given such spatial constraint, how would the time complexity change compared to the original Grover's algorithm?

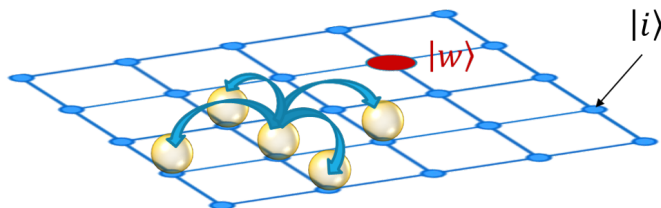


Figure 3.5: Benioff's problem illustrated as a situation to find a marked state $|w\rangle$ on the two-dimensional lattice using a quantum particle hopping locally between adjacent sites.

The first work that considered such search problem was by Benioff [34] in 2002. Benioff considered the situation where the database is embedded in the two-dimensional lattice, and considered a quantum particle (stated as quantum robot in the original paper) that is allowed to make local moves to the adjacent lattice site at each time step. The state of the quantum robot is represented by the linear combination of the N position basis state. Utilizing the nature of quantum mechanics, the initial state of the quantum robot is prepared as the uniform superposition state of all positions, $|s\rangle = \sum_{i=1}^N |i\rangle/\sqrt{N}$. This corresponds to the initial Hadamard operator applied to all of the qubits in the Grover's algorithm. The local move to the adjacent four sites is done by applying a unitary operator $D_{loc} = \sum_{x,y} |x+1\rangle\langle x| + |x-1\rangle\langle x| + |y+1\rangle\langle y| + |y-1\rangle\langle y|$. This corresponds to the diffusion operator D_f in the Grover's algorithm, although in this case the diffusion is limited to the adjacent four states. After the local move, the oracle operator is applied, which flips the phase of the position state $|w\rangle$ corresponding to the marked state. Now the question is the time complexity of this algorithm. How many time steps of the above iteration is required in order to measure the marked state with approximately probability 1?

Benioff stated that the time complexity of this algorithm is $O(N)$, which is no better than the classical brute-force search. This suggests that on a physical, locally distributed database, a quantum search algorithm cannot achieve the quantum speedup of $O(\sqrt{N})$, the optimal search time that was achieved by the Grover's algorithm. The intuitive reason

3.3. INTRODUCTION AND LITERATURE REVIEW OF THE SPATIAL SEARCH ALGORITHMS

for this is the slow diffusion of the complex amplitudes on the two-dimensional lattice. On a two-dimensional lattice, it would take $O(\sqrt{N})$ time steps for the quantum robot to diffuse over the lattice and interfere with each other to simulate the Grover's diffusion operator D_f (application of D_{loc} for $O(\sqrt{N})$ times, while the Oracle operator is also applied between each D_{loc}). This comes from the fact that the size of the square lattice consists of N lattice points is $\sqrt{N} \times \sqrt{N}$, and the robot is restricted only to move to the adjacent box at each step. As we need $O(\sqrt{N})$ iterations of the above process to amplify the complex amplitude of the marked state, the total time complexity is $[O(\sqrt{N}) \text{ oracle operations}] \times [O(\sqrt{N}) \text{ time steps for the diffusion}]$ which results to $O(N)$.

At a glance, the above explanation is reasonable. The reason for the slowdown against Grover's algorithm is due to the locality of the unitary operator. This also clarifies that the Grover's algorithm is not considering any physical setting of the database, and the algorithm is considered on a search space with no restriction. The Grover's algorithm is assuming a global operation where the particle can explore the whole Hilbert space in one step. Such operation is physically unrealistic as N grows larger, the Benioff's problem raised this fact.

Further investigation on Benioff's problem After the seminal work by Benioff, different authors have investigated the problem of quantum search on the locally constraint search space (namely the spatial search). Remarkably, Benioff's result was re-considered and improved by Aaronson and Ambainis [35] in 2003. They proposed a clever quantum query algorithm to solve spatial search on an arbitrary undirected graph, not limiting to the two-dimensional lattice. Moreover, they mathematically formalized the physics of the database in terms of local unitary operators. The main results derived from the proposed algorithm was that they could find a marked node with optimal time $O(\sqrt{N})$ for a cubic lattice of dimension three or higher, and $O(\sqrt{N} \log^{5/2} N)$ for a two-dimensional square lattice. This showed that with some effort a search faster than the classical algorithm can be still achieved on a local database. Their essential idea was to divide the lattice into sub-squares. For instance, consider dividing the two-dimensional lattice into \sqrt{N} sub-squares. The quantum robot placed at the edge of the lattice can travel to any sub-square within time steps of $2\sqrt{N}$ steps. Within the sub-region the robot classically searches for the marked node locally which takes $O(\sqrt{N})$ steps. If the marked node exists in the searched sub-square, the phase of the state of the robot is flipped. Subsequently, the robot travels back to its initial position within $2\sqrt{N}$ steps. At this point, a total of

3.3. INTRODUCTION AND LITERATURE REVIEW OF THE SPATIAL SEARCH ALGORITHMS

$5\sqrt{N}$ time steps at most are consumed. Now, if we assume such local searching process using a uniform super position state of the robot and apply the Grover's algorithm, the total complexity is $O(N^{1/4}) \times 5\sqrt{N} = O(N^{3/4})$. The first term $O(N^{1/4})$ comes from the square root of $O(\sqrt{N})$, the time complexity of the Grover's algorithm on \sqrt{N} sub-squares. For the two-dimensional square lattice, Aaronson and Ambainis found a lower bound of the time complexity to be $O(\sqrt{N} \log^{5/2} N)$ by dividing the lattice into $N^{1/3}$ sub-squares.

After this, in 2005, Ambainis, Kempe and Rivosh [36] gave an algorithm based on discrete-time quantum walk on d -dimensional lattices (known as AKR algorithm) which achieves optimal search $O(\sqrt{N})$ when $d \geq 3$ and $O(\sqrt{N} \log N)$ for $d = 2$. This generalized the previous algorithm by Aaronson and Ambainis using the framework of discrete-time quantum walk. In 2004, Childs and Goldstone [26] proposed an analogous continuous-time quantum walk algorithm to solve the spatial search. The difference of Childs and Goldstone's algorithm from the previous work (including the Grover's algorithm) was that their unitary operation is the continuous time-evolution operator generated by an Hamiltonian, instead of a consecutive application of unitary operators. Their algorithm achieved to search with optimal time $O(\sqrt{N})$ for $d \geq 5$, and $O(\sqrt{N} \log^{3/2} N)$ for $d = 4$, but no faster than classical for $d \leq 3$. The continuous-time quantum walk framework given by Childs and Goldstone was simple that this paper led to a various study that investigate the time complexity of the search on different types of graphs. Essentially, the search by continuous-time quantum walk can be analyzed on any graph if the adjacency matrix of the graph is given. The hardness of the analysis of the search time complexity comes down to the hardness of analyzing the eigenstate and eigenvalue structure of the graph, which has strong connection to spectral graph theory.

List of works on the spatial search algorithm and the general goal of the analysis Let us list up some results from the various work dealing with the spatial search algorithms using quantum walks, and summarize the general goal of this field.

The main topic of the seminal papers by Ambainis, Kempe and Rivosh [36] or Childs and Goldstone [26] were to analyze the search complexity for d -dimensional lattices. Building up on these work, searching quickly on periodic lattices is one of the big topics in the field. Their essential results are listed in Table 3.1. Essentially, using discrete-time quantum walk, optimal search is achieved when $d > 2$ ($O(\sqrt{N} \log N)$), and using continuous-time quantum walk, optimal search is achieved when $d > 4$ ($O(\sqrt{N} \log^{3/2} N)$). $d = 2$ and $d = 4$ seem to be the critical dimensions where the discrete or continuous-time algorithms

3.3. INTRODUCTION AND LITERATURE REVIEW OF THE SPATIAL SEARCH ALGORITHMS

can perform optimally or not. Whether one can construct an algorithm to speed up the search at these critical dimensions to $O(\sqrt{N})$ is an open question.

Table 3.1: List of the time complexities of the spatial search algorithms on d -dimensional lattices using quantum walk.

d	Discrete-time [36]	Continuous-time [26]
≥ 5	$O(\sqrt{N})$	$O(\sqrt{N})$
4	$O(\sqrt{N})$	$O(\sqrt{N} \log^{3/2} N)$
3	$O(\sqrt{N})$	$O(N)$
2	$O(\sqrt{N} \log N)$	$O(N^2 / \log^3 N)$

The the best speedup achieved on the $d = 2$ lattice so far is a algorithm proposed by Tulsi [37], achieving the complexity of $O(\sqrt{N \log N})$. In Tulsi's method, an ancilla qubit is attached to the Hilbert space of the database, which boosts the success probability (probability to measure the marked state after the unitary operations) up to a constant. The complexity $O(\sqrt{N} \log N)$ given by AKR algorithm is actually composed of two elements; $O(\sqrt{N \log N})$ time steps to localize the state on the marked state, and the probability to measure the marked state, that is $O(1/\sqrt{\log N})$. The total time complexity is derived by multiplying the time steps with the inverse of the success probability, that gives $O(\sqrt{N} \log N)$. Such multiplication is necessary, since to obtain the correct result one needs to repeat the algorithm at least $1/P$ times when the probability of success is P . As Tulsi's method boosts the success probability to $O(1)$, the total time complexity improves.

Observing from Table 3.1, the critical dimension to achieve optimal search for the continuous-time algorithm is $d > 4$, which is higher than the discrete-time case. The reason of such difference comes from the dispersion relation of the Hamiltonian or the unitary operator representing the d -dimensional lattice. The Hamiltonian used in Childs and Goldstone algorithm is based on the tight-binding Hamiltonian of a single electron bounded on a d -dimensional periodic lattice crystal (this will be formally introduced in Section 3.5.1). One can show that since the dispersion relation $\omega(k)$ of a cubic lattice is quadratic, the energy separation between the ground and first excited state is $E(k) - E_0 \sim |k|^2 \sim N^{-2/d}$. The optimality of the spatial search can be roughly predicted by comparing this with the energy separation of the perturbed Hamiltonian, $\Delta E = N^{-1/2}$. The critical

3.3. INTRODUCTION AND LITERATURE REVIEW OF THE SPATIAL SEARCH ALGORITHMS

dimension is $d > 4$ since the ratio $\Delta E/N^{-2/d}$ goes to 0 as $N \rightarrow \infty$. This shows that the larger energy separation between the ground and first excited state of the tight-binding Hamiltonian is an important factor that determines optimal search.

Such critical dimension reduces to $d > 2$ when the lattice has a linear dispersion relation, since $E(k) - E_0 \sim N^{-1/d}$. The unitary operator used in the discrete-time algorithm shows this linear dispersion relation due to the internal degree of freedom of the quantum walker [36]. Childs and Goldstone has soon utilized this fact in their later work [38], by using the Dirac Hamiltonian for the continuous-time search algorithm, which possesses a linear dispersion relation due to the internal spin degree of freedom. Their method allowed to search optimally for $d \geq 3$ and $O(\sqrt{N} \log N)$ for $d = 2$. This direction led to the work by Foulger, Gnutzmann and Tanner [39], who considered a continuous-time algorithm on a hexagonal (graphene) lattice instead of a cubic lattice. A hexagonal lattice ($d = 2$) naturally possesses a linear dispersion relation near the K point, thus allowed to search with complexity $O(\sqrt{N} \log^{3/2} N)$ without requiring the internal degree of freedom of the quantum walker. Afterwards, Childs and Ge [40] generalized the search on hexagonal lattice by discussing how to configure the lattice topology to give a linear dispersion relation on the lattice. However, despite all the challenges, no algorithm have been found that searches optimally on $d = 2$ dimensional lattices. Additionally, there is no proof to say searching optimally on a two-dimensional lattices is impossible. This is still an interesting open question in this field.

Another direction in the field of spatial search is to explore what kind of graphs other than lattices can achieve optimal search. For example, Childs and Goldstone [26] proved that optimal search by continuous-time quantum walk is possible on the complete graph and the hypercube⁴. Janmark, Meyer and Wong [41] analyzed the search on strongly regular graphs, and derived that the search is optimal for known classes of strongly regular graphs. Their result indicated that unlike complete graph or hypercube, a global symmetry of the graph is not a necessary condition for optimal search. Novo *et al.* [42] developed a systematic method to reduce the dimension of the graph's adjacency matrix, which helps when analyzing the spatial search or more generally, continuous-time quantum walk on graphs. They applied their method on star graphs, complete bipartite graphs, and complete graph with broken links, where all graphs achieved optimal search. Meyer and Wong [43] analyzed the search on a joint complete graph (two complete graphs

⁴A hypercube of $2^n = N$ nodes is a regular graph whose degrees are n . The edges are connected between nodes whose hamming distance is 1.

3.3. INTRODUCTION AND LITERATURE REVIEW OF THE SPATIAL SEARCH ALGORITHMS

joint by a single edge) and a simplex of complete graphs (a simplex with each vertex replaced by a complete graph). The former graph possessed optimal search while the latter did not. This result gave a counter example to the intuition that high connectivity of the graph is one indicator for optimal search; there are examples where graphs with low connectivity may possess optimal search. Chakraborty *et al.* [44] analyzed the search on Erdős-Rényi random graphs. This is a probabilistic graph model where an edges between every pair of nodes exists with a constant probability p independent of all other edges. Chakraborty *et al.* proved a powerful lemma indicating that a certain large gap in the eigenvalues of the graph (which means the need of certain large connectivity) is a sufficient condition for optimal search. Their analysis clearly proved that a very high connectivity like a complete graph is unnecessary, and we can cut links from the complete graph up to a threshold value while keeping the fast speed of the search.

Given a lot of instances of graphs that possess optimal search, the ultimate goal for spatial search on arbitrary graphs is to find out and formulate the necessary and sufficient condition of the graph for optimal search. In other words, we want to formulate the success criteria of spatial search. We want a criteria such that when we give a particular instance of graph, the criteria determines whether it possesses optimal search or not with some systematic analysis. However, finding this criteria still seems to be a challenging path.

Moving toward spatial search on heterogeneous graphs Still few, but some work moved toward exploring inhomogeneous or non-regular graphs where to analyze the spatial search algorithm. Such graphs are different from lattices or highly symmetric graphs mentioned above due to the unequivalence of the nodes. Therefore, the dynamics of the quantum walker can be complex and different depending on which node in the graph is marked. Agliari *et al.* [45] explored spatial search on fractal structures such as the Sierpinski gasket and the Cayley tree. They studied how the transition in the eigenstates of the Hamiltonian depends on the marked node. Berry and Wang [46] studied spatial search using the discrete-time algorithm on the Cayley tree, and examined the relation between centrality measures of the graph and the time complexity of the spatial search. Philipp *et al.* [47] examined the continuous-time algorithm on balanced trees, and derived that the search performance changes depending whether the marked node is towards the root or the leaves of the graph. Glos *et al.* [48] examined how the inhomogeneity of a random graph causes variation to the optimal measurement time of the search algorithm.

This thesis is especially focusing the interest on this direction; how the spatial search

3.4. WHAT THIS THESIS TACKLES IN THE FIELD OF SPATIAL SEARCH

algorithm behaves on a complex and non-regular structure.

3.4 What this thesis tackles in the field of spatial search

Based on the review of the field in the previous section, here we explain the motivation and aim of this thesis' analysis. Our aim and its analysis on the spatial search problem is composed of two individual parts.

Part 1: Spatial search on the long-range percolation graph

In this part, we approach to the spatial search problem from the perspective of connectivity of the graph, and examine explicitly how the time complexity of the search changes depending on the connectivity. We consider the spatial search algorithm using continuous-time quantum walk (CG algorithm) on a graph known as the long-range percolation (LRP) model.

The LRP model [49–51] is a probabilistic graph generation model where we initially have periodic lattice points (say a two-dimensional square lattice), and generate edges between lattice points i and j with probability $p_{ij} = |i - j|^{-\alpha}$. Here, $|i - j|$ is the Euclidean distance between the lattice points and $\alpha \geq 0$ is a constant taking real value. As the probability p_{ij} is defined as a decaying function of the Euclidean distance between the lattice points, the non-nearest neighbour will be more likely to be added between spatially close lattice points (see Figure 3.10).

Our motivation of analyzing spatial search on the LRP model is to first discuss the effect of connectivity of the graph on the spatial search algorithm. This was also discussed in the work by Chakraborty *et al.* [44] using the Erdős-Rényi random graph, but the LRP model considers more of a physically realistic situation as the probability to generate long-range edges decays with the distance of the nodes. Distance-decaying functions naturally arise in the nature such as the coulomb interaction. On the other hand, the Erdős-Rényi random graph generates edges between nodes with a constant probability. We analyze the search by gradually changing the connectivity of the graph from a periodic lattice (a

3.4. WHAT THIS THESIS TACKLES IN THE FIELD OF SPATIAL SEARCH

local structure) to a fully connected graph (non-local structure).

We will show that there exists a threshold connectivity where the time complexity of the search switches from optimal $O(\sqrt{N})$ to non-optimal. This threshold will be represented by a critical value of the exponent $\alpha = \alpha_c$. We will also examine some graph properties of the LRP model such as average degree, diameter and clustering coefficient, which we will discuss some relation between these properties and the time complexity of the search. From the analytical calculation of the average degree, we will show that the LRP model has a improved connectivity threshold over the Erdős-Rényi random graph.

Part 2: Spatial search on the Bollobás scale-free network

In the second part we explore how the time complexity of the spatial search algorithm behaves in a real-world complex network structure. Although the spatial search on various graphs have been investigated in the literature, spatial search on complex networks or real world networks have been almost never unexplored, to the best of our knowledge. Complex networks are important class of graphs as they represent the common structures that appears in the social and natural system. We go beyond lattice or regular structures, and analyze the spatial search algorithm on a scale-free network, which is one of the most important class of complex networks.

We select a probabilistic network generation model known as the Bollobás model [52, 53] where to analyze the spatial search algorithm. This model essentially simulates the preferential attachment rule to generate a network with power-law degree distribution

$$P(k) \propto k^{-\beta}. \tag{3.16}$$

Here, k is the degree of a node while $\beta > 2$ is a real constant value. This degree distribution represents that most nodes in the network have small degree, while some few nodes has very large degree (corresponding to the tail of the power-law distribution). We call the node having the largest degree as the *hub* node.

We will first show that the speed of the spatial search will greatly depend on the properties of the marked node. These properties can be for example the degree, shortest path distance from the hub, or some centrality measures. This is a critically different result compared to periodic lattices, since all nodes are equivalent due the translational symmetry, and they all share the common property. We analyze the distribution of the

3.5. PRELIMINARIES OF THE SPATIAL SEARCH ALGORITHM

search time which is well fit to a multimode log-normal distribution.

To characterize the relation between the network structure and the performance of the search, we examine the correlation between some centrality measures of the network and the time complexity of the spatial search. We find a strong correlation to the eigenvector centrality and closeness centrality. We also show how our results are different from the classical random walk process to search for a marked node, which has high correlation to the degree centrality. These observations cannot be seen from purely random graphs [44], and this is another critical difference from the previous studies. We also point out one advantage of using a scale-free network for the spatial search, which is that one can perform the search starting from a localized initial state instead of a global superposition state conventionally used in the spatial search and Grover's algorithm. Taking advantage of this fact, one can naturally translate the spatial search to a efficient state transfer protocol between the hub node and another arbitrary node.

These results indicate that the hub node in the scale-free network plays a crucial role on the quantum dynamics, and the distance measures of the network is one important factor that determines the time complexity of the spatial search algorithm.

3.5 Preliminaries of the spatial search algorithm

3.5.1 Definitions of the spatial search algorithm by continuous-time quantum walk

Here we start by formally defining the spatial search algorithm we are going to examine. The comparison with the Grover's algorithm explained in Section 3.2 is summarized in Figure 3.6. The essential difference between the Grover's algorithm and the spatial search algorithm we analyze here is that the latter uses a continuous-time evolution during the algorithm, as well as having more freedom in defining the diffusion operator corresponding to D_f defined in Section 3.2, Eq. (3.4).

Define $G(V, E)$ as a graph with a set of nodes $V = \{1, 2, \dots, i, \dots, N\}$ and a set of edges E . We consider an N -dimensional Hilbert space spanned by the basis states $\{|1\rangle, |2\rangle, \dots, |i\rangle, \dots, |N\rangle\}$, and assign each states to the N nodes of the graph $G(V, E)$. We will call these states as node basis states. We view that each state corresponds to the situation where a quantum walker or a single excitation is localized at node i . Quantum

3.5. PRELIMINARIES OF THE SPATIAL SEARCH ALGORITHM

walk is a coherent quantum dynamics where quantum particle(s) hop between the nodes of graph. We define the state of the quantum walker at time t using the node basis states as

$$|\psi(t)\rangle = \sum_{i=1}^N c_i(t)|i\rangle \quad (3.17)$$

with the complex amplitudes $c_i(t)$ constrained such that $\sum_{i=1}^N |c_i(t)|^2 = 1$.

	Grover's algorithm	Spatial search algorithm
Goal of the algorithm	Identify the marked state $ w\rangle$ among N states	Identify the marked state $ w\rangle$ among N states
Definition of the state	$ \psi(t)\rangle = \sum_{x \in \{0,1\}^n} c_i(t) x\rangle b\rangle$ <ul style="list-style-type: none"> • $\{ x\rangle\} = \{ a_1 a_2 \dots a_n\rangle\}_{a_1, \dots, a_n=0,1}$ $= \{ 0 \dots 00\rangle, 0 \dots 01\rangle, \dots, 1 \dots 11\rangle\}$ \Rightarrow n-qubit ($N = 2^n$ dimension) • $b\rangle, b = 0,1 \Rightarrow$ 1-qubit ancilla 	$ \psi(t)\rangle = \sum_{i=1}^N c_i(t) i\rangle$ $\{ i\rangle\} = \{ 1\rangle, 2\rangle, \dots, N\rangle\}$ \Rightarrow N orthogonal basis states (not necessarily qubits)
Initial state before iteration	$ \psi(0)\rangle = \frac{1}{\sqrt{2N}} \sum_{x \in \{0,1\}^n} x\rangle(0\rangle - 1\rangle)$	$ \psi(0)\rangle = \frac{1}{\sqrt{N}} \sum_{i=1}^N i\rangle$
Black box unitary	$U = (D_f U_f)^t$ Discrete time operations D_f : Diffusion operator \longleftrightarrow A : Adjacency matrix (diffusion term) U_f : Oracle operator \longleftrightarrow $ w\rangle\langle w $: Oracle term (Definition in Section 3.2) correspondence (Definition in Section 3.5.1)	$U(t; 0) = \exp(-iH_s t/\hbar)$, Continuous time evolution where $H_s = -\gamma A - \epsilon_w w\rangle\langle w $
Probability to measure the marked state	$P = \left \langle w (D_f U_f)^t \psi(0) \rangle \right ^2 = 1 - 1/N$	$P = \langle w \exp(-iH_s t/\hbar) \psi(0) \rangle ^2 = \text{depends on } A$
Search time	Always $O(\sqrt{N})$ since the definition of D_f is fixed.	Depends on the structure of A. Fastest case is $O(\sqrt{N})$ when A corresponds to the complete graph, $A = N \psi(0) \rangle \langle \psi(0) - \mathbb{I}$.

Figure 3.6: Correspondence between the Grover's algorithm and the spatial search algorithm.

In order to search for a single marked node which we label as $|w\rangle$, we define a search Hamiltonian that gives constraint to the system and generates the time evolution of the quantum walker. Following Childs and Goldstone's [26] definition, the search Hamiltonian

3.5. PRELIMINARIES OF THE SPATIAL SEARCH ALGORITHM

is defined as

$$H_s = -\gamma A - \epsilon_w |w\rangle\langle w| \quad (3.18)$$

$$= -\gamma \sum_{i,j}^N A_{ij} (|i\rangle\langle j| + |j\rangle\langle i|) - \epsilon_w |w\rangle\langle w|. \quad (3.19)$$

Here, A is the adjacency matrix of graph $G(V, E)$ whose entries are defined as $A_{ij} = A_{ji} = 1$ if nodes i and j are connected by an edge $e_{ij} \in E$, and $A_{ij} = 0$ if no edge exists between i and j . The real value constant $\gamma \geq 0$ globally controls the transition energy between the node basis states. $\epsilon_w > 0$ is the on site energy on node w . With some appropriate balance of the parameters γ and ϵ_w (we fix $\epsilon_w = 1$ in most cases), the adjacency matrix term causes the complex amplitudes of the quantum walker to diffuse over the graph, while the projection $|w\rangle\langle w|$ term causes the amplitude to accumulate and localize on the marked node w . This term corresponds to the Oracle part of the search algorithm.

In some cases, the adjacency matrix term can be instead replaced by the Laplacian matrix L of the graph. Here, L is defined as $L = A - D$, where $D = \sum_{i=1}^N k_i |i\rangle\langle i|$ is a diagonal matrix with its diagonal entries D_{ii} corresponding to the degree of node i , $k_i = \sum_{j=1}^N A_{ij}$. For the dynamics of the quantum walk, the diagonal terms acts as the on-site energy of the tight-binding Hamiltonian. If the graph is regular (i.e. all nodes have equal degree $k_i = k$), these diagonal terms only affects the global phase of the state since $D = k\mathbb{1}$. If the graph is non-regular, these on-site energies can affect the dynamics non-trivially.

Now we consider the unitary time evolution of the system which is given by the Schrödinger equation,

$$i\hbar \frac{d}{dt} |\psi(t)\rangle = H_s |\psi(t)\rangle. \quad (3.20)$$

Assume that we make a measurement in the node basis at a time t , the probability of getting the outcome $|w\rangle$ (in other words the probability to measure the quantum walker on node w) is $P(t) = |\langle w | \exp(-iHt/\hbar) |\psi(0)\rangle|^2$. The goal of the spatial search algorithm is to maximize $P(t)$ (make $P(t)$ as close as possible to 1) with shortest t possible. Such manipulation of the measurement probability can be achieved by properly adjusting the the parameters γ and ϵ , and this will be further explained in the following sections.

The time complexity of the spatial search algorithm or the “search time” T , in units of ϵ_w , is evaluated by finding the shortest time $t = \tau$ that maximizes $P(t)$. As one can find

3.5. PRELIMINARIES OF THE SPATIAL SEARCH ALGORITHM

the quantum walker on node w with probability $P(\tau)$ at the optimal measurement time τ , the algorithm can identify the marked node with success probability $P(\tau)$. This concept of *success probability* is very fundamental for quantum algorithms and has to be always taken into account since measurements in quantum systems are always probabilistic. The simple way to take the success probability into account of the time complexity of the search algorithm, is to consider the repetition of algorithm for $1/P(\tau)$ times. For example if $P(\tau) = 1/3$, we need to repeat the algorithm from the beginning for 3 times (or more) to confirm that the outcome is the correct marked state $|w\rangle$. Therefore, the time complexity of the search T is finally determined as $T = \tau/P(\tau)$.

3.5.2 Spatial search on the complete graph: analytical approach

As we defined the spatial search algorithm by continuous-time quantum walk in the previous section, in this section we will explain the basic mechanism of how the algorithm actually works. We will explain that with a proper choice of parameters γ and ϵ_w (defined in Eq. (3.19) in the previous section), one can manipulate the quantum walker to localize on the marked node with high probability $P(\tau)$. We will assume that the graph where the spatial search is considered is a complete graph (fully connected graph), in order to make some analogy with the Grover's algorithm, and to also make the calculation simple. This explanation of the search on the complete graph is based the original paper by Child and Goldstone [26].

Assume that graph $G(V, E)$ is a complete graph (see left panel of Figure 3.7), where the adjacency matrix A_{comp} is

$$A_{comp} = \begin{pmatrix} 0 & 1 & \dots & 1 \\ 1 & 0 & \dots & \vdots \\ \vdots & \dots & \ddots & 1 \\ 1 & \dots & 1 & 0 \end{pmatrix}. \quad (3.21)$$

The matrix entries are all ones except the diagonals are all zeros. Let us define a state $|s\rangle = \sum_{i=1}^N |i\rangle/\sqrt{N}$, which is a uniform superposition of all node basis states. Using $|s\rangle$, A_{comp} can be written as

$$A_{comp} = N|s\rangle\langle s| - \mathbb{I}. \quad (3.22)$$

Observe that A_{comp} has a similar form as the Grover's diffusion operator D_f in Eq. (3.4).

3.5. PRELIMINARIES OF THE SPATIAL SEARCH ALGORITHM

Now we plug A_{comp} into the search Hamiltonian Eq. (3.19), which gives

$$H_s = -\gamma N |s\rangle\langle s| + \gamma \mathbb{I} - \epsilon_w |w\rangle\langle w|. \quad (3.23)$$

The term including the identity will only change the global phase under the time evolution, so we can remove that term (in other words, we re-scale the energy by subtracting $\gamma \mathbb{I}$). If we choose $\gamma = 1/N$ and $\epsilon_w = 1$, Eq. (3.23) will become

$$H_s = -|s\rangle\langle s| - |w\rangle\langle w|. \quad (3.24)$$

Note that the states $|s\rangle$ and $|w\rangle$ has an overlap of $|\langle s|w\rangle| = 1/\sqrt{N}$. If we instead rewrite this Hamiltonian in the mutually orthogonal basis $|r\rangle = \sum_{i \neq w}^N |i\rangle / (\sqrt{N-1})$ and $|w\rangle$, the Hamiltonian becomes

$$H_s = -\left(\frac{1}{N} + 1\right) |r\rangle\langle r| - \frac{\sqrt{N-1}}{N} |r\rangle\langle w| - \frac{\sqrt{N-1}}{N} |w\rangle\langle r| - \left(1 - \frac{1}{N}\right) |w\rangle\langle w|. \quad (3.25)$$

Assuming $N \gg 1$, the above Hamiltonian can be simplified as

$$H_s = -\begin{pmatrix} 1 & \frac{1}{\sqrt{N}} \\ \frac{1}{\sqrt{N}} & 1 \end{pmatrix}, \quad (3.26)$$

written in a 2×2 matrix form. This means that we have reduced the complete graph of N nodes into simplified graph of 2 nodes (see right panel of Figure 3.7). Such reduction is possible since the dynamics inside the $N - 1$ nodes excluding w is equivalent. As the complex amplitudes travel between the node w and the rest with the equal rate γ , we can still capture the time evolution of the system from the reduced graph.

From the matrix Eq. (3.26), now we can see that the two energy levels corresponding to the eigenstates of $|r\rangle\langle r| + |w\rangle\langle w|$ are degenerated (up to $1/N$), and a perturbation is applied which splits the eigenstates. The time evolution under this situation drives the oscillation between the two levels $|r\rangle$ and $|w\rangle$. Diagonalizing H_s we can obtain the new eigenstates,

$$|E_0\rangle = (|w\rangle + |r\rangle)/\sqrt{2}, \quad (3.27)$$

$$|E_1\rangle = (|w\rangle - |r\rangle)/\sqrt{2}, \quad (3.28)$$

3.5. PRELIMINARIES OF THE SPATIAL SEARCH ALGORITHM

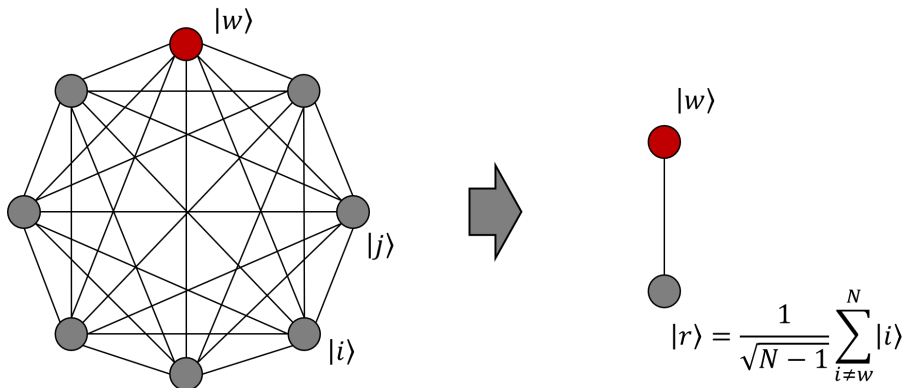


Figure 3.7: Complete graph of 8 nodes (left) and its reduction to a graph of two nodes (right). As the dynamics on the nodes except the marked node $|w\rangle$ is equivalent, one can reduce the nodes into a single node $|r\rangle$.

up to terms of order $1/N$. We defined the energy eigenstates and eigenvalues of H_s as $H_s|E_{0,1}\rangle = E_{0,1}|E_{0,1}\rangle$. We define and compute the energy gap between the two energies as $\Delta E \equiv E_1 - E_0 = 2/\sqrt{N}$. When $N \gg 1$, we can assume that uniform superposition state $|s\rangle$ is close enough to $|r\rangle$ as the overlap is $|\langle s|w\rangle| = \sqrt{1 - 1/N}$. Therefore, if we prepare the initial state as $|s\rangle$ and let the system evolve under the action of the Hamiltonian H_s , the state will approximately rotate to $|w\rangle$ after time $t = \pi/\Delta E = \pi\sqrt{N}/2$. It is important that we are preparing the initial state $|s\rangle$ instead of $|r\rangle$, since the person who executes the search algorithm does not know the marked state $|w\rangle$ in advance (i.e. it is impossible to prepare $|r\rangle$ without knowing the answer of the search in advance).

Now we derived that the system constraint by the Hamiltonian H_s rotates between the states $|s\rangle$ and $|w\rangle$ if we prepare the initial state at $|s\rangle$. The probability to measure the marked state $P(t) = |\langle w|\exp(-iHt/\hbar)|\psi(0)\rangle|^2$ oscillates between $1/N$ and $1 - 1/N$ with period $\pi\sqrt{N}$. If we measure the quantum walker at time $\tau = \pi\sqrt{N}/2$, the state $|w\rangle$ will be measured with probability $1 - 1/N \sim 1$, hence the time complexity of the search is $\pi\sqrt{N}/2$ which is the optimal order $O(\sqrt{N})$.

3.5.3 Spatial search on a general graph

In the previous section, we have considered how the dynamics of the spatial search algorithm is determined by analyzing the eigenvectors of the search Hamiltonian H_s . The key feature of the Hamiltonian lies in the equation

$$H_s = -\gamma N|s\rangle\langle s| - |w\rangle\langle w|. \quad (3.29)$$

3.5. PRELIMINARIES OF THE SPATIAL SEARCH ALGORITHM

Here we set $\epsilon_w = 1$ and omitted $\gamma\mathbb{I}$ from Eq. (3.23). We can learn from this Hamiltonian that state $|s\rangle$ is the ground state of the diffusion part of the Hamiltonian $-A_{comp}$ (in other words, the ground state of H_s is close to $|s\rangle$ when $\gamma N \gg 1$). On the other hand, state $|w\rangle$ is the ground state of Oracle term $|w\rangle\langle w|$ (the ground state of H_s is close to $|w\rangle$ when $\gamma N \ll 1$). All other eigenstates (excited states) are degenerated for both A_{comp} and $|w\rangle\langle w|$. Due to this isolated ground states of A_{comp} and $|w\rangle\langle w|$, when γ is set to $\gamma N = 1$ which equally mixes the two ground states, an isolated two-dimensional subspace is created in the form of Eqs. (3.27) and (3.28). In other words, an avoided crossing between the two lowest energy eigenstates, with a energy gap of $\delta E = 2\sqrt{N}$, were formed. Now, if we assume a general graph besides the complete graph in H_s , would the same situation hold? The answer to this question lies in the spectral property of the graph, especially how well separated the ground state and the excited states are.

Let's consider an adjacency matrix of a connected, undirected graph A_g . This matrix can be decomposed by their eigenvectors and eigenvalues, as $A_g = \sum_{l=1}^N \lambda_l |\lambda_l\rangle\langle \lambda_l|$. The eigenvalues are ordered such that $\lambda_1 > \lambda_2 \geq \lambda_3 \geq \dots \geq \lambda_N$. The search Hamiltonian can be written as

$$H_s = -\gamma \lambda_1 |\lambda_1\rangle\langle \lambda_1| - \gamma \sum_{l=2}^N \lambda_l |\lambda_l\rangle\langle \lambda_l| - |w\rangle\langle w|. \quad (3.30)$$

Here we again set $\epsilon_w = 1$, and separated the $l = 1$ term (the leading eigenvector term) and the rest ($l \geq 2$). When we set $\gamma = 1/\lambda_1$,

$$H_s = -|\lambda_1\rangle\langle \lambda_1| - \sum_{l=2}^N \frac{\lambda_l}{\lambda_1} |\lambda_l\rangle\langle \lambda_l| - |w\rangle\langle w| \quad (3.31)$$

$$\equiv -|\lambda_1\rangle\langle \lambda_1| - |\tilde{w}\rangle\langle \tilde{w}|. \quad (3.32)$$

Here we defined the last term as

$$|\tilde{w}\rangle\langle \tilde{w}| \equiv \sum_{l=2}^N \frac{\lambda_l}{\lambda_1} |\lambda_l\rangle\langle \lambda_l| + |w\rangle\langle w|. \quad (3.33)$$

We have written the Hamiltonian in the similar fashion as Eq. (3.24), although the latter term got a correction due to the higher energy levels. From Eq. (3.32), we can see that if we start the dynamics from the initial state $|\lambda_1\rangle$, the state will rotate to $|\tilde{w}\rangle$ with time $t = |\langle \lambda_1 | w \rangle|$, since $|\langle \lambda_l | \lambda_m \rangle| = \delta_{lm}$.

3.5. PRELIMINARIES OF THE SPATIAL SEARCH ALGORITHM

Recalling the case of the complete graph, the eigenvalues of A_{comp} is $\lambda_1 = N - 1$ while $\lambda_{l \geq 2} = -1$. Therefore, the ratio λ_l/λ_1 quickly approaches to 0 as $N \rightarrow \infty$. And thus $|\tilde{w}\rangle = |w\rangle$, which matches Eq. (3.24). From this treatment, we can see that all graphs whose eigenvalue ratio $\lambda_{l \geq 2}/\lambda_1$ converging to 0 in the $N \rightarrow \infty$ limit can achieve optimal search. This means that the graph has to have a large spectral gap, which generally requires the graph to be highly connected. In the other extreme case where the eigenvalue ratio is $\lambda_{l \geq 2}/\lambda_1 \rightarrow 1$ as $N \rightarrow \infty$, the search algorithm would not work as the dynamics starting from $|\lambda_1\rangle$ highly leaks out to the higher energy levels through $|w\rangle$.

In the intermediate region of $0 < (\lambda_{l \geq 2}/\lambda_1) < 1$, the dynamics will be non-trivial depending on the actual structure of the eigenstates $|\lambda_l\rangle$. We need to know the full spectrum and eigenstates in order to exactly know the dynamics, but we can still extract important information from Eq. (3.32). Let us write the two lowest energy eigenstates of Eq. (3.32) as

$$|E_0\rangle = (|\tilde{w}\rangle + |\lambda_{1,\tilde{w}}\rangle)/\sqrt{2}, \quad (3.34)$$

$$|E_1\rangle = (|\tilde{w}\rangle - |\lambda_{1,\tilde{w}}\rangle)/\sqrt{2}, \quad (3.35)$$

where $|\lambda_{1,\tilde{w}}\rangle$ is a state that approximately achieves $|\langle\tilde{w}|\lambda_{1,\tilde{w}}\rangle| = 0$. We assume $|\langle w|\lambda_1\rangle|$ is small (up to order of $1/\sqrt{N}$) so that $|\lambda_{1,\tilde{w}}\rangle$ is very close to $|\lambda_1\rangle$ as $N \rightarrow \infty$. By considering the characteristic equation $H_s|E_{0,1}\rangle = (-A_g/\lambda_1 - |w\rangle\langle w|)|E_{0,1}\rangle = E_{0,1}|E_{0,1}\rangle$, we can derive that

$$\Delta E = E_1 - E_0 = 2|\langle\lambda_1|w\rangle\langle w|\tilde{w}\rangle|. \quad (3.36)$$

We can extract important information from Eq. (3.36).

1. By starting the dynamics from $|\lambda_1\rangle$, the state will rotate to $|\tilde{w}\rangle$ with time $\tau = \pi/\Delta E = \pi/2|\langle\lambda_1|w\rangle\langle w|\tilde{w}\rangle|$, which is the necessary length of time evolution that maximizes $P(\tau)$.
2. The success probability is $P(\tau) = |\langle w|\tilde{w}\rangle|^2$.

The first point tells us that τ will depend on the w -th component of the leading eigenvector of A_g , which can be different depending on w . If the graph is regular, $|\lambda_1\rangle$ is always uniform vector $|s\rangle$, which gives $|\langle s|w\rangle| = 1/\sqrt{N}$ independent of N . For non-regular graphs (including complex networks we are going to deal with), the components are non-

3.5. PRELIMINARIES OF THE SPATIAL SEARCH ALGORITHM

uniform. The second point tells us that the success probability will depend on how much the dynamics can stay within the two dimensional subspace spanned by $|\lambda_1\rangle$ and $|w\rangle$.

It is important to note that there are cases where $\gamma = 1/\lambda_1$ is not the optimal choice to obtain the best time complexity for the given graph. From our observations from some numerical analysis in the later sections, the optimal value of γ that maximizes $P(\tau)$ (without increasing τ substantially) tends to take a value smaller than $1/\lambda_1$ as the connectivity of the graph decreases. This is probably because γ also has a role to suppress the higher energy level terms (the second term of Eq. (3.30)).

In summary, we can clearly see that the dynamics and time complexity of the spatial algorithm crucially depends on the structure of the energy eigenspace of the graph. Optimal search can be achieved on graphs whose largest and second largest eigenvalues of the adjacency matrix are well separated. In terms of the difficulty of the analysis, eigenvectors and eigenvalues of some simple graphs can be obtained analytically, but generally this is a difficult problem especially when the graph is a complex network. One needs to use numerical diagonalization or simulations of the quantum walk dynamics in order to obtain the time complexity of the algorithm.

3.5.4 Numerical method to analyze spatial search

In this section, we develop a numerical strategy to efficiently compute time complexity of the spatial search algorithm. In principle, if all of the eigenvalues of the adjacency matrix can be obtained analytically, we can derive the time complexity with some analytical calculations. However, this is a very rare case and especially for complex networks analyzed in this thesis, we need to rely on numerical calculations. Additionally, we need to run computations such as diagonalization and matrix exponentiations of large matrices (dimensions up to order of 10^4) to obtain reliable results both in the perspective of statistical convergence of the network models, and the perspective of algorithm evaluation (as we are interested in the scaling of the time complexity in the large N region). In the following paragraphs, we will see step by step how we can numerically analyze the spatial search algorithm for any graphs. At the end of the section, in Figure 3.9, the flow of the analysis is summarized.

1. Optimization of γ Let's assume that we have a search Hamiltonian $H_s = -\gamma A_g - |w\rangle\langle w|$ we would like to analyze. We assume the adjacency matrix A_g is given, and we

3.5. PRELIMINARIES OF THE SPATIAL SEARCH ALGORITHM

have selected a certain node w to search for. First of all, we need to find the optimal value of $\gamma = \gamma_{opt}$ which equally mixes the ground states of A_g and w , and drive the transition between the states $|\lambda_1\rangle$ and $|\tilde{w}\rangle$ defined in Eq. (3.32). The optimization of γ is necessary for the algorithm to run in a most efficient way, which means that setting γ to an non-optimized value can lead to low success probability $P(\tau)$.

To understand how we can find the optimal γ , we will look at how the eigenvalues and eigenstates of H_s depends on γ . See Figure 3.8. We have plotted some quantities relevant to the dynamics of the spatial search against γ . First, we can observe that $\Delta E \equiv E_1 - E_0$, the energy gap between the first excited state and the ground state of H_s , takes a curve which has a minimum at a certain value of γ . Remember that at $\gamma = 0$, $H_s = -|w\rangle\langle w|$ and thus $\Delta E = 0 - (-1) = 1$. Increasing γ from zero, the gap starts to shrink, take a minima, and starts to open up where the effect of the term $-|w\rangle\langle w|$ becomes negligible. Conclusions first, the point where ΔE takes the minimum value is where the avoided crossing between the two lowest energy eigenstates is formed, and thus this point corresponds to the optimal value $\gamma = \gamma_{opt}$. This is further supported by looking at the quantities $|\langle\lambda_1|E_1\rangle|^2$ and $|\langle\lambda_1|E_0\rangle|^2$, the squared overlaps between the leading eigenvector of A_g and the two lowest eigenstates of H_s . The quantities take $|\langle\lambda_1|E_0\rangle|^2 \approx |\langle\lambda_1|E_1\rangle|^2 \approx 0.5$ where ΔE takes the minimum, indicating the equal mixture of the eigenstates (i.e. formation of $H_s = -|\lambda_1\rangle\langle\lambda_1| - |\tilde{w}\rangle\langle\tilde{w}|$). It is also interesting to see how the quantities $|\langle w|E_1\rangle|^2$ and $|\langle w|E_0\rangle|^2$ behave. Sum of these quantities indicates the success probability $P(\tau)$, since this measures how much the state $|w\rangle$ communicate with only with $|\lambda_1\rangle$ and not with the higher energy levels.

Therefore, in order to find γ_{opt} , we need to compute two smallest eigenvalues of H_s (which are in most cases the eigenvalues with the largest two magnitude), and minimize against γ . This is actually computed numerically using the power method. In the procedure of the optimization, we initialize γ at $1/\lambda_1$ (again λ_1 is computed via power method), and minimize ΔE by shifting γ by $\delta\gamma = 0.01 \times 1/\lambda_1$ at each step. As E_0, E_1 or λ_1 are eigenvalues with large magnitudes, they are rather easily computed that the other eigenvalues that could be small in magnitude.

2. Computation of the evolution time τ Computing the necessary length of the time evolution of the quantum walk τ is rather easy as τ is given by $\tau = \pi/\Delta E$, derived in the previous section.

3.5. PRELIMINARIES OF THE SPATIAL SEARCH ALGORITHM

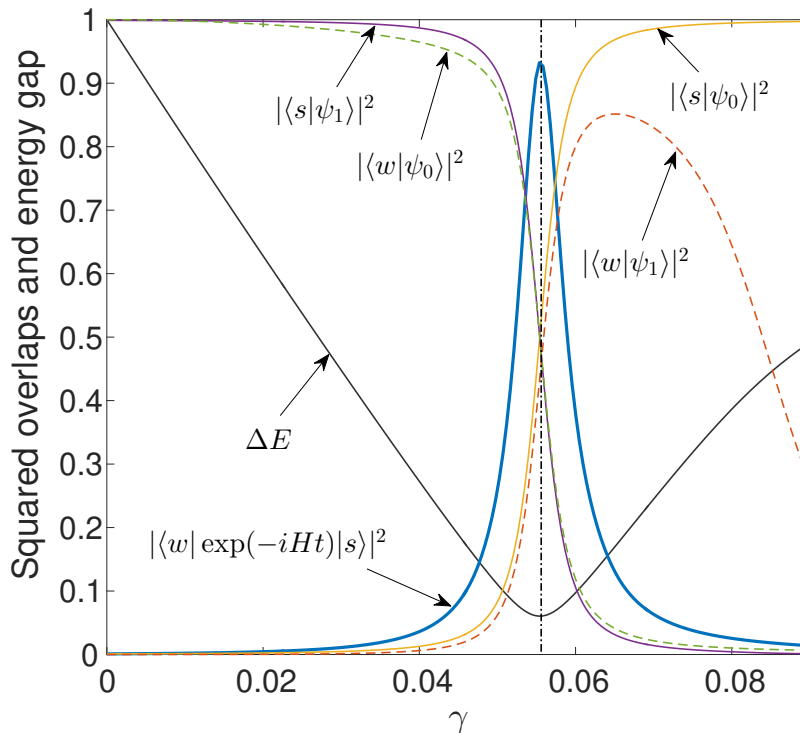


Figure 3.8: Energy gap ΔE , success probability $|\langle w | \exp(-iHt) | s \rangle|^2$, and squared overlaps plotted against the parameter γ . The plot is created using an instance of the long-range percolation graph (defined in Section 3.6.1) with size $N = 1024$ and $\alpha = 2$. In the vicinity where ΔE takes the minimum, the success probability (blue line) takes the peak value. We evaluate the algorithm by using this peak value as the success probability, and use ΔE at this point to calculate the evolution time as $\tau = \pi/\Delta E$.

3. Computation of the success probability $P(\tau)$ Finally we need to compute the probability to measure the quantum walker on the node $|w\rangle$ after the time evolution of length τ , which is given by

$$P = |\langle w | \exp(-\frac{i}{\hbar} H_s \frac{\pi}{\Delta E}) | \psi(0) \rangle|^2. \quad (3.37)$$

The direct computation of the matrix exponential is a burden as it requires diagonalization of the matrix H_s . However, in our case, we just need to know the resulting *state* after the time evolution $|\psi(\tau)\rangle = \exp(-\frac{i}{\hbar} H_s \frac{\pi}{\Delta E}) |\psi(0)\rangle$, rather than the unitary operator itself. We can use the efficient Chebyshev series expansion [54] in such occasion. The matrix exponential is approximated with a polynomial function and multiplied to the initial state vector simultaneously until sufficient accuracy is achieved. This method is especially memory and time saving if H_s is sparse.

3.5. PRELIMINARIES OF THE SPATIAL SEARCH ALGORITHM

An important factor we have left to discuss is the choice of the initial state $|\psi(0)\rangle$. The ideal choice is $|\lambda_1\rangle$, which is clear from the previous section. However, in realistic experimental settings, preparing an eigenstate of a system accurately can be a hard task. Some eigenstate may be composed of complex amplitudes and relative phases. In such cases we can still run the algorithm using a initial state that has substantial overlap with $|\lambda_1\rangle$. Let's say the overlap approaches to a constant, $|\langle\psi(0)|\lambda_1\rangle| \rightarrow c$, as $N \rightarrow \infty$. Starting the dynamics from such initial state, the success probability will be only decreased by a constant factor compared to starting from the state $|\lambda_1\rangle$. On the other hand, an initial state whose overlap with the leading eigenvector decreases as the growth of N is an poor choice as the time complexity will get an additional factor which increases as N grows.

We think the numerical strategy developed in this section is universal for computing the time complexity of the spatial search algorithm by continuous-time quantum walk on any connected, undirected graph.

3.5. PRELIMINARIES OF THE SPATIAL SEARCH ALGORITHM

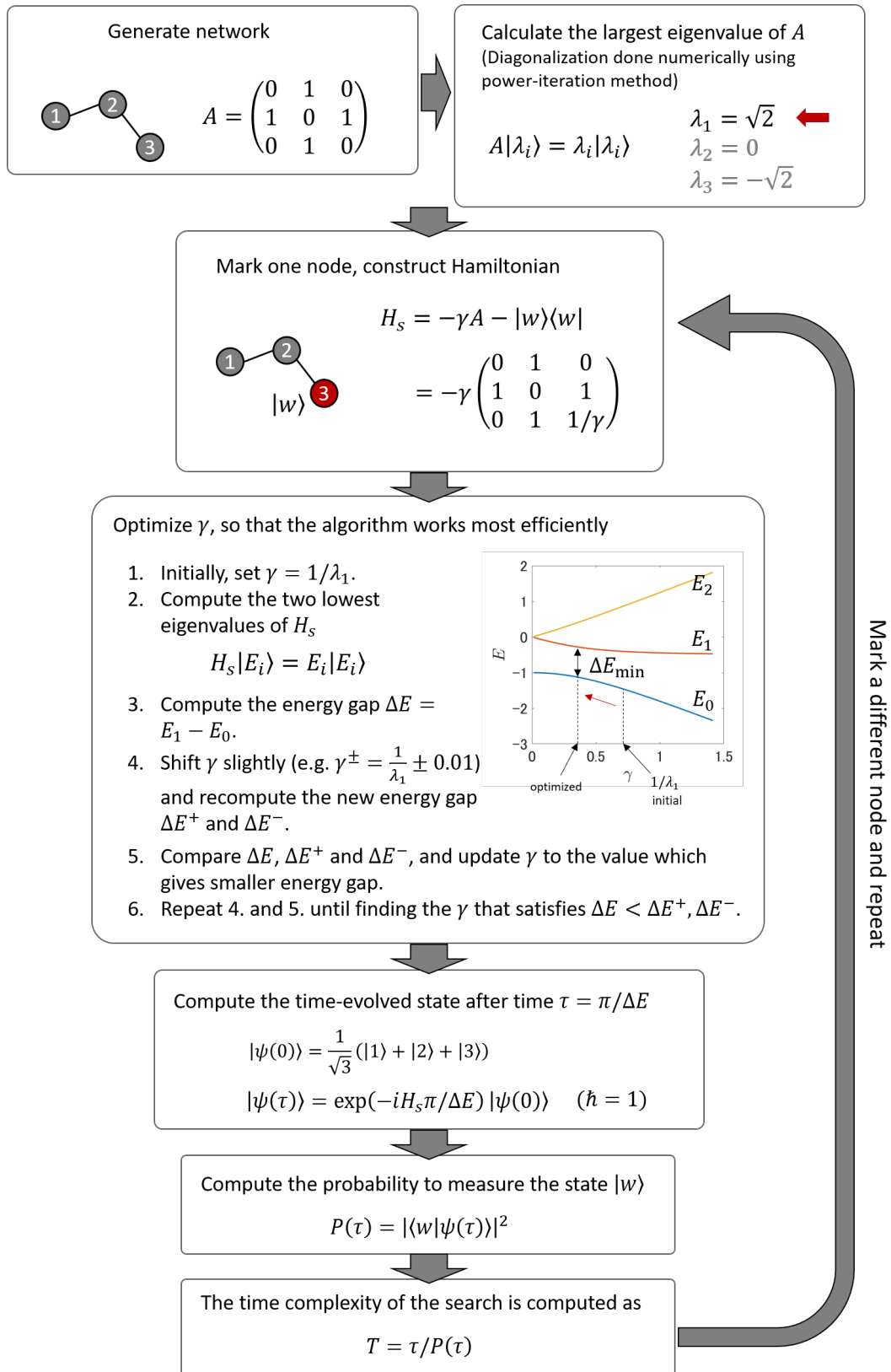


Figure 3.9: Flowchart of the numerical calculation of the search time.

3.6 Spatial search on the long-range percolation model

In this section, we will present our result on the analysis of the spatial search algorithm on the long-range percolation (LRP) model. First, we will introduce the formal definition of the LRP model, and then present the result on how the time complexity depends on the parameter of the network model. We discuss the behaviour of the time complexity against the change of connectivity of the graph. After that, we show some network measures computed on the LRP model, and discuss some relation between the property of the network and the optimality of the search.

3.6.1 Defining the LRP model

Here we introduce definition of the long-range percolation (LRP) model. Such model was originally introduced by Schulman [49, 50], who considered the classical percolation transition on this graph. Also, similar graph models are considered in the field of complex network theory as a network to describe the small-world phenomena [55, 56].

The model we consider here is a probabilistic graph generation model described as follows. N nodes are placed on the cubic lattice points of \mathbb{Z}^d . As an example, if $d = 2$ we consider the lattice points of a \sqrt{N} by \sqrt{N} square lattice, and if $d = 1$ this is a simple line of length N . We assume the lattice to have toric or periodic boundary condition in order to exclude effects that may come from the boundary of the lattice. An edge exists between all pair of nodes i and j by a probability p_{ij} , independently of all other edges. Here, we choose p_{ij} to be a power law decaying function

$$p_{ij} = |i - j|^{-\alpha}, \quad (3.38)$$

where $|i - j|$ is the Euclidean distance between the pair of nodes i and j , and $\alpha \geq 0$ is a constant taking real value. The exponent α controls the decay speed and magnitude of the probability function, and thus controls the connectivity (average of total number of edges) of the graph. The feature of the form of p_{ij} is that the geometric layout of the nodes are taken into account. Therefore, the graph will likely have edges if the nodes are spatially close to each other, and an edge will rarely exist if they are spatially far apart. We define the distance between the nearest-neighbour lattice points as $|i - j| = 1$. This allows us to always generate nearest neighbour edges for any value of α , and put additional long-range (non-nearest neighbour) edges on top of it. This setting also allows

3.6. SPATIAL SEARCH ON THE LONG-RANGE PERCOLATION MODEL

the graph to result as a simple lattice in the $\alpha \rightarrow \infty$ limit. The graph will be a complete graph when $\alpha = 0$, since $p_{ij} = 1$. As a note, if we choose p_{ij} to be a constant value independent of the Euclidean distance between the nodes, this model is equivalent to the Erdős-Rényi random graph. See Figure 3.10 for the schematic picture.

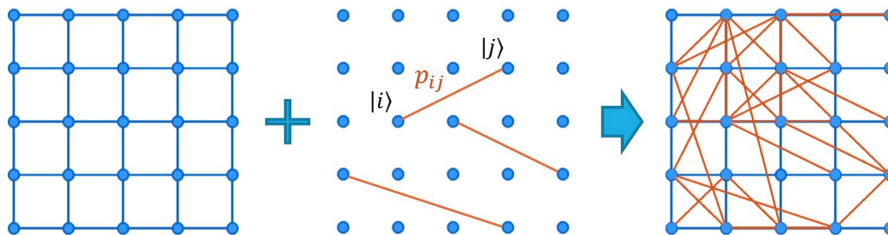


Figure 3.10: Schematic representation of the long-range percolation model. Assume a two-dimensional square lattice, and long-range edges are added between pair of nodes i and j by probability $p_{ij} = |i-j|^{-\alpha}$, which is a power-law decaying function depending on the Euclidean distance between the nodes.

Since p_{ij} in this form is scale invariant (i.e. does not include the system size N), we expect the search time on this graph to be $O(\sqrt{N})$ in a certain region of α , which should be $0 \leq \alpha \leq \alpha_c$. The scaling of the search time would grow with the increase of α , when $\alpha > \alpha_c$. Our primary goal is to determine α_c , the critical point where the search time switches from optimal to non-optimal.

3.6.2 Time complexity of the spatial search on the LRP model

In this section we will present the critical α_c for the LRP model with $d = 2$ and $d = 1$. We will show how α_c is derived through the numerical calculations introduced in the previous section.

We first clarify the setting of our analysis. The search Hamiltonian is constructed using the Laplacian matrix of the LRP model,

$$H_s = -\gamma L_{lrp}(\alpha) - |w\rangle\langle w|. \quad (3.39)$$

$L_{lrp}(\alpha)$ depends on the connectivity exponent α defined in Eq. (3.38). Additionally, as the graph is generated by a stochastic process, the graph will not be exactly same at each trial of the generation. Therefore, when we compute the time complexity of the search algorithm (τ and $P(\tau)$), we compute 200 samples of them at each fixed α and took the average. This consists of 20 samples of the graph, with 10 different nodes chosen randomly as the marked node w . For each realization of the network, we follow the

3.6. SPATIAL SEARCH ON THE LONG-RANGE PERCOLATION MODEL

numerical analysis described in the previous section to optimize γ , compute τ and $P(\tau) = |\langle w | \exp(-iH_s\tau/\hbar) | \psi(0) \rangle|^2$. τ is the necessary length of time-evolution under the action of H_s (i.e. the optimal measurement time), and $P(\tau)$ is the success probability of the algorithm. We evaluate the spatial search algorithm via these two quantities (details are explained in Section 3.5.4). When computing $P(\tau)$, we choose the initial state of the time evolution as the uniform superposition state over all nodes $|\psi(0)\rangle = |s\rangle = \sum_{i=1}^N |i\rangle/\sqrt{N}$, as this state is the lowest energy eigenstate of L_{lrp} .

Our result on the evolution time τ for $d = 2$ is shown in Figure 3.11. The figure shows how τ depends on α for different system sizes N . We can see that the curves stays almost flat between $\alpha = 0 \sim 2$. The evolution time grows dramatically (especially as N is larger) after $\alpha \sim 2$.

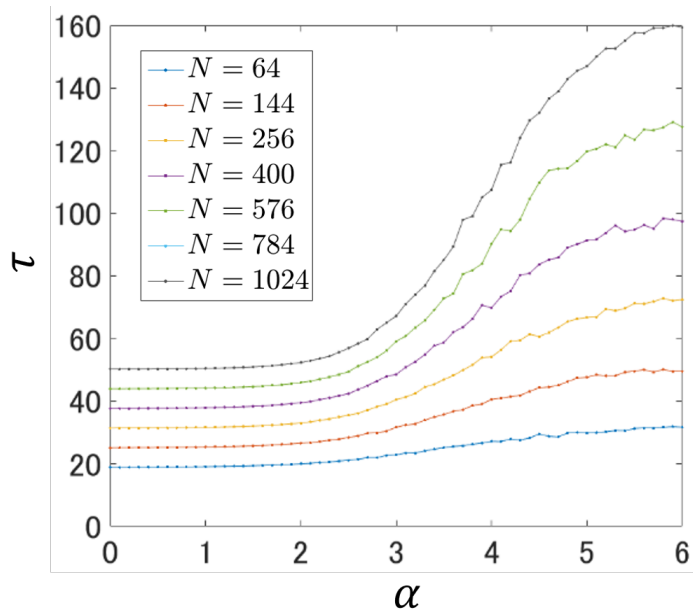


Figure 3.11: The optimal measurement time τ plotted against α , on the $d = 2$ LRP model. The curves with different colours correspond to different network sizes N . The optimal measurement time grows as α increases, which is associated to lowering the connectivity of the graph.

In order to apply a quantitative analysis, we converted τ to another quantity we name as the normalized energy gap, $\Delta E_{norm} = \Delta E \sqrt{N}/2$. The relation between the two is $\Delta E_{norm} = \pi \sqrt{N}/2\tau$, using $\tau = \pi/\Delta E$. We define this quantity so that when the search is optimal (i.e. $\Delta E = 2/\sqrt{N}$), $\Delta E_{norm} = 1$. Moreover as long as ΔE scales as $N^{-1/2}$, ΔE_{norm} scales as a constant $O(1)$. The plot of ΔE_{norm} against α is shown in Figure 3.12(a). Now the curves lives within $[0, 1]$, and we can see a single intersecting point of the curves with different system sizes.

3.6. SPATIAL SEARCH ON THE LONG-RANGE PERCOLATION MODEL

In Figure 3.12(b), we have shown the result on the success probability $P(\tau)$, plotted against α . $P(\tau)$ naturally lives within $[0, 1]$ from definition, and we can see a similar behaviour as the normalized energy gap. A single intersecting point of the curves with different system sizes exists in the plot as well.

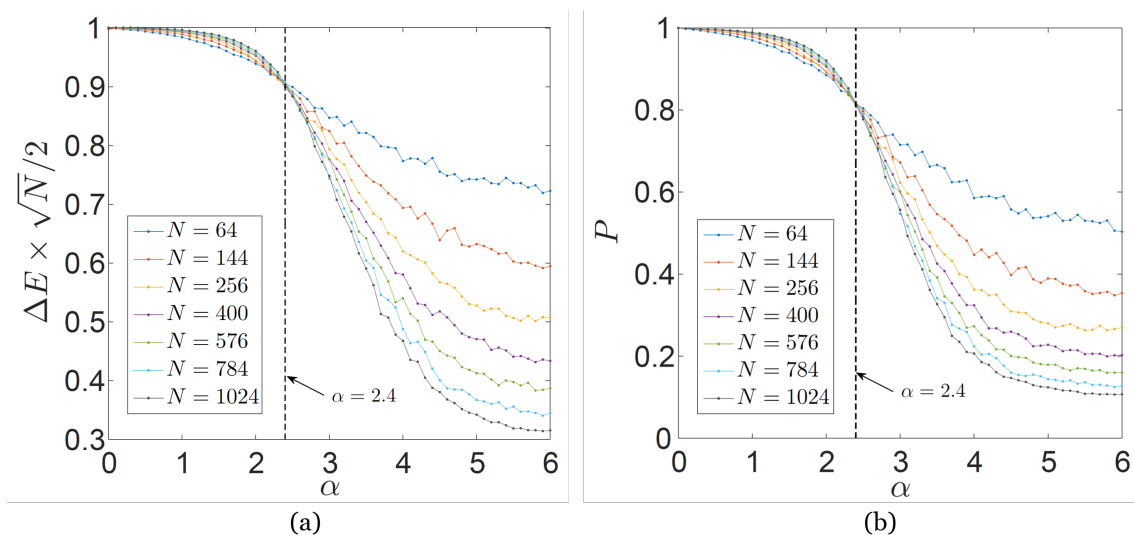


Figure 3.12: (a) The normalized energy gap $\Delta E \sqrt{N}/2 = \pi \sqrt{N}/2\tau$ and (b) the success probability $P(\tau)$ plotted against α , on the $d = 2$ LRP model. The curves with different colours correspond to different network sizes N . The data points represent the averaged values of 200 samples of computation, where error bars are not shown for the visibility of the plots (see Figure 3.13). The curves intersect at $\alpha \approx 2.4$ for both plots. This indicates that at $\alpha = \alpha_c$ the spatial search is optimal, since the optimal measurement time scales as $\tau \propto \sqrt{N}$ and the success probability $P(\tau)$ scales as a constant.

Let us explain the interpretation of the result. First of all, when $\alpha = 0$, a complete graph is generated using the LRP model. As derived in the previous section, the spatial search on the complete graph achieves optimal search with $\tau = \pi \sqrt{N}/2$ and $P(\tau) = 1 - 1/N$. We can see this result is reproduced in Figure 3.12, at $\alpha = 0$. When α is increased from 0, the graph gradually loses edges, getting sparse. This is reflected in the plots as the gradual decrease of the curves. However, interestingly, the curves of different system sizes cross at one point, which is around $\alpha \approx 2.4$ for both ΔE_{norm} and $P(\tau)$. This point is the critical α_c where the scaling of the time complexity switches from optimal to non-optimal. At $\alpha = \alpha_c \approx 2.4$, The scaling of ΔE_{norm} and $P(\tau)$ are constant as they are fixed against the change of N . Therefore, we get $\tau = \pi \sqrt{N}/2 \Delta E_{norm} = \pi \sqrt{N}/2 c_\tau$ and $P(\tau) = c_P$, where c_τ, c_P are constants, and thus the time complexity of the search is $T = \tau/P(\tau) = O(\sqrt{N})$. On the other hand, in the region of $\alpha > \alpha_c$, ΔE_{norm} and $P(\tau)$ decreases as N grows. This suggests $\Delta E_{norm} = f(N)$ and $P(\tau) = g(N)$ where $f(N), g(N)$

3.6. SPATIAL SEARCH ON THE LONG-RANGE PERCOLATION MODEL

are decreasing functions of N . This straightforwardly suggests that the time complexity is $T = \tau/P(\tau) = O(\sqrt{N}f^{-1}(N)g^{-1}(N))$ which is slower than optimal. As the $\alpha \rightarrow \infty$ limit the graph is the simple square lattice, the time complexity in the region of $\alpha > \alpha_c$ can be bounded by $O(\sqrt{N}) < T \leq O(N^2/\log^3 N)$, referring to Table 3.1.

In Figure 3.13, we plotted $\Delta E, P(\tau)$ and $T = \pi/\Delta EP(\tau)$ for $N = 1024$ with the standard deviations of the data included as the error bars. We can see that the slope of the energy gap and success probability (Figure 3.13(a) and 3.13(b)) maximizes in the region of $2 < \alpha < 4$. The standard deviation is also larger in this region. The time complexity T (Figure 3.13(c)) starts to increase sharply after $\alpha = 2$. We can also see that the quantities converges to the value for the simple square lattice (the blue dashed lines in the plots) as α increases.

We have also obtained the critical α_c for the LRP model with $d = 1$. The results are shown in Figure 3.14(a) and 3.14(b). The plots of ΔE_{norm} and $P(\tau)$ shows the same tendency as in the $d = 2$ case, where we see the intersecting point at $\alpha \approx 1.3$. It is interesting that we could find that the critical α_c actually exists, and their values are slightly above the dimension of the underlying lattice, $\alpha_c > d$.

3.6.3 Average degree of the LRP model at the critical connectivity

In this section, we discuss the structure and connectivity of the LRP model at α_c , the critical point where the optimal search is achieved. We will derive that the average degree of the LRP model at α_c scales as a constant, and compare our result with the case of the spatial search on the Erdős-Rényi random graph.

Let us first compute the average degree of the LRP model with $d = 2$. We consider how many long-range edges are actually added on the square lattice when the optimal search was achieved. To compute the average degree (expectation value of the degree) of node j , we sum up the edge existence probability function $p_{ij} = |i - j|^{-\alpha}$ over all pair of nodes as,

$$\langle k_j \rangle = \sum_{i \neq j}^N p_{ij} = \sum_{i \neq j}^N |i - j|^{-\alpha}. \quad (3.40)$$

We upper bound this sum by the integral of p_{ij} over a disk of radius $\sqrt{2N}/2$, which covers the whole lattice. Replacing the Euclidean distance as $r \equiv |i - j|$, and writing the integral

3.6. SPATIAL SEARCH ON THE LONG-RANGE PERCOLATION MODEL

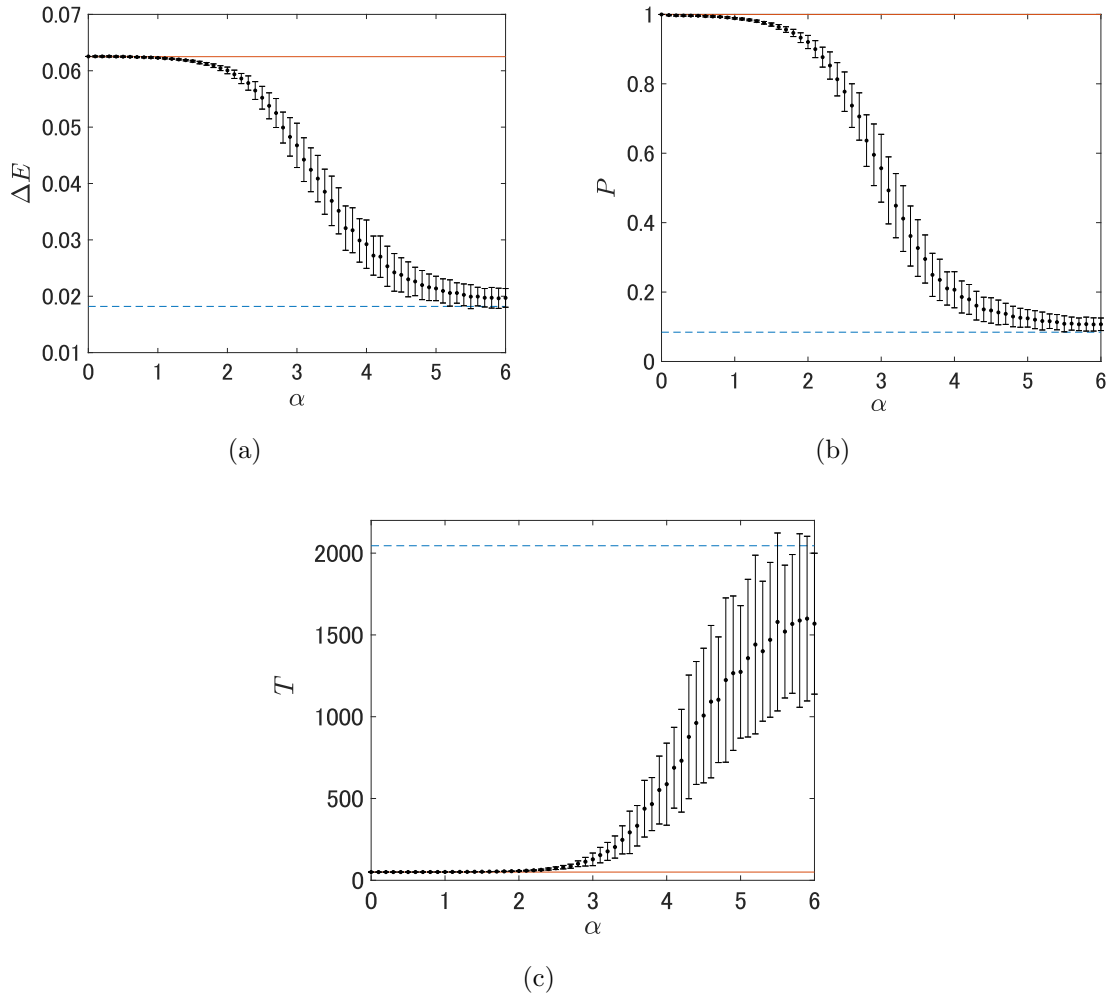


Figure 3.13: (a) The energy gap ΔE , (b) success probability $P(\tau)$ and (c) total search time $T = \pi/(\Delta EP)$ plotted against α , on the $d = 2$ LRP model. The network size is $N = 1024$ for all plots. The data points and their error bars are the average and standard deviation of the quantities obtained from 200 samples. In each plot, the values computed from the complete graph and the two-dimensional square lattice is indicated as the red solid line and the blue dashed line, respectively.

3.6. SPATIAL SEARCH ON THE LONG-RANGE PERCOLATION MODEL

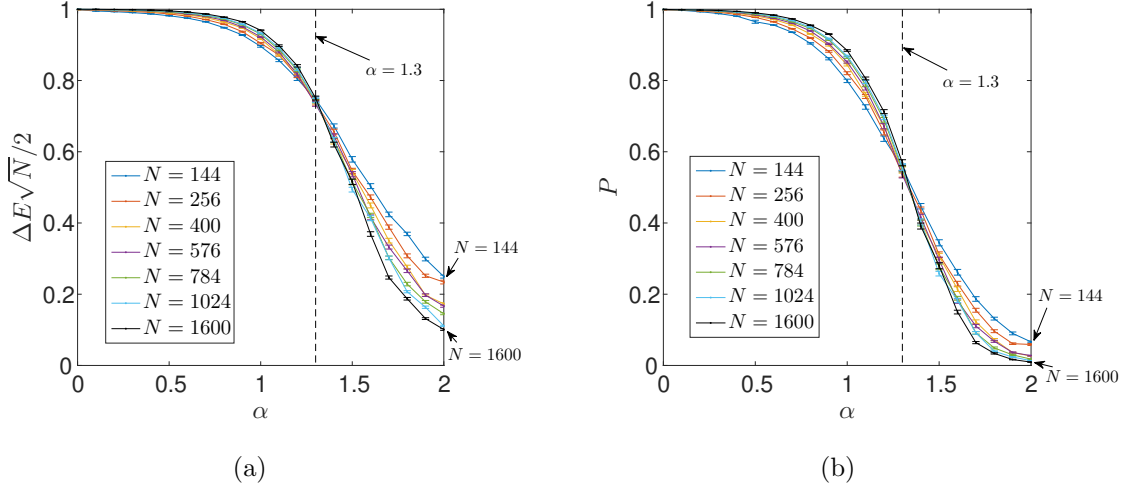


Figure 3.14: (a) The normalized energy gap $\Delta E \sqrt{N}/2 = \pi \sqrt{N}/2\tau$ and (b) the success probability $P(\tau)$ plotted against α , on the $d = 1$ LRP model. The curves with different colours correspond to different network sizes N . The data points represent the averaged values of 200 samples of computation, where error bars are their standard deviation. The curves intersect at $\alpha \approx 1.3$ for both plots.

in polar coordinates, we can upper bound $\langle k_j \rangle$ as

$$\langle k_j \rangle < 4 + \int_1^{\sqrt{N/2}} (r^{-\alpha}) r dr d\theta. \quad (3.41)$$

We separated the contribution from $r = 1$ nodes into the first term of Eq. (3.41), since the four nearest neighbour edges are generated with probability 1 in our setting. The latter term counts the average number of long-range edges that are connected to node j . When $\alpha \neq 2$, the integral can be solved as

$$\langle k_j \rangle < 4 + \int_1^{\sqrt{N/2}} (r^{-\alpha+1}) dr d\theta \quad (3.42)$$

$$= 4 + 2\pi \left[\frac{1}{-\alpha + 2} r^{-\alpha+2} \right]_1^{\sqrt{N/2}} \quad (3.43)$$

$$= 4 + \frac{2\pi}{-\alpha + 2} \left\{ \left(\sqrt{\frac{N}{2}} \right)^{-\alpha+2} - 1 \right\}. \quad (3.44)$$

3.6. SPATIAL SEARCH ON THE LONG-RANGE PERCOLATION MODEL

When $\alpha = 2$,

$$\langle k_j \rangle < 4 + \int_1^{\sqrt{N/2}} (r^{-1}) dr d\theta \quad (3.45)$$

$$= 4 + 2\pi [\log r]_1^{\sqrt{N/2}} \quad (3.46)$$

$$= 4 + \pi (\log N - \log 2). \quad (3.47)$$

We can see from Eq. (3.44) that the leading term is $N^{-\alpha/2+1}$ when $\alpha \neq 2$, and from Eq. (3.47) that the leading term is $\log N$ when $\alpha = 2$. We are especially interested in the case of $\alpha = \alpha_c \approx 2.4$, where we get from Eq. (3.44) as

$$\langle k_j \rangle < 4 + \frac{2\pi}{\alpha - 2} \left\{ 1 - \left(\frac{2}{N} \right)^{\alpha/2-1} \right\} \quad (3.48)$$

$$= 4 + 5\pi \left\{ 1 - \left(\frac{2}{N} \right)^{0.2} \right\}. \quad (3.49)$$

From this equation it is clear that the average degree grows with N , but slowly converges to constant value as $N \rightarrow \infty$.

The average degree for the LRP model with $d = 1$ can be straightforwardly computed following the similar calculation as with $d = 2$. The average degree is upper bounded by the integral,

$$\langle k_j \rangle < 2 + \int_1^{N/2} (r^{-\alpha}) dr, \quad (3.50)$$

and we can show for $\alpha = \alpha_c \approx 1.3$, the average degree is

$$\langle k_j \rangle < 2 + \frac{2}{\alpha - 1} \left\{ 1 - \left(\frac{2}{N} \right)^{\alpha-1} \right\} \quad (3.51)$$

$$= 2 + \frac{20}{3} \left\{ 1 - \left(\frac{2}{N} \right)^{0.3} \right\}. \quad (3.52)$$

The average degree again converges to a constant value.

This lets us conclude that $O(\sqrt{N})$ search time can be achieved on the $d = 2$ or $d = 1$ LRP model with a constant, or at least less than $O(\log N)$ average degree. To indicate a specific value, the average degree calculated numerically by generating the LRP graph with $\alpha = 2.4$ and $N = 1024$ was $\langle k_j \rangle = 13.5$, which means 4 nearest neighbour edges plus

3.6. SPATIAL SEARCH ON THE LONG-RANGE PERCOLATION MODEL

9.5 long-range edges in average. Note that most of the long-range edges do not connect far apart nodes going across the whole lattice.

The results also suggest that when one uses the LRP graph, independent of the choice of $d = 1$ or $d = 2$, one can achieve the optimal search time of $O(\sqrt{N})$ with almost identical scaling of average degree (just a constant factor difference between $d = 1$ and $d = 2$). However, if we take into account the length of the edges, $d = 1$ will have more chance to generate long-distance edges than $d = 2$, since the probability of generating an edge of length r is proportional to $r^{-\alpha}$.

It is interesting to compare our results with the case of Erdős-Rényi random graph. The spatial search by continuous-time quantum walk on the Erdős-Rényi random graph has been analyzed by Chakraborty *et al.* [44]. This graph model corresponds to the case where we set the edge generation probability p_{ij} to a function independent of the Euclidean distance between the nodes. In [44], it was shown that optimal search is achieved as long as $p_{ij} \geq p_c = (\log^{3/2} N)/N$. This tells us that the average degree of the graph at $p_{ij} = p_c$ is $\langle k_j \rangle = p_c(N - 1) = (\log^{3/2} N)(N - 1)/N \approx \log^{3/2} N$. In contrast, we got a result that on the LRP model, one can achieve optimal search with an average degree converging to constant. Therefore, in principle, the LRP model requires less amount of edges (i.e. less connectivity) in average than the Erdős-Rényi random graph in order to achieve optimal search. This is an interesting observation, as the LRP model is a model that has constraint by the Euclidean distance between the node, while the Erdős-Rényi random graph has no such constraint, and connects any pair of nodes with equal probability. In terms of graph measures, such difference of the models results the the difference in the clustering coefficient of the graphs. See Figure 3.15(a) which compares how the average clustering coefficient changes depending on the average degree of the two graphs. The LRP model has a high clustering coefficient, resulting from the fact that the model generates edges densely in local regions.

This comparison suggests that quantum search is more efficient when the quantum walker explores the space within some local space densely, rather than exploring the entire space sparsely. We can assume that when the quantum walker hops around in a local region, it has more chance to come back to its initial node and cause more interference with itself. As the interference of the complex amplitudes is the key feature of the quantum search algorithm, the more interference of the quantum walker leads to a efficient spatial search algorithm.

3.7. SPATIAL SEARCH ON THE SCALE-FREE NETWORK

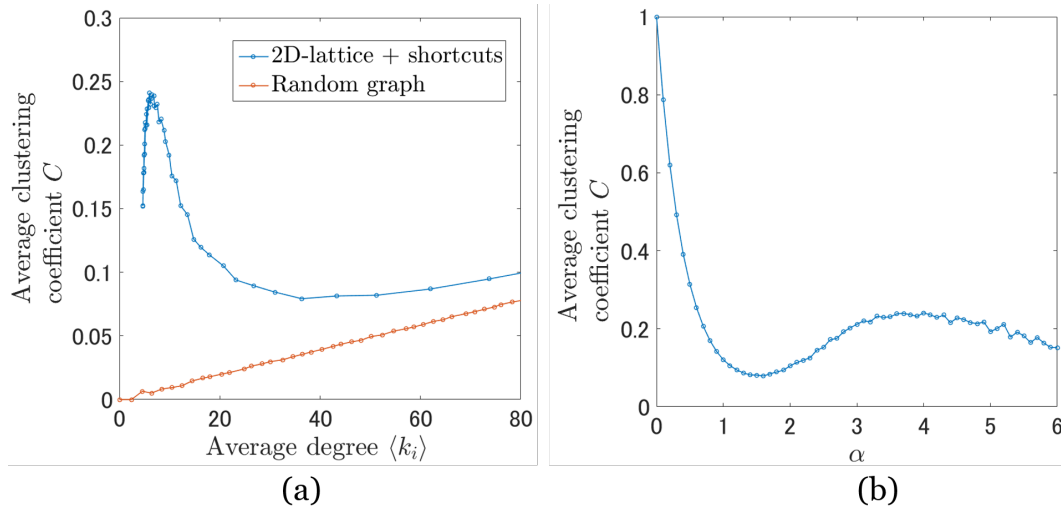


Figure 3.15: Average clustering coefficient of the LRP model. (a) Comparison between the $d = 2$ LRP model (blue dots) and the ER graph (red dots), plotted against the average degree of each graph. The quantities are computed from networks of size $N = 1024$. (b) The average clustering coefficient of the $d = 2$ LRP model, plotted against α . Interestingly, there is a local maximum around $\alpha = 3.5$.

We also point out that when $d < \alpha < 2d$, the LRP model has a diameter of $\log^\delta N/d$, where $\delta^{-1} = \log_2(2d/\alpha)$, which was derived by Biskup [57]. This means that the graph has a small-world property in this region of α , a common and important feature of real-world networks. Essentially, the small-world property in this context means that the long-range edges added on the lattice creates shortcuts, such that one can reach from one node to another in small (order of $\log N$) number of steps. A simple lattice ($\alpha \rightarrow \infty$) is not small-world as the diameter is the order of $N^{1/d}$. It is clear that the fact that the graph has small-world property is helping to speed up the search.

3.7 Spatial search on the Scale-free network

In this section we will present our results on the time complexity of the spatial search algorithm on the Bollobás scale-free network. First we will introduce the definition and the network generation process of the Bollobás scale-free network. Next we will show how the spatial search algorithm behaves of such network, by considering the distribution and the scaling of the search time. After that, we will present some results on the relations between the network measures of the Bollobás scale-free network and the search time.

3.7. SPATIAL SEARCH ON THE SCALE-FREE NETWORK

3.7.1 Definition of the Bollobás scale-free network

Here, we will describe how the generation process of the Bollobás scale-free network. We are following the process defined by Bollobas [52, 53], and the explanation is based on such definitions.

The process of generating the network with N nodes is as follows. At the initial time step $u = 1$, the network $G_{\{u=1\}}$ starts with a single node v'_1 with one edge connecting to itself. At every subsequent time step $u \geq 2$, one node v'_u having one outgoing edge is added into $G_{\{u-1\}}$ and connects to one of the nodes in $G_{\{u\}}$ with its outgoing edge. Defining the degree of node v'_i at time u as $d_u(v'_i)$, the node to connect to is chosen by the following probability distribution [52]

$$Pr(i = s) = \begin{cases} d_{u-1}(v'_s)/(2u - 1) & 1 \leq s \leq u - 1 \\ 1/(2u - 1) & s = u. \end{cases} \quad (3.53)$$

This means that the probability for a node to be chosen is proportional to its degree, which resembles the “preferential attachment”. After repeating the above process until a certain time step $u = m$ ($m \in \mathbb{N}$), the set of nodes v'_1, v'_2, \dots, v'_m forms a single node v_1 . The edges that were connecting the nodes within the set is converted to m self loops on v_1 . The process of adding new nodes v'_u is continued until time step $u = 2m$, and again the the set of nodes v'_{m+1}, \dots, v'_{2m} forms another node v_2 . If $m' \leq m$ nodes in the set of nodes v'_{m+1}, \dots, v'_{2m} are connected to v_1 , they are converted to m' edges between v_1 and v_2 . Following the rule described above, the process is repeated until time step $u_{\text{end}} = mN$, which results as a network $G_{\{mN\}}$ with N nodes and mN edges. The obtained network has a power law degree distribution $P(k) \propto k^{-\beta}$ with exponent $\beta = 3$ [52]. In order to change the value of β , we use the method introduced by Dorogovtsev *et. al* [58].

A more friendly word that would summarize the process above is, the richer gets richer. In this model, a node and an edge is added one by one to the network until the number of nodes reaches N . The node who existed earlier in the network will have higher probability to acquire the edge due to the probability function Eq. (3.53), which tells that the nodes who already have more edges than the others will have higher probability to get the new edge. Therefore, a large number of edges will concentrate on the few nodes that existed early in the generation process, while most other nodes will have limited number of edges.

From the construction described above, we have three control parameters when generating the network; the total number of nodes N , the parameter which controls the

3.7. SPATIAL SEARCH ON THE SCALE-FREE NETWORK

connectivity of the network m , and the degree distribution exponent β . The average degree of the network is $2m$, while the minimum degree is m and the largest degree is $\sim N^{1/(\beta-1)}$. Note that we allow self loops and parallel edges between nodes in our network in order to keep consistency, that is to fix the total number of edges to mN for every trial of generating $G_{\{mN\}}$. When converting $G_{\{mN\}}$ to the adjacency matrix A , the number of self loops or parallel edges contributes to the weight of the diagonal or the off-diagonal entries of A , respectively. The degree distribution and visualization of an instance of $G_{\{mN\}}$ is shown in Figure 3.16.

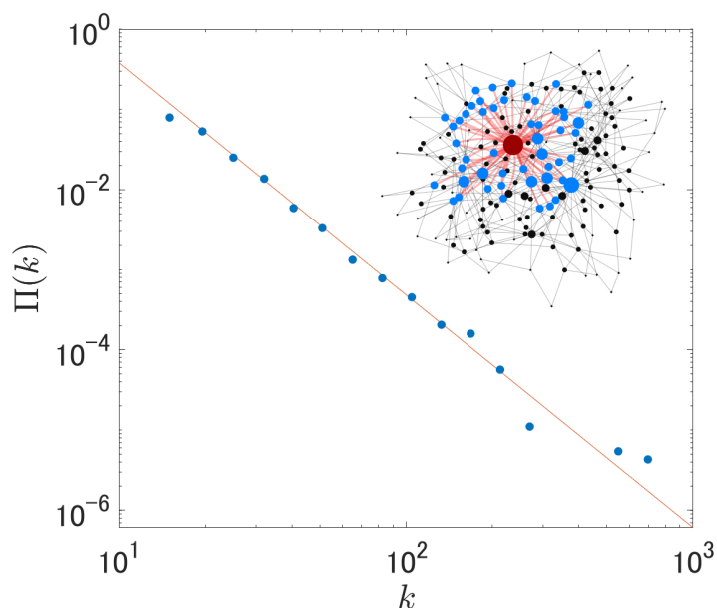


Figure 3.16: Plot of the degree distribution of the Bollobás model. One instance of the network with size $N = 10000$ and minimum degree $m = 5$ is generated, and the degree distribution was fit to a power law function with $P(k) \propto k^{-2.9}$. The inset is a visualization of the network with parameters $N = 200$, $m = 2$, $\beta = 3$.

The Bollobás scale-free network is one of the simplest mathematical model that generates a complex network with power-law degree distribution. The generated network has no high clustering coefficient, community structure, or a self-similar structure, which suggests that the connections are mostly random besides there are large degree hub nodes, which makes crucial difference against the Erdős-Rényi random graph. We choose such model to concentrate the analysis on how the power-law degree distribution affects the spatial search.

3.7. SPATIAL SEARCH ON THE SCALE-FREE NETWORK

3.7.2 The distribution and the scaling of the search time

Now let us describe the results on the time complexity of the spatial algorithm on the Bollobás scale-free network. The search Hamiltonian we use is

$$H_s = -\gamma A_{sf}(m, \beta) - |w\rangle\langle w|, \quad (3.54)$$

where $A_{sf}(m, \beta)$ is the adjacency matrix of the Bollobás scale-free network which depends on the parameter m and β . As the graph is generated by a stochastic process, the graph will not be exactly same at each trial of the generation. Therefore, we computed 1000 samples of networks at with a fixed m and β , chose randomly at least 400 nodes as the marked node w for each sample, and computed the time complexity of the spatial search algorithm. For each realization of the network, we follow the numerical analysis described in Section 3.5.4 to optimize γ , compute τ and $P(\tau)$.

When $P(\tau)$ is computed, we choose the initial state of the time evolution as a state where the quantum walker is fully localized on the largest degree node. We label this state as $|\psi(0)\rangle = |hub\rangle$. This is a initial state very different from the states usually used in spatial search algorithms in other graphs, which is the uniform superposition state $|s\rangle = \sum_{i=1}^N |i\rangle/\sqrt{N}$. The reason for this can be understood by analyzing $|\lambda_1\rangle$, the leading eigenvector of A_{sf} . In Figure 3.17, we have plotted each components c_w of $|\lambda_1\rangle = \sum_{w=1}^N c_w |w\rangle$, and the squared overlap between the eigenvector and the initial state $|\langle hub|\lambda_1\rangle|^2$ in the inset. It is clear that $|\lambda_1\rangle$ is localized around some nodes, which are the large degree nodes. It has a dominantly large component on node 1, which is the largest degree hub node. On the preferential attachment network, it was shown by Goh *et al.* [59] that the components of $|\lambda_1\rangle$ is localized on the largest degree node, and c_i varies from $1/\sqrt{2}$ to $1/(2\sqrt{N})$. Our plot confirms this result by Goh *et al.*. We can see from the inset that $|\langle hub|\lambda_1\rangle|^2$ does not decrease as N increases, and tends to converge to a value below 0.5. Therefore, we can conclude that our the localized state $|hub\rangle$ has a substantial overlap with the leading eigenvector, and it is a good state to choose as the initial state of the dynamics.

Recalling Eq. (3.36), we derived that τ and $P(\tau)$ depend on the index of the marked node w , when $|\lambda_1\rangle$ is not uniform. Therefore we need to take into account which node in the network was marked when evaluating the search. To this end, we first analyze and show the distribution of the search time $T = \tau/P(\tau)$. We get the distribution by

3.7. SPATIAL SEARCH ON THE SCALE-FREE NETWORK

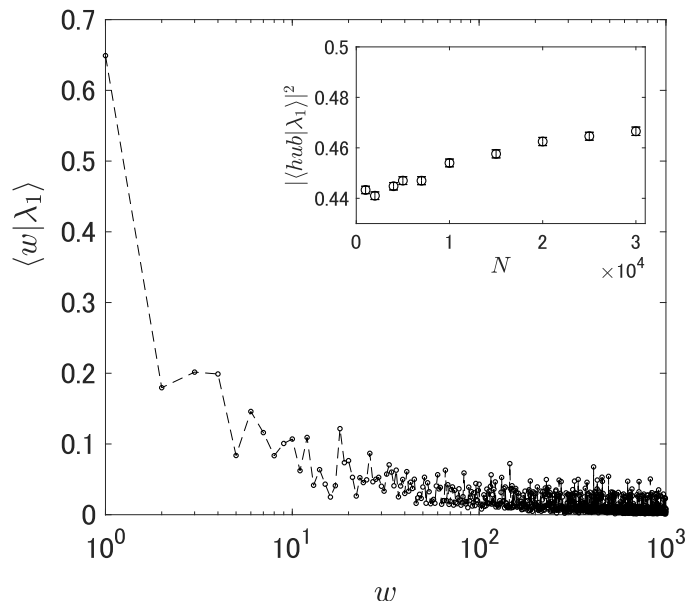


Figure 3.17: Plot of all of the components of the leading eigenvector $|\lambda_1\rangle$ of Bollobás model with network parameters $N = 1000$, $m = 10$, $\beta = 3$. We can see that the components are strongly localized around $w = 1$, which is the largest degree hub node. The inset shows the square of the component on the hub $|\langle hub|\lambda_1\rangle|^2$, plotted against the network size N . $|\langle hub|\lambda_1\rangle|^2$ tends to converge to a value close to 0.5 as the network size increases.

generating multiple samples of the Bollobás model with a fixed $\{N, m, \beta\}$, for each network repetitively mark a random node, find γ_{opt} and compute T , and finally take the histogram of T . We have excluded the largest degree hub node when randomly marking a node, since we initialize the quantum walker on that node. Figure 3.18 shows the distribution for three different values of $\beta = 2.5, 3, 3.5$, with fixed $N = 10000$ and $m = 10$. Note that the distribution is taken in logarithmic scale. The main feature in this distribution is that they have multiple peaks, meaning that there are classes of nodes that can be searched faster or slower than each other. A good fit to the distributions was a sum of log-normal functions in the form of

$$f(T) = \sum_i p_i g(T; \mu_i, \sigma_i), \quad (3.55)$$

where

$$g(T; \mu, \sigma) = \frac{1}{\sqrt{2\pi}\sigma T} \exp\left(-\frac{(\ln T - \mu)^2}{2\sigma^2}\right). \quad (3.56)$$

Therefore the distribution $f(T)$ is characterized by the mean values μ_i , standard deviations σ_i and the mixing parameters p_i (constraint such that $\sum_i p_i = 1$). For the

3.7. SPATIAL SEARCH ON THE SCALE-FREE NETWORK

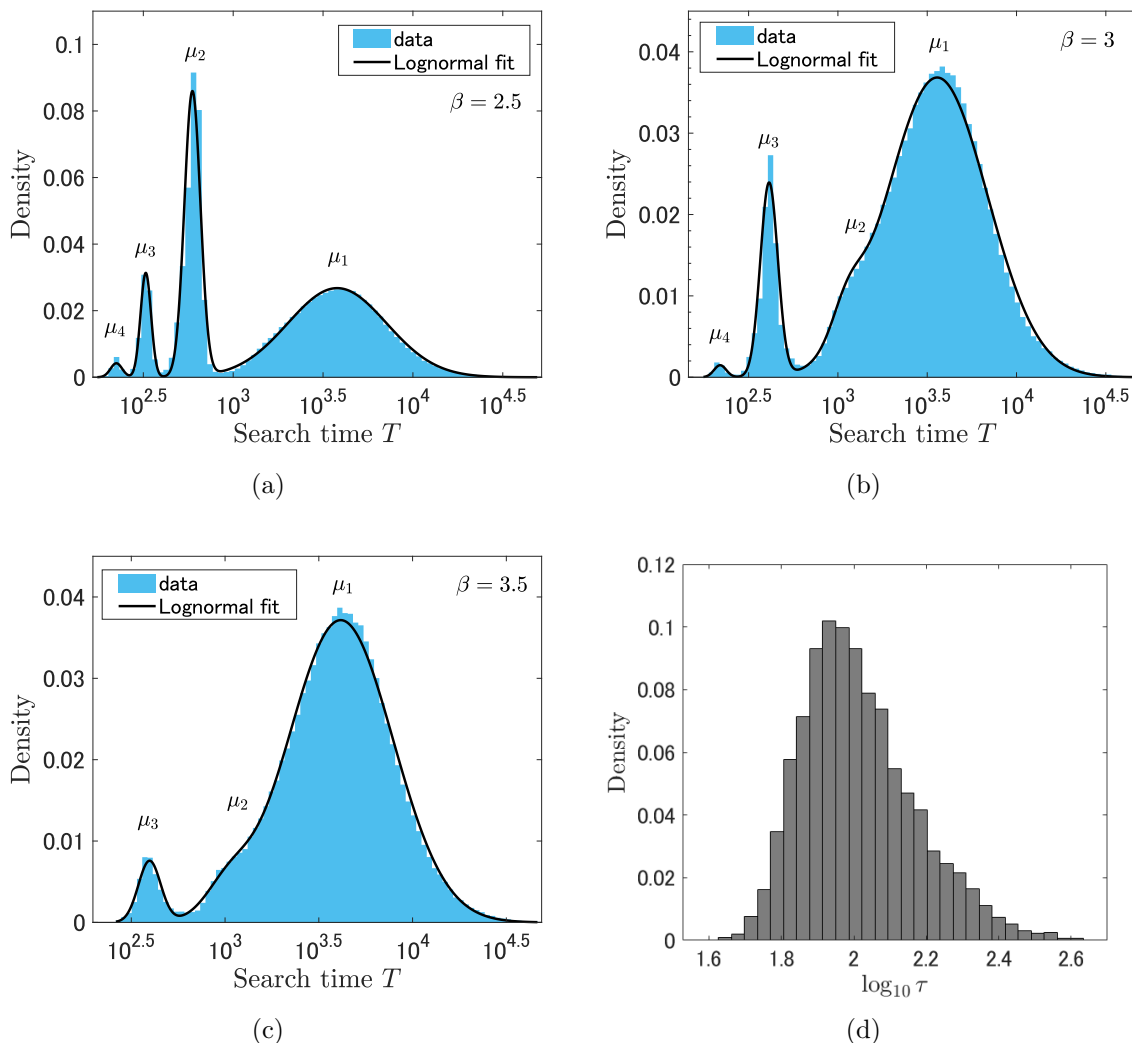


Figure 3.18: Distributions of the search time T on the Bollobás model. The data is obtained from 1000 instances of the Bollobás model with network size $N = 10^4$ and minimum degree $m = 10$, as well as randomly marking different nodes in the network. Plots from (a) to (c) corresponds to networks with different degree distribution exponents, (a) $\beta = 2.5$, (b) $\beta = 3$, and (c) $\beta = 3.5$. Plot (d) corresponds to the search time distribution of the LRP model as a comparison. The distribution tells us that the search time is 1 \sim 2 orders of magnitude different depending on which node in the network is marked. The distribution from (a) to (c) is fit to a sum of log-normal function defined as Eq (3.55).

distributions with $\beta = 2.5$ and $\beta = 3$ we take up to $i = 4$, and for $\beta = 3.5$ we take up to $i = 3$.

We understand that this multi-mode log-normal distribution results from the combination of randomness of the network and the effect of the hub node. When we take a distribution of the search time on the Erdős-Rényi random graph, or the LRP model we see a single-mode log-normal distribution (see Figure 3.18(d)). Likewise, the connec-

3.7. SPATIAL SEARCH ON THE SCALE-FREE NETWORK

tions of the nodes in the Bollobás model is mostly random, meaning that there are no characteristic structures such as communities or self-similarity, except the overall degree distribution follows a power law. However, this power law degree distribution, or the existence of the large degree hub node heavily influences the nodes around it, leading to the multi-mode distribution. In fact, we find that the narrower modes μ_3 and μ_4 (and μ_2 for $\beta = 2.5$) corresponds to the nodes that are directly connected to the largest degree hub. We will discuss this further in the next section.

Next we evaluate the scaling of the parameters μ_i, σ_i, p_i by examining their dependence on N , specifically by fitting to the function $\propto N^\xi$. The obtained scaling exponents ξ are shown in Table 3.2, as well as the plots of μ_i versus N are shown in Figure 3.19. We find two features in our results. First, for all β , μ_1 has $\xi > 0.5$ while $\mu_{i \geq 2}$ has $\xi < 0.5$. As $\xi = 0.5$ is the best known scaling of the spatial search algorithm, the scaling of $\mu_{i \geq 2}$ being $\xi < 0.5$ has to be interpreted carefully, and we are not claiming here that a spatial search faster than $T \propto N^{0.5}$ can be achieved. The search time evaluated here is the case when the measurement of the quantum walker is done at the exact optimal time τ when the probability $P(\tau)$ maximizes. In order to know the optimal time, one needs to know in prior the properties of the marked node, or at least know that the node is in one the modes of $\mu_{i \geq 2}$ in order to make a reasonable guess of the measurement time. Therefore, our result does not mean a search faster than $N^{0.5}$ can be achieved for some nodes in the

Table 3.2: Exponent ξ of each parameters of the search time distribution fit to $\propto N^\xi$. Obtained from networks with $N = 2000 \sim 10000$, $m = 10$ and $\beta = 2.5, 3, 3.5$. *const.* represents that the quantity is independent of N .

	$\beta = 2.5$	$\beta = 3$	$\beta = 3.5$
μ_1	0.731 ± 0.021	0.620 ± 0.024	0.681 ± 0.032
μ_2	0.295 ± 0.010	0.254 ± 0.040	0.256 ± 0.027
μ_3	0.253 ± 0.009	0.194 ± 0.014	0.172 ± 0.014
μ_4	0.240 ± 0.006	0.155 ± 0.012	N/A
σ_1	0.147 ± 0.026	0.180 ± 0.032	0.155 ± 0.029
σ_2	-0.013 ± 0.005	-0.133 ± 0.035	<i>const.</i>
σ_3	<i>const.</i>	-0.016 ± 0.004	<i>const.</i>
σ_4	<i>const.</i>	<i>const.</i>	N/A
p_1	0.213 ± 0.018	0.211 ± 0.022	0.112 ± 0.030
p_2	-0.132 ± 0.034	-1.65 ± 0.54	-0.942 ± 0.096
p_3	-0.478 ± 0.043	-0.423 ± 0.061	-0.613 ± 0.057
p_4	-0.847 ± 0.055	-0.920 ± 0.086	N/A

3.7. SPATIAL SEARCH ON THE SCALE-FREE NETWORK

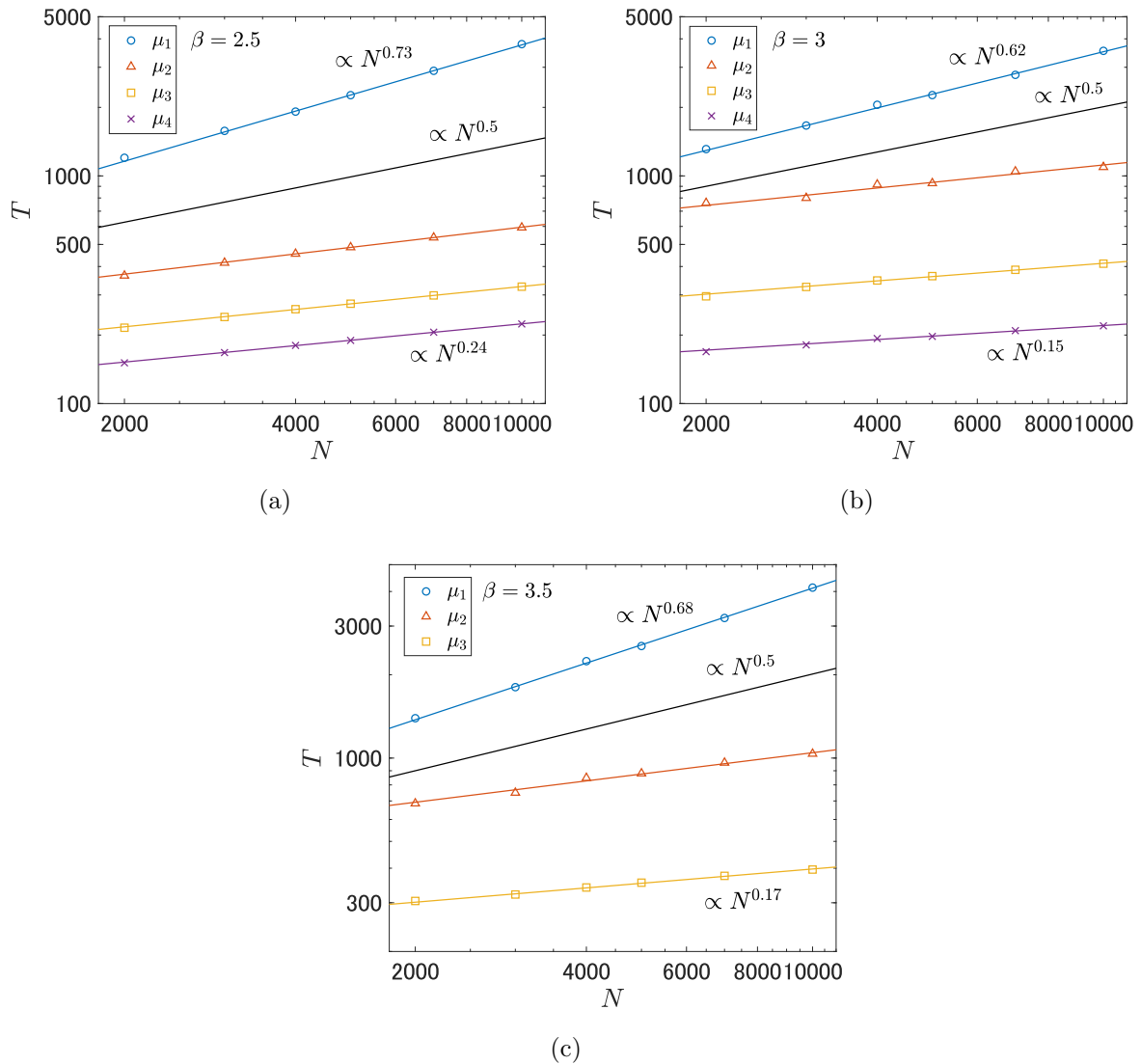


Figure 3.19: Scaling of the search time on the Bollobás model. The search time T is plotted against the network size N , while the minimum degree is fixed to $m = 10$. The three figures corresponds to different degree distribution exponents, (a) $\beta = 2.5$, (b) $\beta = 3$, and (c) $\beta = 3.5$. Each data labels μ_1, \dots, μ_4 corresponds to the average values of the search time distribution fit to the multi-mode log-normal function Eq. (3.55). The black solid line of $N^{0.5}$ is drawn as a reference to compare with the optimal search time.

3.7. SPATIAL SEARCH ON THE SCALE-FREE NETWORK

network, but rather means the quantum walker can be localized to those nodes quickly.

The second feature in our result is the agreement between the scaling of p_i and the property of the network. From Table 3.2, we see that $p_{i \geq 2}$ decays as N grows. This corresponds to the decay of the fraction of nodes those are neighbours the largest hub node, $N^{1/(\beta-1)}/N$. The result suggests that the modes $\mu_{i \geq 2}$ corresponds to the nodes those are neighbouring to the hub, or the nodes heavily influenced by the hub. This argument is also supported by the change of the distributions depending on β (see Figure 3.18). As β increases, edges will be less concentrated on the large degree nodes, letting the network to become closer to a random graph. This effect is observed as the shrinking of the $\mu_{i \geq 2}$ modes when β increases. We note that these scaling obtained from numerical simulations are only guaranteed for $N = 2000 \sim 10000$, the region where we executed the simulations.

As a conclusion of this section, the distribution of the search time T obtained by marking different nodes in the network strictly reflects the structure of the network; the combination randomness and scale-free property (i.e. existence of the hub) leads to a multi-mode log-normal distribution of T . The existence of the hub allows the quantum walker to localize on nodes that are neighbours of the hub especially fast.

3.7.3 Correlations with network measures

In this section, we interpret the search time T and the dynamics of the spatial search by investigating some centrality measures of the network. This will bridge the knowledge in complex network science and quantum dynamics. We investigate the correlation between the search time and six different centrality measures: degree centrality, eigenvector centrality [60], closeness centrality [61], betweenness centrality [62], random walk closeness centrality [63] and random walk betweenness centrality [64]. The essential result we show here is that the search time is dependent on how close the marked node is to all other node in the network, in terms of shortest path distances.

The scatter plots where the search time T is plotted against different centrality measures are shown in Figure 3.20. Here we used one instance of the Bollobás scale-free network with parameters $N = 2000, m = 5, \beta = 3$, and computed T for every single node except the hub.. Figure 3.20(a) shows the case of degree centrality $C_w^d = \sum_j^N A_{wj}/(N-1)$, which measures the fraction of nodes that are connected to the node w . This plot tells that when the marked node has large degree, the quantum walker will likely to be localized on that node quickly, but if the node has low degree, the search time is almost

3.7. SPATIAL SEARCH ON THE SCALE-FREE NETWORK

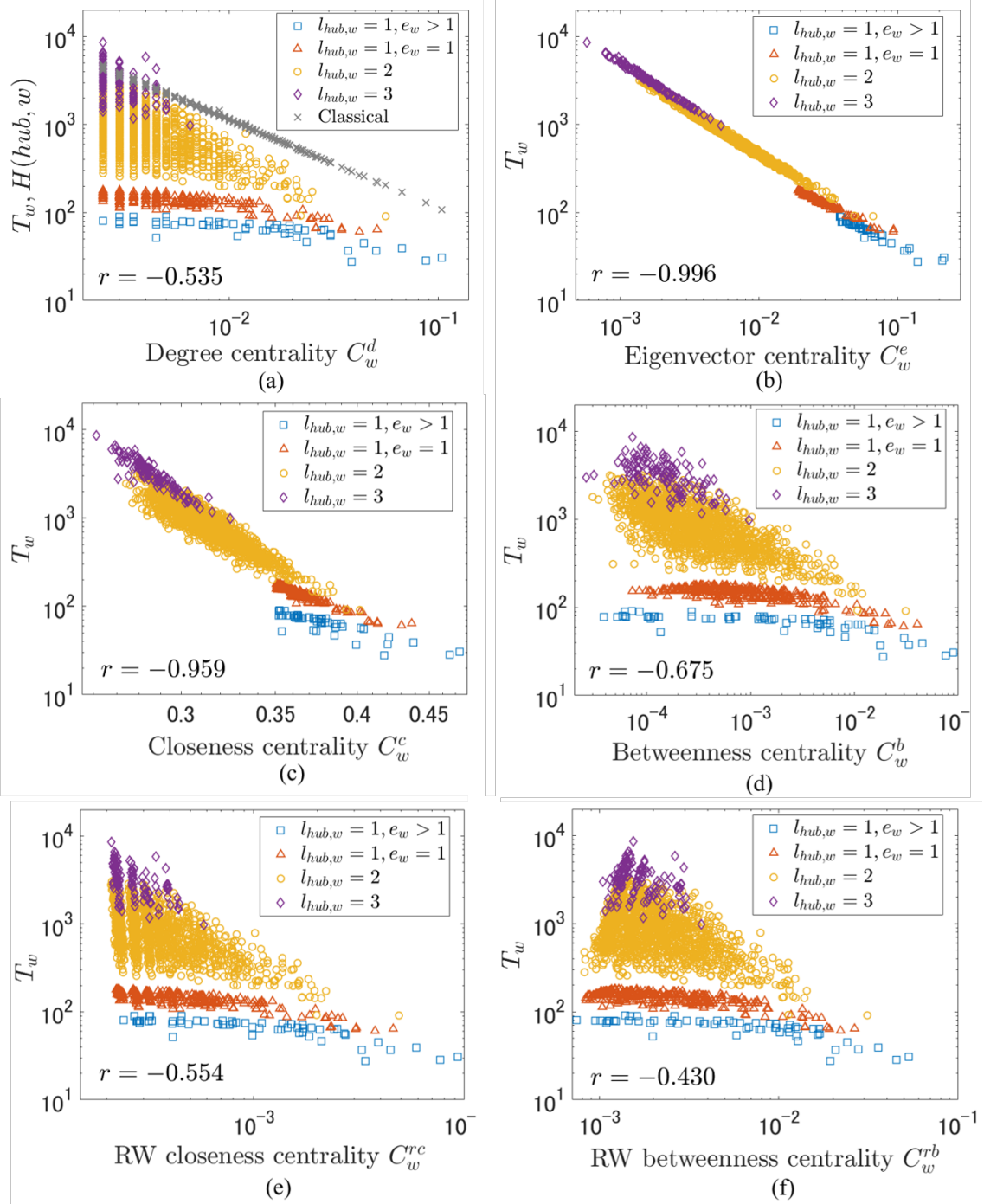


Figure 3.20: The correlation between the search time T and six different network centrality measures. The data is obtained from a network with $N = 2000, m = 5, \beta = 3$. The definition of each centrality measures are defined in the main text of this section. The data points are coloured according to the shortest path distance between the hub and the marked node $l_{hub,w}$, as well as the number of parallel edges between the hub and the marked node e_w . The clustering of the data points of different colours tells us that the search time tends to be faster as the marked node is closer to the hub. The value r in each plots represents the Pearson correlation coefficient. The best correlation is found in the eigenvector centrality (b), followed by the closeness centrality (c). In panel (a), the classical search time, namely the mean first passage time $H(hub,w)$, is also plotted.

3.7. SPATIAL SEARCH ON THE SCALE-FREE NETWORK

independent of the degree. This feature is quite different from the case of classical random walk, where the difference can be seen by comparing with the mean first passage time $H(hub, w)$ computed numerically and plotted in the same figure. The mean first passage time $H(i, j)$ is defined as the average time for the classical random walker to visit node j for the first time, starting the walk from node i . We can interpret $H(hub, w)$ as the average time to search the marked node by starting the classical random walk from the hub node. From Figure 3.20(a), we can confirm that the time it takes to search a node using random walk is proportional to its degree, which was also confirmed in [65], as well as revealing that the search using quantum walk clearly shows a different feature. The result also shows indicates that typically on the Bollobaá network, the quantum search is faster than searching by classical random walk, although there are some purple data points exceeding the classical search time.

Figure 3.20(b) shows the case of eigenvector centrality $C_w^e = |\langle \lambda_1 | w \rangle|$, which is a centrality measure based on the leading eigenvector of the adjacency matrix. The plot shows a high correlation as expected from Eq. (3.36). We also see a good correlation in Figure 3.20(c) which shows the case of closeness centrality $C_w^c = (N-1) / \sum_{j \neq w}^{N-1} l_{wj}$ where l_{wj} is the shortest path distance between nodes w and j . This measure represents how fast one can move from the node w to all other nodes using the shortest paths.

Figure 3.20(d) shows the betweenness centrality $C_w^b = \sum_{i \neq w \neq j} \sigma_{ij}(w) / \sigma_{ij}$, where σ_{ij} is the number of shortest paths from node i to j , and $\sigma_{ij}(w)$ is the number of shortest paths that goes through node w among them. The random walk closeness centrality $C_w^{rc} = N / \sum_j H(j, w)$ in Figure 3.20(e) is an alternative measure of the closeness centrality, where path lengths between nodes are measured based on the random walk process. The random walk betweenness centrality C_w^{rb} in Figure 3.20(f) is an alternative measure of betweenness centrality, where instead of counting only shortest paths, all paths contribute to the measure with a certain weight. All three of these measures are correlated with the search time in a similar way as the degree centrality.

The results presented in Figure 3.20 tells us that the quantum walk or the spatial search is a dynamics relying on the shortest paths of the network, unlike classical random walk. In the case of classical random walk, the walker chooses one neighbour randomly at each time step, and thus it is natural to understand that a node having larger degree will have higher probability to receive the walker, leading to shorter time of the search. In contrast, since the quantum walker spreads to all of the neighbours as a superposition

3.7. SPATIAL SEARCH ON THE SCALE-FREE NETWORK

state, the length of shortest paths between the nodes determines the time for the complex amplitudes to reach from a node to another, rather than the degrees. As indicated by the high correlation to the closeness centrality C_w^c , if the marked node w is averagely close to all other nodes (i.e. has high C_w^c), the quantum walker can localize on that node faster since the complex amplitudes of the quantum walker can be collected from the whole network with a shorter time.

The importance of the distances is emphasized by distinguishing the data points in Figure 3.20 based on the shortest path distances between the hub node and the marked node (see the legend of the figure). The data is well clustered depending on $l_{hub,w}$. Especially when the marked node is adjacent to the hub ($l_{hub,w} = 1$), these nodes have small shortest path distances with the other nodes by going through the hub, leading to the shortness of T .

We also examined the how the scaling of the search time $T \propto N^\alpha$ depends on the distance between the hub and the marked node $l_{hub,w}$. We computed multiple samples of T_w from network with parameters $N = 2000 \sim 10000, m = 5, \beta = 3$ and took the averaged of T_w for each $l_{hub,w}$. The obtained scaling α is shown in Table 3.3. Although we get large standard deviations of T_w since the factor determining the search time is not only $l_{hub,w}$, the scaling α roughly increases linearly as $l_{hub,w}$ grows. We assume this comes from the ballistic spread of the quantum walker.

Table 3.3: Exponent α of the average search time $T \propto N^\alpha$ for nodes with different distances from the hub $l_{hub,w}$. Networks with parameters $N = 2000 \sim 10000, m = 5, \beta = 3$ are used to obtain α .

$l_{hub,w}$	1	2	3
α	0.120 ± 0.019	0.638 ± 0.122	1.127 ± 0.205

Note that the especially short T when the marked node is adjacent to the hub is not due to the localized initial state of the quantum walker. The quantum walker does not instantaneously hop from the hub to the marked node, but instead has to traverse the entire network and acquire some phase to localize on the marked node. In fact, from Eq. (3.36) we can see that the optimal evolution time $\tau = \pi/\Delta E$ is independent of the initial state. The initial state determines the fraction of the complex amplitude that stays in the two-dimensional subspace spanned by $|E_0\rangle$ and $|E_1\rangle$, and thus only affects the maximum success probability $P(\tau)$.

3.7. SPATIAL SEARCH ON THE SCALE-FREE NETWORK

Although the high correlation between the search time and the eigenvector centrality is expected from Eq. (3.36), there are small corrections from the factor $|\langle w|\tilde{w}\rangle|$, which is essentially the success probability P . In our results, we did not see a particularly high correlation between the centrality measures and P . The best correlation we could observe was with the eigenvector centrality, with correlation coefficient $r = 0.363$. The distribution of the success probability taken over different nodes of the network is plotted in Figure 3.21, where we observe a single mode distribution peaked around 0.4.

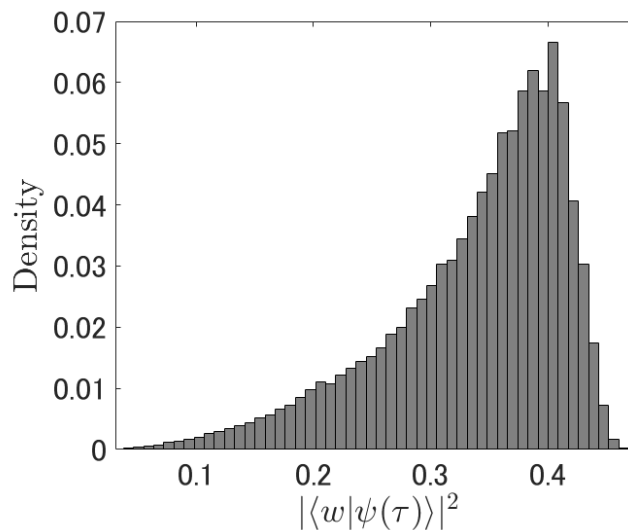


Figure 3.21: Distribution of the success probability $P(\tau) = |\langle w|\psi(\tau)\rangle|^2$, with network parameters $N = 10^4$, $m = 10$ and $\beta = 3$. The distribution is peaked around 0.4, with a long tail on the lower values. The distribution suggests that there are some nodes who are very hard to localize (i.e. very low success probability), but as we did not find a clear correlation between P and the six correlation measures investigated in this Section, we could not make a conclusion about nodes having what kind of properties are very hard to localize.

3.7.4 Limitation of the search algorithm on complex networks and translation to a state transfer protocol

As we have shown in the previous sections that the search time T is actually different depending on which node in the network is marked. This means that τ is different depending on the marked node, and thus the optimal measurement time will be different. This leads to a limitation when actually performing the search, because one will need the information of the marked in prior to performing the search algorithm. This actually breaks the rule of the search problem, as the one who aims to search for the marked

3.7. SPATIAL SEARCH ON THE SCALE-FREE NETWORK

node must not have any information about the marked node before using the search Hamiltonian.

However, we can think of some strategies to overcome this limitation. One is to give restriction on which node to mark. If we restrict to choose the marked node from the subset of nodes in the individual modes μ_i , we can make a reasonable guess of the measurement time τ . This essentially restricts the space of the search.

Another strategy we can consider is to adjust the network parameters so that τ of different modes are in harmonics. See Figure 3.22 for the conceptual explanation. For example, let's focus on the dominant modes τ_1 and τ_3 in the distribution. If we can adjust the network parameters m and β and get $\tau_1 = (2n - 1)\tau_3$ where $n = 1, 2, \dots$, we can measure at the time τ_3 at which the oscillation of $P(t)$ corresponding to the τ_1 mode is also maximized. Such adjustment is possible, as τ_1 and τ_3 can be changed by adjusting m . See Figure 3.23, where we plotted the relation between $\tau_{1,3}$ and m , with other parameters fixed at $N = 10^4$ and $\beta = 3$.

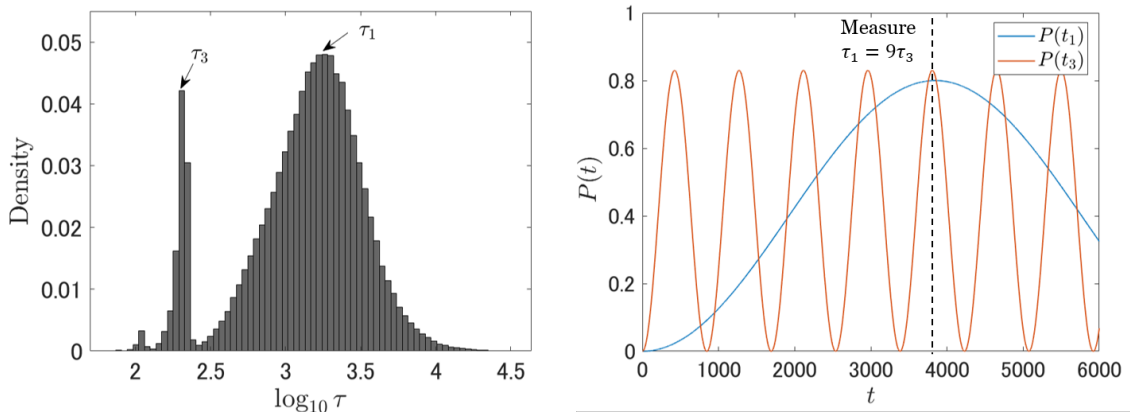


Figure 3.22: Measuring the final state at harmonic times to overcome the difference of the optimal measurement time τ . The left panel shows the distribution of the optimal measurement time of the search algorithm τ in logarithmic scale. As we have seen in Figure 3.18 that the search time $T = \tau/P$ follows a multi-mode log-normal distribution, we see here that τ is also following a very similar distribution. The right panel shows the schematic explanation of choosing the measurement time at $\tau_1 = 9\tau_3$, the moment where the success probability $P(t)$ maximizes for both modes.

One application of the spatial search algorithm on the Bollobás scale-free network is to translate the algorithm into a state transfer protocol. A state transfer protocol is a task to transfer a state, usually an arbitrary qubit state $|\phi\rangle = a|\uparrow\rangle + b|\downarrow\rangle$, between two points in the Hilbert space with high fidelity. We can assume that the quantum walker has a spin-1/2 internal degrees of freedom, and the internal degree of freedom is untouched during the time evolution on the network. If we prepare the quantum walker localized on

3.7. SPATIAL SEARCH ON THE SCALE-FREE NETWORK

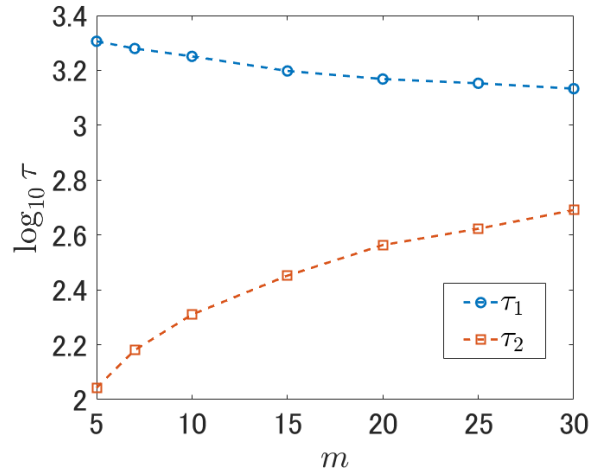


Figure 3.23: Logarithm of the optimal measurement time (the peaks τ_1 and τ_3 of the modes shown in Figure 3.22 left panel) plotted against the minimum degree of the Bollobás network m . The network size and the degree distribution exponent is fixed to $N = 10^4$ and $\beta = 3$, respectively. We can see that the optimal measurement time of the two modes approach closer to each other as m is increased, indicating the merging of the two modes. As the average degree of the network is $2m$, increasing m will increase the connectivity of the network.

the hub node, decide the target node w where to transfer the state, and then adjust the parameters of the Hamiltonian $H_s = -\gamma A_{sf} - \epsilon_w |w\rangle\langle w|$ in the same way we perform the search algorithm, we can obtain the spin state at node w after time τ with probability $P(\tau)$. Such protocol is useful as a short range quantum data bus in quantum computation or communication settings.

3.8 Conclusions and discussions

In this chapter, we have analyzed the spatial search algorithm by continuous-time quantum walk on two types of complex networks, the long-range percolation (LRP) model and the Bollobás scale-free network. We initially introduced the classical and quantum search problem in a computer science perspective, and introduced the Grover's algorithm, the first quantum algorithm that runs on a quantum computer that solves the unstructured search problem in time $O(\sqrt{N})$. We next introduced the spatial search algorithm as the physically restricted version of the Grover's algorithm. We reviewed the literature by discussing the different challenges on the field, explained the aim of our analysis based on such background. The brief summary of our aim was to analyze how the spatial search algorithm behaves on complex networks, and explore whether we can see novel features of the algorithm or find usefulness of quantum complex networks.

Next we began our analysis by starting from the basic calculation of the spatial search algorithm on the complete graph. The calculation was extended to the case for searching on arbitrary graphs, and we derived some relation between the eigenspace structure of the graph's adjacency matrix and the time complexity of the spatial search algorithm. The explanation of our numerical calculation method to analyze the spatial search algorithm followed. Next we moved on to our actual analysis and results of the spatial search algorithm on the LRP model and the Bollobás scale-free network. The novel results from our analysis can be summarized as follows.

1. On the LRP model, there is a threshold connectivity of the graph where the search time switches from optimal to non-optimal. We have found that on the LRP model with lattice dimensions $d = 1, 2$, there is a clear threshold connectivity, indicated by the exponent $\alpha = \alpha_c$, where the time complexity of the search algorithm switches from $O(\sqrt{N})$ when $\alpha \leq \alpha_c$, to a slower time complexity $O(\sqrt{N}) < T \leq O(N^2/\log^3 N)$. The average degree of the graph converges to a constant as $N \rightarrow \infty$. The existence of α_c was non-trivial and such finding of α_c provides an interesting perspective to find the general optimal condition of the spatial search algorithms. The result of α_c also indicates that the structure of the eigenspace of the LRP model changes at α_c , which is also a novel result.

3.8. CONCLUSIONS AND DISCUSSIONS

2. Having locally dense connections in the graph leads to efficient speedup of the search. The characteristic of the LRP model is in its definition of the edge generation probability function, $p_{ij} = |i - j|^{-\alpha}$, where $|i - j|$ is the Euclidean distance between pair of nodes i, j . This rule allows the model to generate edges with relatively short length, while limiting the chance to generate edges bridging large distance of the lattice to be low. Therefore, edges are rather locally concentrated around each nodes. We have compared our result against the case of the Erdős-Rényi random graph which generates edges of any length with equal probability, and found that the LRP model requires less resource (less number of edges in the large N region) to achieve optimal search. Interestingly, this result suggests that having dense connections locally is a resource efficient way to achieve optimal search rather than globally connecting random nodes.

3. The search time depends on the shortest path distances between the marked node and the rest of the nodes in the network. From the analysis on the Bollobás scale-free network, we have found there is a high correlation between the search time and the closeness centrality of the marked node. The closeness centrality of a node is a network measure which represents how much the node is close to all other nodes using the shortest paths between the nodes. Results tell us that the more the node having high closeness centrality, the more the node can be searched faster. This was purely a representation of quantum effect, which we confirmed by examining the difference with the classical random walk on the same network. The mean first passage time of the classical random walk was proportional to the degree of the node, rather than the closeness centrality. This observation could not have been possible if we have used regular graphs, since such graphs will have identical centrality for all nodes.

4. Randomness of the connections in the network leads to a log-normal distribution of the search time We have analyzed the distribution of the search time in a network, by repetitively marking different nodes in the network and computing the search time. From the LRP model, we obtained a single log-normal distribution, while from the Bollobás scale-free network we obtained a multimode log-normal distribution. We understood that the log-normal distribution appears due to the randomness of the networks. The scale-free network showed a multimode distribution due to the existence of the dominant hub node. To the best of our knowledge, the distribution of the search time was never examined before on any graphs (although statistical analysis of graphs are

3.8. CONCLUSIONS AND DISCUSSIONS

common strategy, such as measuring the distribution of eigenvalues), and we were able to discuss an interesting relation between the structure of the network and the quantum search.

5. Using networks whose leading eigenvector is localized, one can perform the search algorithm from a localized initial state We have shown that the leading eigenvector of the Bollobás scale-free network was a localized state around the hub node. This led to the availability to perform the spatial search algorithm from an initial state fully localized on the hub node. This can be helpful for experimental implementations of the algorithm, since preparing a superposition state with a carefully manipulated relative phase [66]. We can generally say that using a Hamiltonian whose leading eigenvector is a localized state, one can perform the search from a localized initial state. A star graph is another good instance of this.

We can conclude that the two complex network models we have analyzed is useful to perform the spatial search algorithm, as we can achieve the search algorithm faster than the classical algorithm. Although there are limitations in the case of Bollobás scale-free network as the optimal measurement time is different depending on which mode of the distribution the marked node belongs to. Nevertheless, it is possible to overcome such limitation with an constant factor overhead in the time complexity, if we adjust the network parameters so that the optimal measurement time of the different modes are in harmonics. Finally, it is also important that the network structure in these complex networks can be noisy in a sense that each of the edge does not need to be in a fixed position, and only the statistical property of the network is important.

Chapter 4

Simulation of complex quantum networks using driven quantum systems

4.1 Simulating complex network structures with effective Floquet Hamiltonians

In the previous chapter, we have shown that complex quantum networks are useful for quantum search algorithm, and from these networks one can see fruitful dynamics correlated with the network structure that cannot be observed from regular or lattice structures. Now the problem comes down to how to actually engineer such complex quantum networks. The system needs to contain complex, non-regular and long-range transitions between states in the Hilbert space. As we reviewed in the Chapter 1, the technologies to manipulate and generate interactions between multiple single qubit systems are becoming available in the labs. Few body systems with network-like, non-regular interaction structures may be available using these technologies. However, this approach may come to a bottleneck when we want to scale up the system to actually get a large-scale complex network structure. Also, manipulating the interactions spatially can have limitations. For example, superconducting qubits are usually placed on a planar two-dimensional surface, limiting the ability to couple qubits those are spatially far apart.

In this chapter we present a strategy to *simulate* complex quantum networks using driven quantum systems. We will use the term *simulate* rather than *engineer*, as we

4.2. SIMULATING RANDOM NETWORKS WITH PERIODICALLY MODULATED OPTICAL WAVEGUIDES

are going to create an effectively complex transition between the states via the effective Hamiltonian of a time-periodic Floquet system, rather than engineering spatially complex interactions. Based on Floquet theory, we look at the periodic times of the dynamics generated by the time-periodic Hamiltonian $H(t + T) = H(t)$, such that

$$U(T; 0) = \mathcal{T} \exp \left(-i \int_0^T H(\tau) d\tau / \hbar \right) = \exp(-iH^{\text{eff}}T/\hbar), \quad (4.1)$$

where \mathcal{T} is the time ordering operator. H^{eff} is the effective Hamiltonian where we find the complex quantum network. H^{eff} contains the effective transitions during one period of the time evolution by $H(t)$. As we will see in the two examples analyzed in the following sections, H^{eff} can have transition structures which has the properties of random graphs or scale-free networks, when the system is driven with certain conditions. This is shown by computing the matrix representation of H^{eff} and viewing this as the adjacency matrix of a network. The method of such analysis can be found in Sections 2.4 and 2.9 of Chapter 2. The specific physical systems analyzed here to simulate the complex quantum networks are the coupled optical waveguides and the time crystalline system. Some experimental schemes for such systems are also shown to discuss the possibility of future experimental realizations.

4.2 Simulating random networks with periodically modulated optical waveguides

The first example we propose to simulate complex quantum networks is a photonic system where photons propagate through an array of coupled optical waveguides. We will show theoretically that by modulating the coupling constants between the waveguides periodically in the propagation direction, this can be analyzed as a time-periodic Hamiltonian system. We analyze the corresponding system Hamiltonian using Floquet theory, and show that the derived effective time-independent Hamiltonian will have a structure similar to random graphs, when displayed in the tight-binding Hamiltonian matrix form. To start the discussion, we will first consider a simple case where one photon propagates through N statically coupled waveguides. This corresponds to a unitary time evolution generated by a N -dimensional time-independent tight-binding Hamiltonian with its transition structure equal to the coupling constants between the waveguides. Next we

4.2. SIMULATING RANDOM NETWORKS WITH PERIODICALLY MODULATED OPTICAL WAVEGUIDES

will consider a case where two photons propagate through the same N statically coupled waveguides, and show that this corresponds to a unitary time evolution generated by a $N(N + 1)/2$ -dimensional tight-binding Hamiltonian. Finally we add a drive to the Hamiltonian by designing a periodically modulated waveguide array.

4.2.1 Single or two-photon state propagating through an coupled waveguide array

First we introduce and define the quantum system we consider. We assume a system composed of optical waveguides. A optical waveguide is a narrow (order of microns to sub-microns) dielectric material whose refractive index is higher than the surrounding material. When photons or classical laser is input to a waveguide, the light propagates through the waveguide due to the total internal reflection. The loss of light during the propagation is very low in a ideal waveguide, allowing to characterize the system as closed coherent dynamics. Such device is typically fabricated by focusing a femtosecond pulse laser in a silica glass medium which writes the waveguide structure. This utilizes the property of the silica with germanium atoms doped, which changes its refractive index when an ultraviolet pulse is focused. See [67, 68] for a review. When two waveguides are placed next to each other orthogonal to the propagation direction, the light can tunnel through between the waveguides. Such waveguides are stated as coupled waveguides. The origin of the tunneling of light is the evanescent field that propagates outside the waveguide, which decays exponentially after propagating for a distance about the wavelength of the light. Therefore, the waveguides are strongly coupled when they are as close as the order of the light wavelength.

Let's consider the situation where a single mode photon propagates through an array of N coupled waveguides. The Hamiltonian of the system can be written as

$$H_{wg} = \sum_i^N D_i \hat{a}_i^\dagger \hat{a}_i + \sum_{i,j}^N C_{i,j} \hat{a}_i^\dagger \hat{a}_j. \quad (4.2)$$

Here \hat{a}_i and \hat{a}_i^\dagger are the annihilation and creation operator of mode i (equivalently annihilates/creates one photon in the propagation mode of waveguide i). D_i is the propagation constant and $C_{i,j}$ is the coupling constant between waveguides i and j . As the system can be considered as a closed system, the dynamics is unitary with the time evolution

4.2. SIMULATING RANDOM NETWORKS WITH PERIODICALLY MODULATED OPTICAL WAVEGUIDES

operator given by $U(t) = \exp(-iH_{wg}t/\hbar)$.

First we consider a case where a single photon, initially injected into waveguide i , propagates through the waveguide, which can be described by the time evolution of the creation operator \hat{a}_i^\dagger . To obtain time evolution of \hat{a}_i^\dagger , we consider the Heisenberg equation of motion,

$$\frac{\partial \hat{a}_i^\dagger}{\partial z} = \frac{n}{c} \frac{\partial \hat{a}_i^\dagger}{\partial t} = i \left[H_{wg}, \hat{a}_i^\dagger \right] = i D_i \hat{a}_i^\dagger + i \sum_j^N C_{ij} \hat{a}_j^\dagger, \quad (4.3)$$

where we used commutation relation of bosonic operators $[a_i, a_j^\dagger] = a_i a_j^\dagger - a_j^\dagger a_i = \delta_{ij}$ and $[a_i^\dagger, a_j^\dagger] = [a_i, a_j] = 0$ to obtain the final expression. We also used the phase velocity of the light $c/n = \partial z / \partial t$, where c is the speed of the light in vacuum, n is the effective refractive index of the waveguides, z is the position of the photon in the propagation direction and t is the time. Note that evolution of the photon along the spatial direction z corresponds to the time evolution of the system. The solution of the equation is

$$\hat{a}_i^\dagger(z) = \sum_j^N (e^{izC})_{ij} \hat{a}_j^\dagger(0) = \sum_j^N U_{ij} \hat{a}_j^\dagger(0). \quad (4.4)$$

Here, the coupling constants C_{ij} can be viewed as the matrix elements of a $N \times N$ symmetric matrix C . The diagonal entries of C is equal to the propagation constant $C_{ii} = D_i$. U_{ij} is the matrix elements of the unitary matrix e^{izC} . Importantly, from Eq. (4.4), the matrix $-C$ is equivalent to a tight-binding Hamiltonian,

$$H_{tb} = -C = - \sum_i^N D_i |i\rangle \langle i| - \sum_{i \neq j}^N C_{ij} (|i\rangle \langle j| + |j\rangle \langle i|). \quad (4.5)$$

The basis states $\{|i\rangle\}$ corresponds to the single photon Fock states $\{|1\rangle_i\}$.

Next we consider a case where two indistinguishable photons propagate through the waveguide array. To obtain the propagation of two photons initially injected into waveguides i and j , we use Eq. (4.3) while replacing \hat{a}_i^\dagger by $\hat{a}_i^\dagger \hat{a}_j^\dagger$, which yields to

$$\frac{\partial \hat{a}_i^\dagger \hat{a}_j^\dagger}{\partial z} = i \left[H_{wg}, \hat{a}_i^\dagger \hat{a}_j^\dagger \right]. \quad (4.6)$$

For simplicity, if we consider the waveguides are coupled in a one dimensional chain with

4.2. SIMULATING RANDOM NETWORKS WITH PERIODICALLY MODULATED OPTICAL WAVEGUIDES

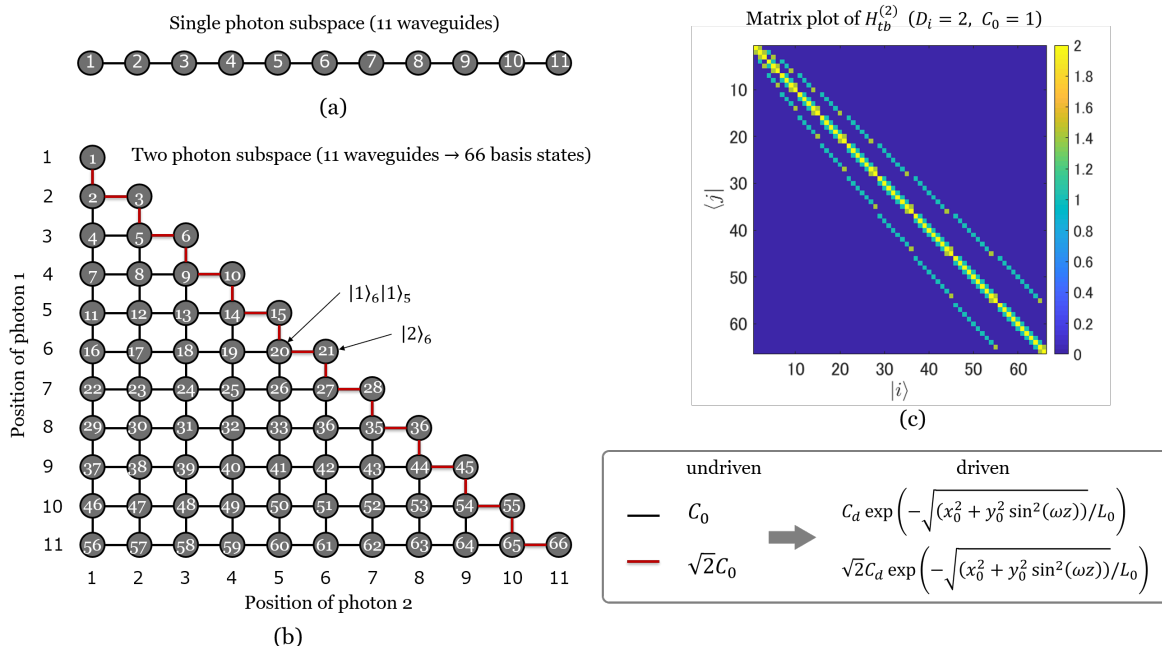


Figure 4.1: Graphical representation of the (a) single and (b) two-photon subspace of Eq. (4.2). The waveguide array is assumed to be in a one-dimensional nearest-neighbour coupled configuration of $N = 11$ waveguides. The dimension of the single-photon and two-photon subspaces are $N = 11$ and $N_b = N(N + 1)/2 = 66$, respectively. The black and red coloured edges between the nodes corresponds to different coupling strength of the modes. (c) is the tight-binding Hamiltonian matrix plot of Eq. (4.8), which corresponds to the subspace in panel (b). By assuming a periodically modulated waveguide array introduced in Section 4.2.2, we simulate a periodic drive on the couplings as indicated in the box below (c).

uniform coupling constants C_0 , we get

$$\frac{\partial \hat{a}_i^\dagger \hat{a}_j^\dagger}{\partial z} = i(D_i + D_j) \hat{a}_i^\dagger \hat{a}_j^\dagger + iC_0 \left[\hat{a}_i^\dagger \hat{a}_{j-1}^\dagger + \hat{a}_i^\dagger \hat{a}_{j+1}^\dagger + \hat{a}_{i-1}^\dagger \hat{a}_j^\dagger + \hat{a}_{i+1}^\dagger \hat{a}_j^\dagger \right]. \quad (4.7)$$

In this two-photon situation, it is still possible to obtain a tight-binding form of the Hamiltonian by only focusing on the two-photon subspace of the whole Hamiltonian shown in Eq. (4.2). We shall consider the subspace of the Hilbert space spanned by $\{|1\rangle_i|1\rangle_j, |2\rangle_l\}$. Note that the photons are indistinguishable (photons commute) here. We take out from H_{wg} the matrix elements according to this basis set (e.g. $\langle 1|_i \langle 1|_j H_{wg} |1\rangle_k |1\rangle_l$), and define a tight-binding Hamiltonian matrix form, that can be conventionally written as

$$H_{tb}^{(2)} = - \sum_r^{N_b} D_r |r\rangle \langle r| - \sum_{r \neq s}^{N_b} C_{rs} (|r\rangle \langle s| + |s\rangle \langle r|), \quad (4.8)$$

4.2. SIMULATING RANDOM NETWORKS WITH PERIODICALLY MODULATED OPTICAL WAVEGUIDES

where r, s are the numbering of the two-photon Fock states, and $N_b = \binom{N}{2} + N = N(N+1)/2$. Importantly, the dimension of the subsystem has grown to the order of N^2 . We are effectively treating the two photon Fock states at 2 of the N sites as a single particle at one of the N_b sites. The diagonal entries $D_r = D_i + D_j$ depends on the propagation constants of the two waveguides where the pair of photons propagate. The off diagonal entries C_{rs} are equal to C_0 or $\sqrt{2}C_0$ depending on the coupled states. A graphical representation of $H_{tb}^{(2)}$ is shown in Figure 4.1. Panel (a) represents the one-dimensionally coupled N waveguides (i.e. single photon subspace of H_{wg}), while panel (b) represents the two photon subspace of H_{wg} , which is equivalent to $H_{tb}^{(2)}$. The matrix entries of $H_{tb}^{(2)}$ is also plotted in panel (c) with parameters set to $N = 11, D_i = D = 1, C_0 = 1$.

4.2.2 Periodically modulated waveguide array and it's effective Hamiltonian

The treatment of the Hamiltonian of a coupled waveguide array with a bi-photon input, as discussed above, is already explored in the literature [69–71]. Now we move one step forward by applying a time-periodic (i.e. periodic in propagating z -direction) drive on the system to obtain a time periodic Hamiltonian in the form of

$$H_{tb}^{(2)}(z) = - \sum_r^{N_b} D_r |r\rangle\langle r| - \sum_{r \neq s}^{N_b} C_{rs}(z) (|r\rangle\langle s| + |s\rangle\langle r|). \quad (4.9)$$

Waveguides are static objects and in principle cannot dynamically modify their coupling or propagation constants in time. However, as the distance in the z direction corresponds to the time for the propagating photons, we can spatially modify the waveguides along the z direction to let the photons feel the change of the coupling and propagation constants in time.

We designed a $N = 11$, one-dimensional nearest-neighbour coupled, on-site static disordered, periodically modulated waveguides as shown in Figure 4.2. The waveguides are designed to oscillate in the y axis direction, as a function of $y_0 \sin(i\pi + \omega z)$. $i = 1, 2, \dots, N$ is the index of the waveguide, while ω is the frequency of the drive. We shall consider how the coupling constants $C_{ij}(z)$ would change. First, we fix the spacing between the waveguides along the x axis direction to x_0 . We assume the waveguides are cylindrical and calculate the distance between the center of the cylindrical waveguides, $L_{ij}(z)$. We

4.2. SIMULATING RANDOM NETWORKS WITH PERIODICALLY MODULATED OPTICAL WAVEGUIDES

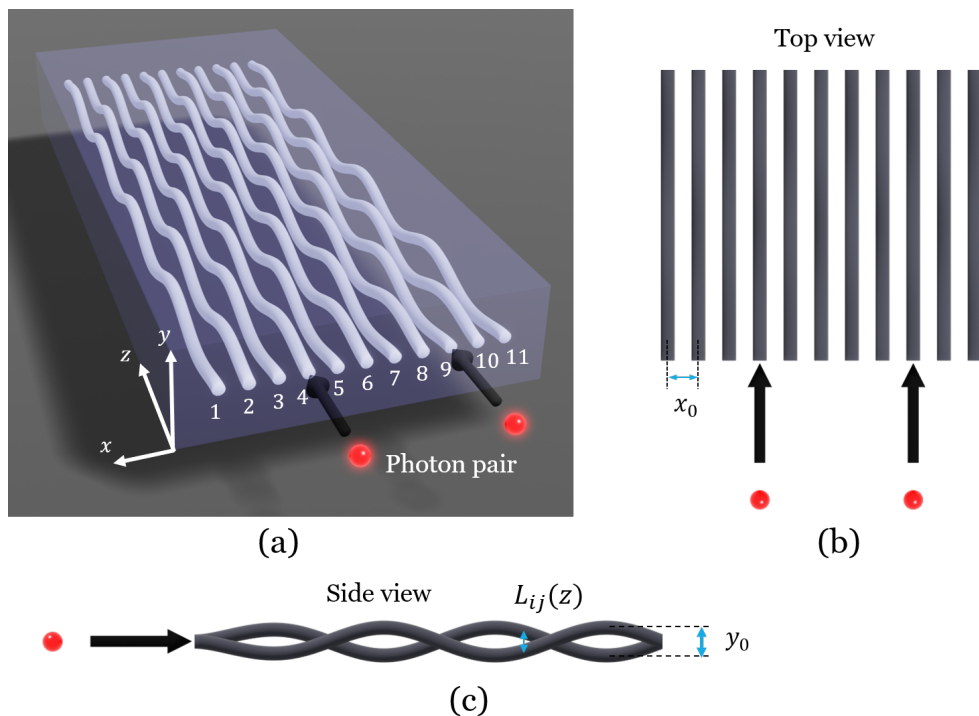


Figure 4.2: Illustration of the periodically modulated optical waveguides. Each panel corresponds to (a) the overall view, (b) the top view and (c) the side view. Two photons which are temporally indistinguishable are injected into arbitrary modes of the array. The spacing between adjacent waveguides in the x -axis direction is fixed to x_0 , while the waveguides are periodically bent up to distance y_0 in the y -axis direction to periodically change their spacing in the y -axis direction. The actual distance between the waveguides in the xy -plane is represented as $L_{ij}(z)$. This leads to a periodic change of the coupling constant between the waveguides, as shown in Eq. (4.11).

can calculate that

$$L_{ij}(z) = \sqrt{x_0^2 + y_0^2 \sin^2(i\pi + \omega z)} = \sqrt{x_0^2 + y_0^2 \sin^2(\omega z)}. \quad (4.10)$$

The coupling constant is known to depend exponentially on the distance between the waveguides [70], such as $C \sim C_d e^{-L/L_0}$. We substitute Eq. (4.10) and get

$$C_{ij}(z) = C_d \exp\left(-\sqrt{x_0^2 + y_0^2 \sin^2(\omega z)}/L_0\right). \quad (4.11)$$

The coupling constant oscillates between $C_d \exp(-x_0/L_0)$ and $C_d \exp(-\sqrt{x_0^2 + y_0^2}/L_0)$ with frequency 2ω . Given the coupling constants between the waveguides, the coupling constants between the two-photon states represented as $C_{rs}(z)$ in Eq. (4.9) will be equal to $C_{ij}(z)$ or $\sqrt{2}C_{ij}(z)$ depending on the photon number of the states (see the box below

4.2. SIMULATING RANDOM NETWORKS WITH PERIODICALLY MODULATED OPTICAL WAVEGUIDES

panel (c) of Figure 4.1).

The propagation constant must also depend on z as the direction of the propagation mode varies with z . However we can replace it with an effective shift of the propagating constant $D_i \rightarrow D_i - \Delta D$. As all of the waveguides are modulated equally, we consider all waveguides acquire an equal constant shift ΔD .

We also add a diagonal disorder into the Hamiltonian, in order to induce randomness in the time evolution. This is modelled by setting D_i for each waveguide as a random number which fluctuates around the mean value with a range of W . The disorder is physically modelled by the small radius differences among the waveguides, which changes their propagation constants. We must note that changing the propagation constants (i.e. the propagation modes) of each waveguide will induce changes in the coupling constants as well. We may also need a multi-mode photon source as an input in order to couple the photons to the slightly different propagation modes of each waveguide. This can lead to a dephasing effect during the time-evolution, and thus the actual dynamics when this situation is experimentally implemented can be different from the Hamiltonian of Eq. (4.9). We leave this discussion as a future work, and at this point investigate how the periodic coupling constant $C_{ij}(z)$ and the diagonal disorder D_i can simulate dynamics on complex quantum networks.

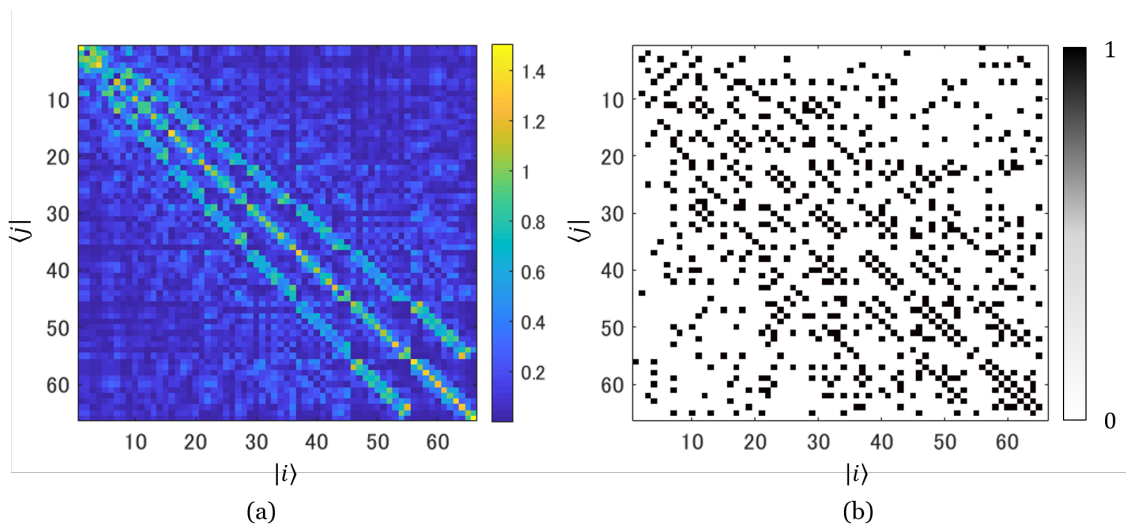


Figure 4.3: (a) The matrix plot of the effective Hamiltonian H^{eff} and (b) the resonance-rule-applied adjacency matrix A of the driven waveguide array with two-photon input. The dimension of the matrix is 66.

Given these conditions, a numerical calculation was conducted to obtain the Floquet

4.2. SIMULATING RANDOM NETWORKS WITH PERIODICALLY MODULATED OPTICAL WAVEGUIDES

operator and the effective Hamiltonian H^{eff} of one period of the Hamiltonian, as defined in Eq. (4.1). The parameters are set to satisfy $C_d \exp(-x_0/L_0) = C_0 = 1$ and $C_d \exp\left(-\sqrt{x_0^2 + y_0^2}/L_0\right) = C_0 e^{-2} = e^{-2}$, while $D_i = D + W$ with $D = 1, W \in [-0.1, 0.1]$. The frequency was set to a low frequency regime $\omega = 2\pi$ to obtain non-trivial effects [72]. Once the effective Hamiltonian was obtained, we interpret this as a graph and applied the resonance rule $|D_r - D_s| < |C_{rs}|$ to draw the edges between the nodes. The effective Hamiltonian H^{eff} and the adjacency matrix A is shown in Figure 4.3. The graph corresponding to A is visualized in Figure 4.4.

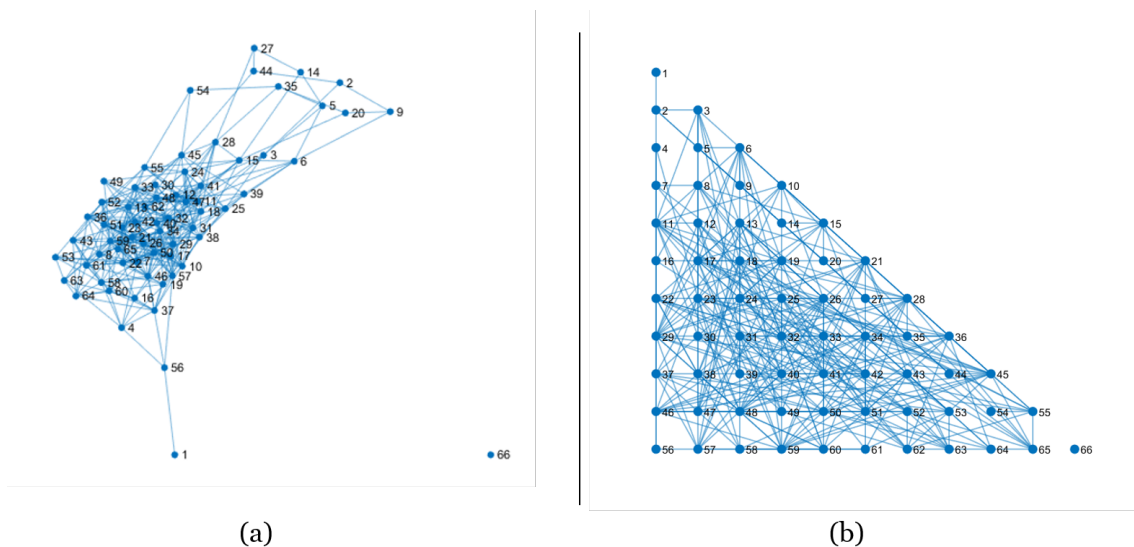


Figure 4.4: The graph visualization of the adjacency matrix plotted in Figure 4.3(b), which corresponds to the driven waveguide array with two-photon input. The graph contains $N_b = 66$ nodes, and in panel (a) the nodes are positioned according to the force-directed drawing method. In panel (b), the same graph is plotted with a different positioning of the nodes, which is the same way took in Figure 4.1(b). We can clearly see that the graph topology and connectivity has dramatically changed compared to the undriven counterpart.

From the effective Hamiltonian and the graph, we can see that the structure contains non-nearest neighbour hopping that were not present in the undriven counterpart (Figure 4.1(c)). One can see from the effective Hamiltonian matrix plot (Figure 4.3(a)) that the original nearest neighbour entries are still present, but blurred, giving rise to the non-local entries. The diagonal entries are also modified compared to the undriven Hamiltonian. In order to visualize the major transitions in the effective Hamiltonian, the resonance-condition-applied adjacency matrix A is obtained as Figure 4.3(b), with the graph drawn in Figure 4.4. For the visualized graph in Figure 4.4(a), the nodes of the graph is positioned based on the force-directed graph drawing method [73] in order to

4.2. SIMULATING RANDOM NETWORKS WITH PERIODICALLY MODULATED OPTICAL WAVEGUIDES

show that the graph is connected densely in certain regions (the positions of the nodes and the length of the edges does not have any correspondence to the coupling strength C_{rs}). For the visualized graph in Figure 4.4(b), the nodes of the graph is positioned in the same way as Figure 4.1(b). We can see that many nodes are connected densely (dynamics are complex), while some nodes have small number of connections or some nodes are even isolated.

These results clearly show the appearance of the non-local transitions. By computing the degree of each nodes $k_s = \sum_r A_{rs}$ and obtaining the degree distribution from 30 realizations of the disorder, an broad distribution was obtained (see Figure 4.5). Although the Poisson distribution did not fit the result, we can still understand that the graph has a random graph-like complex structure. The local peak in the distribution around $k = 3, 4$ comes from the nearest-neighbour transitions. The results shows the potential ability of coupled waveguides to simulate complex network structures by combining the multi-photon state and the periodic modulation strategy.

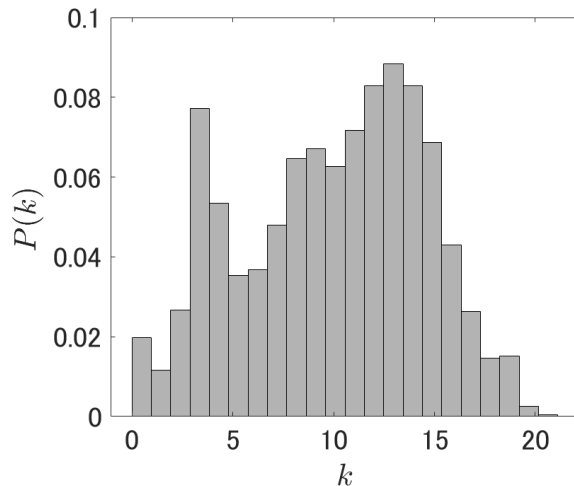


Figure 4.5: The degree distribution of the graph in Figure 4.4. k is the degree of a node. The distribution is taken from 30 realizations of the effective Hamiltonian using different disorder sequence of D_i . We can see a broad distribution, indicating that the graph has random connections.

Trade-off between the complex dynamics and the length of time evolution

Here we discuss why the non-nearest neighbour transitions appear in the driven system, and also mention about the trade-off when realizing such transitions. First we point out that in order to realize the non-nearest neighbour transitions and the complex dynamics, one needs to drive the system in the low frequency regime. Such low frequency regime

4.2. SIMULATING RANDOM NETWORKS WITH PERIODICALLY MODULATED OPTICAL WAVEGUIDES

means that the driving frequency ω is comparable to the energy bandwidth (i.e. the difference between the smallest and largest energy) of the undriven system. For example, it was shown that driving a system with on-site disorder with a low frequency result to chaotic dynamics [24]. In our calculation, we chose $\omega = 2\pi$, which is comparable to the bandwidth of the undriven waveguide Hamiltonian we considered. See Figure 4.6(a) which compares the energy spectrum of the undriven and driven systems. Note that the spectrum (quasi energies) of the driven system is bound by $-\omega/2 \leq E_i \leq \omega/2$. We have observed the complex network structure using this value of ω , but as a consequence, the energy bandwidth of the system has shrank. The undriven system has a bandwidth around 8, from Figure 4.6(a). As the energy scale of the system has decreased by the driving, the time scale of the system will increase. This means that one requires longer length of time evolution in order to realize the complex dynamics.

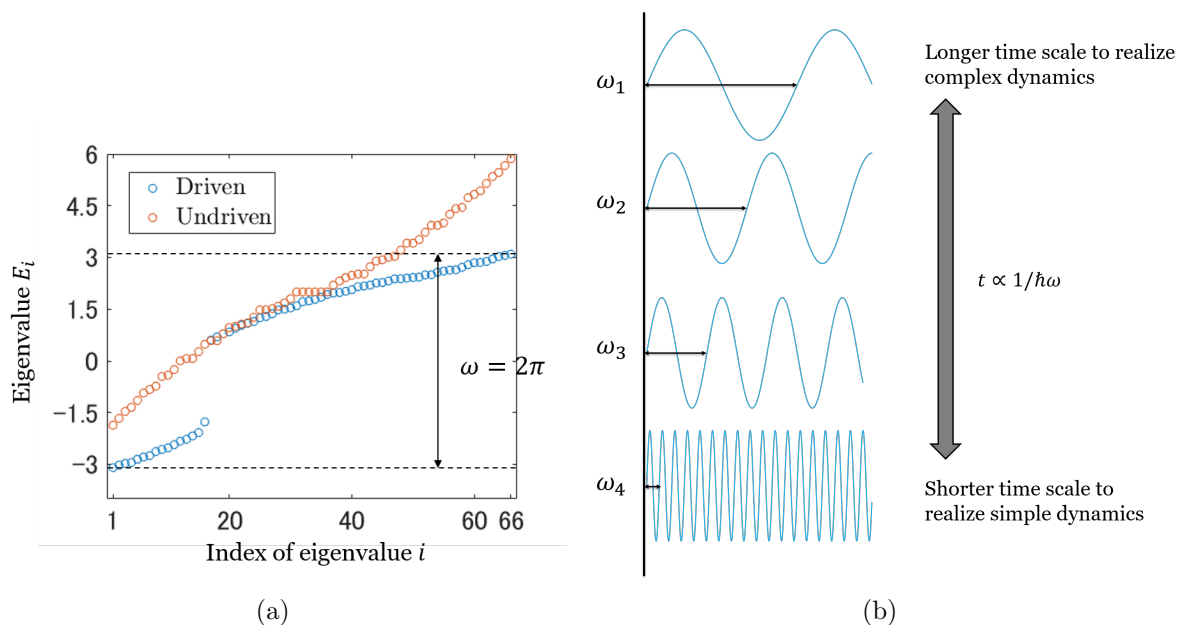


Figure 4.6: (a) The energy eigenvalues of the undriven waveguide and the quasi energies of the effective Hamiltonian of the driven waveguide. (b) A diagram describing that a lower frequency drive generates complex dynamics, while as a trade-off the necessary length of time evolution increases.

We can think this as the trade-off between the time scale of the system and the realization of the complex dynamics. In Figure 4.6(b), the illustrative description of this trade-off is shown. With a high frequency drive, the time to realize one period of the effective Hamiltonian is shorter, but the resulting dynamics is simple (since the high frequency limit corresponds to the undriven case). On the other hand, with a low

4.2. SIMULATING RANDOM NETWORKS WITH PERIODICALLY MODULATED OPTICAL WAVEGUIDES

frequency drive, the time to realize one period of the effective Hamiltonian is longer, resulting to complex dynamics. We can interpret that the complex network structure is captured from the low frequency driven system since the dynamics of a longer time scale is averaged when obtaining the effective Hamiltonian.

4.2.3 Preparation of the two photon source as the input state of the waveguide array

In the previous sections, we have investigated the effective Hamiltonian of the periodically modulated waveguide array, where single or two-photon states were injected. We have seen that in the two-photon case, the dimension of the Hilbert space expands and complex network structures can be observed by mapping the dynamics to the time evolution generated by the single-particle tight-binding Hamiltonian. In order to conduct such experiment in the labs, an indistinguishable two-photon state has to be prepared with high fidelity and rate. In this section we discuss the experimental method to generate such two-photon state, and propose a scheme using the spontaneous parametric down conversion (SPDC) from the non-linear crystal. The key feature of the two-photon source is that (i) one can generate a polarization distinguishable two-photon state (ii) or select to generate a polarization entangled state, (iii) the photons are frequency degenerated, (iv) have high rate of emission and spectral bandwidth due to the usage of type-0 non-linear crystal, (v) and free of postselection.

Such photon source can be used as a reliable two photon input state to observe the dynamics through the driven waveguide array. First of all, the two photons has to be highly indistinguishable in order to simulate the complex dynamics including the interference of the photons. If the photons are completely distinguishable, the output result we get is just a joint probability of two independent photons propagating through a one-dimensional waveguide array (i.e. no quantum interference occurs during the propagation). Furthermore, if we use the photon pair generated from a type-0 quasi-phase matched non-linear crystal, the photons have a broad bandwidth in the frequency domain compared to other types of non-linear crystals [74]. This potentially enables additional controllability on the effective Hamiltonian of the system. If we prepare a spectrally non-degenerate, yet partially overlapping photon pair and conduct a measurement that does not resolve the frequency, we can simulate an open dynamics that has partial loss of coherence to the environment. This can result to an effective Hamiltonian having different structure com-

4.2. SIMULATING RANDOM NETWORKS WITH PERIODICALLY MODULATED OPTICAL WAVEGUIDES

pared to the fully closed dynamics. Therefore, here we select to use the SPDC photons from a type-0 periodically poled non-linear crystal, and propose a scheme to prepare a two-photon state ready-to-use for the input state of the waveguide array.

To start explaining the scheme, let us first define the notations of the polarization states of the photon,

$$|H\rangle = \begin{pmatrix} 1 \\ 0 \end{pmatrix}, \quad |V\rangle = \begin{pmatrix} 0 \\ 1 \end{pmatrix}, \quad |D\rangle = \frac{|H\rangle + |V\rangle}{\sqrt{2}}, \quad |A\rangle = \frac{|H\rangle - |V\rangle}{\sqrt{2}}. \quad (4.12)$$

Each of them represent H : horizontal, V : vertical, D : diagonal, and A : anti-diagonal polarization. The scheme of the photon source is shown in Figure 4.7. We use the spontaneous parametric down-conversion (SPDC) process, where a pump photon is converted to two lower energy photons while satisfying the energy conservation law $\hbar\omega_{pump} = \hbar\omega_{signal} + \hbar\omega_{idler}$. We must use a periodically-poled (pp) non-linear crystal since the converted photons are emitted collinearly. To this end we use the ppKTP crystal. The scheme is constructed by forming an interferometer including the ppKTP crystal, two half-wave plates with angles set to 45° (HWP1) and 22.5° (HWP2).

The input photon is injected into the interferometer by passing through the polarizing beam splitter (PBS). The H-component of the photon that passed through the PBS round trips the interferometer in the clockwise direction [see Figure 4.7(a)]. This photon is converted to the D state by the HWP2, and only the V component of the state contributes to the SPDC conversion $|V\rangle \rightarrow |VV\rangle$ such that the state after the crystal is

$$|\psi_a\rangle = |VV\rangle. \quad (4.13)$$

The down-converted photons are rotated by HWP1 [see Figure 4.7(b)] which leads to

$$|\psi_b\rangle = |HH\rangle. \quad (4.14)$$

The pump photon enters the crystal again after passing through HWP1. The V component again contributes to the SPDC conversion, and will be superposed with the photon pair generated in the first conversion [see Figure 4.7(c)],

$$|\psi_c\rangle \propto |HH\rangle + e^{i\phi}|VV\rangle, \quad (4.15)$$

4.2. SIMULATING RANDOM NETWORKS WITH PERIODICALLY MODULATED OPTICAL WAVEGUIDES

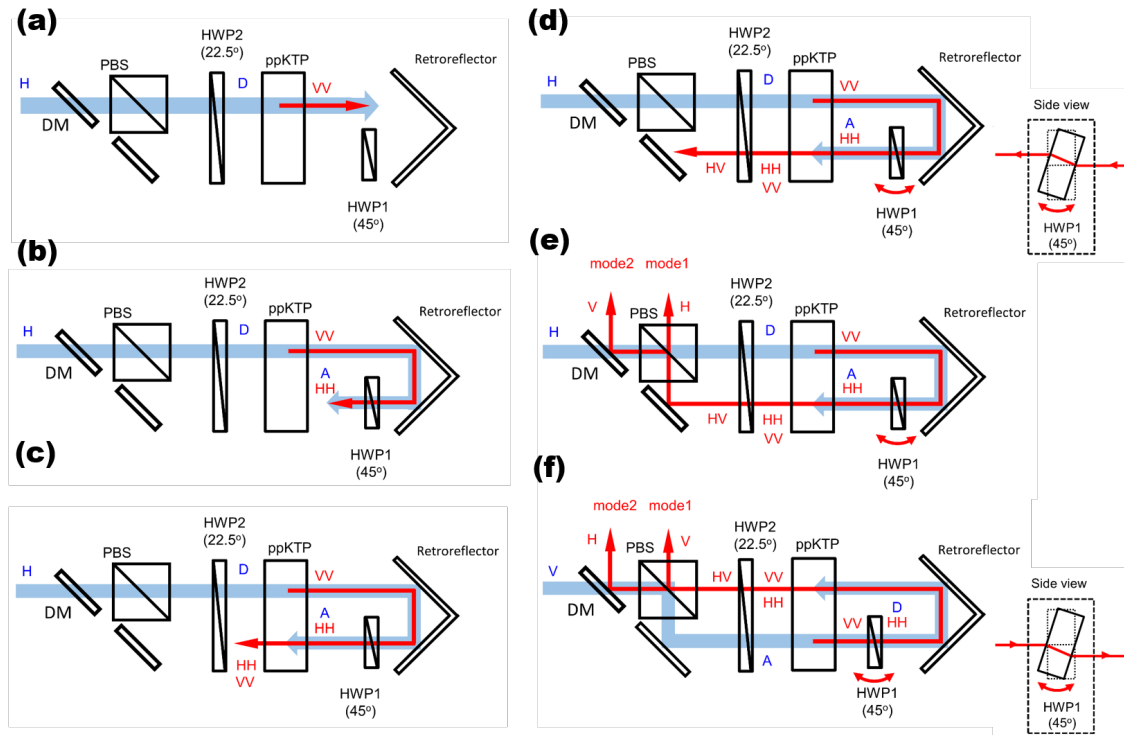


Figure 4.7: The proposed experimental scheme to generate the two-photon state. Essentially, the input photon is separated into two optical paths at the polarizing beam splitter (PBS), propagating the interferometer in the clockwise and counter-clockwise direction. The input photon is converted to a two-photon state via the ppKTP crystal, while their polarization are adjusted by the half-wave-plates (HWP). DM stands for the dichroic mirror which reflects the photon around 800nm, and let through the photon around 400nm.

where ϕ is the relative phase between the first and second conversion. ϕ can be adjusted by tilting the HWP1, which changes the propagation length through the wave plate. This state goes through HWP2, which will rotate H(V) states to D(A) states. The two photon state after HWP2 is [see Figure 4.7(d)],

$$|\psi_d\rangle \propto \sin \frac{\phi}{2} |HV\rangle + \frac{i}{\sqrt{2}} \cos \frac{\phi}{2} (|HH\rangle + |VV\rangle) \rightarrow |HV\rangle \quad (\phi = \pi). \quad (4.16)$$

The relative phase was set to $\phi = \pi$ to obtain the right hand side. This is a quantum interference process corresponding to the reverse Hong-Ou-Mandel(HOM) interference in the polarization basis [75]. After this state passes through PBS, the H and V photons are deterministically separated into different spatial modes 1 and 2 as $|\psi_e\rangle = |H\rangle_1 |V\rangle_2$ [see Figure 4.7(e)].

We can consider the V-component of the initial input photon reflected at the PBS in

4.3. SIMULATING SCALE-FREE NETWORKS WITH TIME CRYSTALS

a similar way discussed above. This time the photon round trips the interferometer in the counter-clockwise direction [see Figure 4.7(f)]. After two down-conversion processes and the reverse HOM interference, the resulting state coming out from the PBS is $|\psi_f\rangle = |V\rangle_1|H\rangle_2$. If we initially input a D state into the interferometer, the process through the clockwise and counter-clockwise direction will occur as a superposition, leading to the entangled output state

$$|\psi_{out}\rangle \propto |H\rangle_1|V\rangle_2 + |V\rangle_1|H\rangle_2. \quad (4.17)$$

On the other hand, if we input the H or V polarized state, we can get a separable state deterministically separated into different optical modes. Note that the round trip process is necessary in order to obtain the photons in different modes deterministically.

The described two-photon source can be injected into different waveguide modes by coupling each spatial mode 1 and 2 after the PBS to the desired waveguide mode. The unique and important point about this photon source is that the two photons are separated into different optical modes with 100% probability, allowing to prepare various initial states for the dynamics through the waveguides. This cannot be achieved if we use a photon pair from single down-conversion from a ppKTP crystal, since the photons propagate collinearly in a single optical mode having the same polarization. One can only prepare an initial state where two photons are injected into a single waveguide, or otherwise have to probabilistically separate the photons using a 50:50 beam splitter. Furthermore, the ability to generate a polarization-entangled state enables to prepare superposed initial states. One can also use one of the paired photons to herald the single-photon state.

4.3 Simulating scale-free networks with time crystals

The second example we propose to simulate dynamics on a complex quantum network is a many-body spin system in a time-crystalline phase. This is a driven system where the Hamiltonian of the system is periodically switched between a many-body localized Ising interaction and the global transversal magnetic field. Such a system shows discrete-time-translational symmetry breaking, where the state of the system has a different periodicity compared to the periodicity of the Hamiltonian. This property is named as the *time crystal*, analogous to the spatial crystal which breaks the spatial-translational symmetry. Using Floquet theory, we compute the effective Hamiltonian of one period of the drive, and analyze its structure when written in the tight-binding Hamiltonian matrix form.

4.3. SIMULATING SCALE-FREE NETWORKS WITH TIME CRYSTALS

We will show that a complex network structure with a scale-free property emerges in such effective Hamiltonian, due to the clustering of energies.

4.3.1 Discrete time crystals in spin systems

First we introduce the many-body spin system that is going to be analyzed in this section. The system is known as the Discrete Time Crystal [76], where a one dimensional chain of n spin-1/2 particles evolves under the action of a sequence of two different Hamiltonians,

$$H(t) = \begin{cases} H_1 = \hbar g (1 - \epsilon) \sum_l^n \sigma_l^x & 0 < t < T_1 \\ H_2 = \hbar \sum_{lm} J_{lm}^z \sigma_l^z \sigma_m^z + \hbar \sum_l B_l^z \sigma_l^z & T_1 < t < T . \end{cases} \quad (4.18)$$

This is a time-dependent Hamiltonian with a period of T . Here $\sigma_l^x, \sigma_l^y, \sigma_l^z$ are the Pauli operators on the l -th spin, $J_{lm}^z \equiv J_0/|l - m|^\alpha$ is the long-range interaction between spins l, m , and $B_l^z \in [0, W]$ is a random longitudinal field. The parameter g satisfies the condition $2gT_1 = \pi$ such that when $\epsilon = 0$, the unitary $U_1 = \exp(-iH_1T_1/\hbar) = \prod_l^n \sigma_l^x$ becomes a global π pulse around the x -axis. $\epsilon \ll 1$ is present as a rotation error around the x -axis. Note that this Hamiltonian is similar to the tilted-field Ising Hamiltonian discussed in Section 2.9, where the difference is that the transversal magnetic field term and the Ising interaction term are separated into a sequence. The Floquet operator of the one period of drive is given by

$$\mathcal{F}_\epsilon = U_\epsilon(T; 0) = \exp(-iH_2T_2/\hbar) \exp(-iH_1T_1/\hbar). \quad (4.19)$$

In order to understand the dynamics of the time crystal, we shall first set to $\epsilon = 0$. We initialize the state of the system in one of the eigenstate of H_2 (states where spins are parallel to the z -direction). Under the action of H_1 , all of the spins globally rotate with an angle of π around the x -axis. Subsequently, under the action of H_2 , the state does not change as the state after the action of H_1 is still an eigenstate of H_2 . This is the state after a single period of the drive. After another period of the drive, the state shall undergo another π rotation and come back to its initial state. See Figure 4.8 which illustrates the situation. Since it takes two periods to rotate for an angle of 2π and return to its initial state, the state has a $2T$ periodicity. On the other hand, the time-periodic Hamiltonian $H(t)$ has a periodicity of T . Such difference of periodicity between the Hamiltonian and the state corresponds to the name time crystal, since the system breaks the discrete-time-

4.3. SIMULATING SCALE-FREE NETWORKS WITH TIME CRYSTALS

translational symmetry.

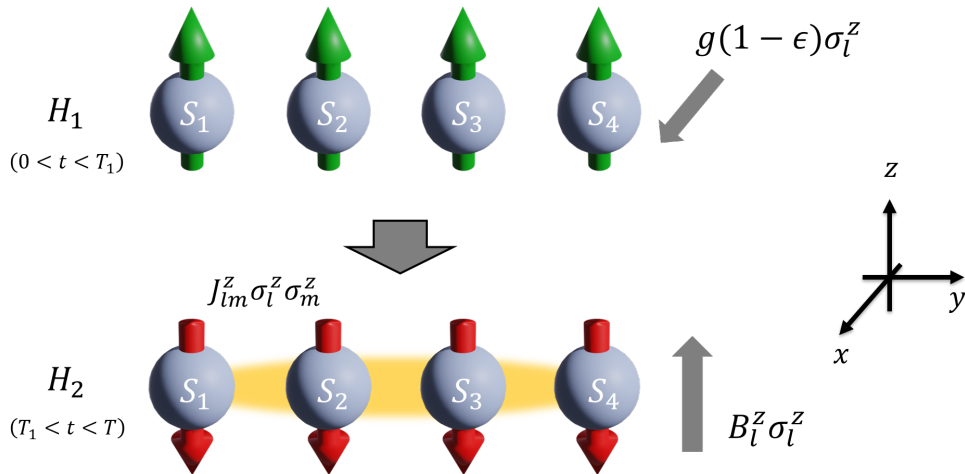


Figure 4.8: Illustration of the two Hamiltonians of the time crystal defined in Eq. (4.18). Assuming that the system is initialized in a state $|\uparrow\uparrow\uparrow\rangle$, all of the spins flips around the x -axis under the action of H_1 . Subsequently, H_2 is applied, which does not change the state $|\downarrow\downarrow\downarrow\rangle$.

Now if the rotation error ϵ is non-zero, the dynamics start to get more complex. As the rotation around x -axis is imperfect, the H_2 term can also non-trivially rotate the spins around the z -axis. The rotation error ϵ essentially breaks the symmetry (the $2T$ response) of the system, and may gradually break the periodicity of the state as the time evolves. However, the H_2 term acts as a correction of the rotation error, since it's a many-body localization Hamiltonian which keeps the spins to localize on its eigenstates. As each of the eigenstate of H_2 are exponentially localized on a certain configuration of the spins $|S_1 S_2 \dots S_n\rangle$, the rotation error is exponentially suppressed. The $2T$ periodicity of the time-evolution will be still present for a long time if ϵ is small due to the presence of H_2 . In the next section, we will focus on this region where a small rotation error is present.

4.3.2 Appearance of scale-free networks in the time crystalline system with a small error

Here we will show that with a small amount of error ϵ in the system, the symmetry of the system will be broken which leads to the appearance of a scale-free network in the effective Floquet Hamiltonian. We choose the parameters to be $\alpha = 1.51$, $J_0(T - T_1) = 0.06$ with a disorder strength $W(T - T_1) = \pi$, which are similar values used in the experiment [76] in the literature. We set the value of error to $\epsilon = 0.012$ and calculated the effective

4.3. SIMULATING SCALE-FREE NETWORKS WITH TIME CRYSTALS

Hamiltonian H_ϵ^{eff} by taking the matrix logarithm of Eq. (4.19). Then we represent H_ϵ^{eff} in the tight-binding Hamiltonian matrix form using the basis set $\{|S_1 S_2 \dots S_n\rangle\}_{S_1, \dots, S_n = \uparrow, \downarrow}$. The obtained Hamiltonian matrix and the resonance-rule-applied adjacency matrix with $n = 8$ is shown in Figure 4.9.

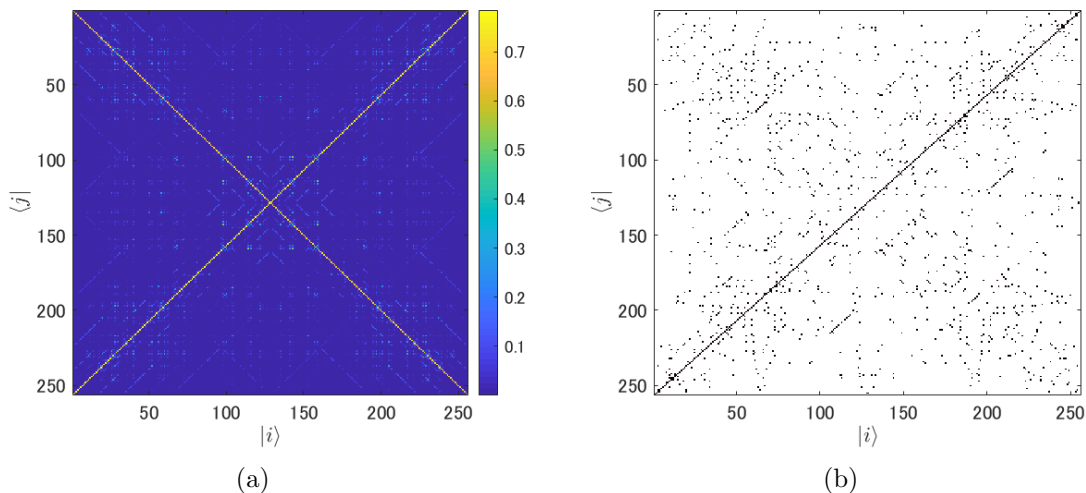


Figure 4.9: (a) The matrix plot of the effective Hamiltonian H_ϵ^{eff} and (b) the resonance-rule-applied adjacency matrix (black= 1, white= 0) of time crystal system with $\epsilon = 0.012$ and $n = 8$.

From the adjacency matrix, the graph is visualized in Figure 4.10. The graph consists of $2^8 = 256$ nodes. Here, again the nodes of the graph is positioned based on the force-directed graph drawing method [73]. The important result is found from the degree distribution in Figure 4.11. The tail of the distribution has a good fit to the power law function, indicating that the obtained graph is a scale-free network. This also means that there are large degree hub nodes in the network. These nodes correspond to the states (in σ_z basis) that has an energy close to other states, which means that the energy levels are clustered at some regions. For example, the hub node in the graph of Figure 4.10 is $|\uparrow\uparrow\downarrow\uparrow\downarrow\downarrow\uparrow\uparrow\rangle$. The number of domain walls in this state is four, and there are ${}_8C_4 = 70$ states which has the same number of domain walls. These states has similar value of energies, and thus have a higher chance to have edges drawn between them by the resonance-rule.

4.3. SIMULATING SCALE-FREE NETWORKS WITH TIME CRYSTALS

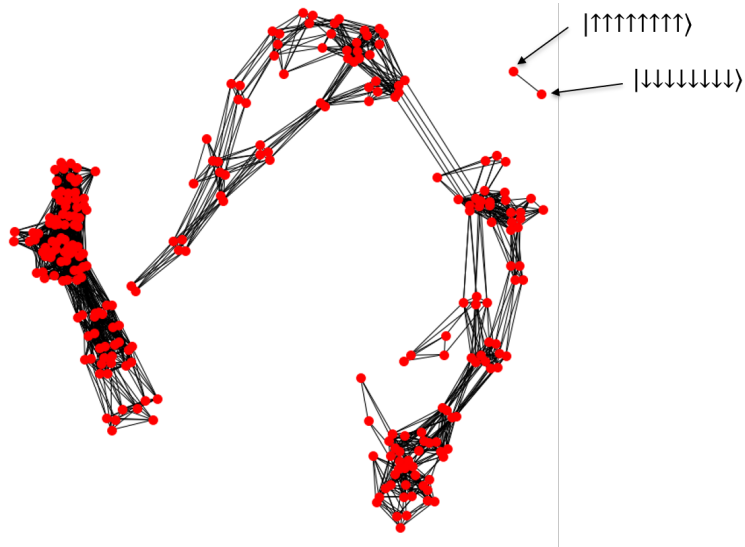


Figure 4.10: The graph visualization of the adjacency matrix plotted in Figure 4.9(b), which corresponds to the time crystal with $n = 8$ spins and the rotation error of $\epsilon = 0.012$. The graph contains $2^n = 256$ nodes, and the nodes are positioned according to the force-directed drawing method. The isolated dimer on the corner corresponds to the basis states where all spins are up or down. This indicates that these states are robust against the rotation error, and the dynamics will stay inside this two-dimensional subspace for a long time.

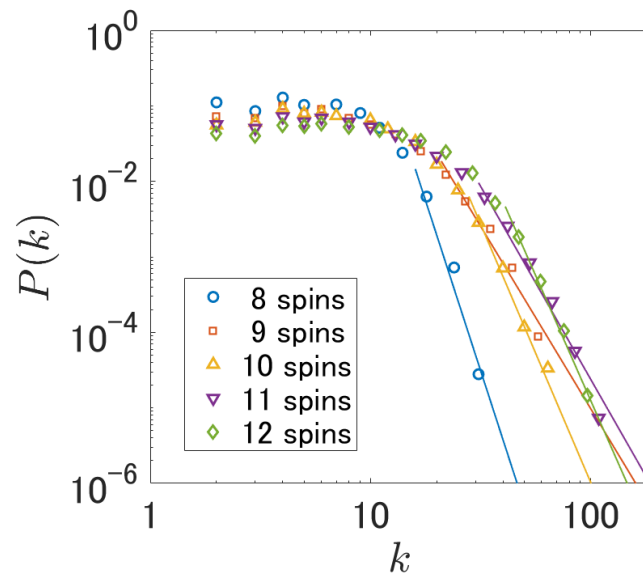


Figure 4.11: The degree distribution of the graph corresponding to resonance-rule-applied adjacency matrix of the time crystalline system. (one instance with $n = 8$ shown in Figure 4.10). k is the degree of a node and n is the number of spins in the system. The distribution is taken from 100 realizations of the effective Hamiltonian using different disorder sequence of B_l^z for each n . We can see a broad distribution, indicating that the graph has random connections. The tail of each plot is fit to a power law function, indicating that the network has a scale-free property.

4.4 Conclusions

In this chapter, we looked at two kinds of quantum system with periodic driving, and utilized the graph interpretation of the Hamiltonians to simulate complex quantum networks. The first system was the periodically modulated waveguide array. We combined two elements to simulate the complex quantum network in this system. One was to consider a two-photon state as the input state, which allowed to extend the Hilbert space in the order of square of the number of waveguides. The other was to utilize the effective Hamiltonian of the time-periodic system. By driving the system in a low frequency regime, we could observe the appearance of non-local terms in the Hamiltonian. We also showed the method to prepare a reliable two-photon source using spontaneous parametric down conversion. The second system we focused was the many body spin system in the time crystalline phase. Breaking of the symmetry of the system by introducing a small error in the rotation of the spins led to the appearance of scale-free network in the effective Hamiltonian.

Chapter 5

Conclusions

This thesis studied quantum dynamics and quantum search algorithm on complex quantum networks, as well as providing some methods to simulate the dynamics in such system. We defined complex quantum networks as closed finite-dimensional quantum systems that contain complex transitions between levels. We especially focused on the transition structure of tight-binding Hamiltonians, and treated these Hamiltonians as complex quantum networks when the matrix has certain properties, such as small-world or scale-free.

We analyzed the quantum search algorithm on complex quantum networks which hold small-world or scale-free property. The main results was that during the network's transition from non-small-world to small world, there exists a clear threshold connectivity of the graph where the search algorithm can be achieved quickly. From the analysis on the scale-free network, a strong correlation between the network's closeness centrality measure and the time complexity of the search was observed. These results provided new perspective on closed quantum dynamics, as well as showing that complex quantum networks are useful for quantum search algorithm.

We have also suggested a method to simulate the dynamics on complex quantum networks using periodically driven systems. When the system Hamiltonian is subject to time-periodic drive with slow frequency, there were cases where the effective Floquet Hamiltonian had complex network structures. The examples considered here was the coupled waveguide system and the many-body spin system, but the idea to use the effective Hamiltonians of driven system as simulators for complex quantum network can be potentially extended to many other systems.

References

- [1] F. Arute *et al.*, *Nature* **574**, 505–510 (2019).
- [2] P. Mundada, G. Zhang, T. Hazard, and A. Houck, *Phys. Rev. Applied* **12**, 054023 (2019).
- [3] I. I. Rabi, J. R. Zacharias, S. Millman, and P. Kusch, *Phys. Rev.* **53**, 318 (1938).
- [4] D. G. Cory, A. F. Fahmy, and T. F. Havel, *Proc. Nat. Acad. Sci.* **94**, 1634–1639 (1997).
- [5] N. A. Gershenfeld and I. L. Chuang, *Science* **275** (5298), 350–356 (1997).
- [6] H. J. Mamin, M. Kim, M. H. Sherwoods, C. T. Rettner, K. Ohno, D. D. Awschalom, and D. Rugar, *Science* **339** (6119), 557-560 (2013).
- [7] W. Paul, *Rev. Mod. Phys.* **62**, 531 (1990).
- [8] R. Blatt and C. F. Roos, *Nature Physics* **8**, 277–284 (2012).
- [9] J. Smith, A. Lee, P. Richerme, B. Neyenhuis, P. W. Hess, P. Hauke, M. Heyl, D. A. Huse and C. Monroe, *Nature Physics* **12**, 907–911 (2016).
- [10] L. Schlipf, T. Oeckinghaus, K. Xu, D. B. R. Dasari, A. Zappe, F. F. D. Oliveira, B. Kern, M. Azarkh, M. Drescher, M. Ternes, K. Kern, J. Wrachtrup, and A. Finkler, *Science Advances* **3**, e1701116 (2017).
- [11] B. J. Brown, D. Loss, J. K. Pachos, C. N. Self, and J. R. Wootton, *Rev. Mod. Phys.* **88**, 045005 (2016).
- [12] S. Boccaletti, V. Latora, Y. Moreno, M. Chavez, and D. U. Hwang, *Phys. Rep.* **424**(4-5), 175 (2006).

REFERENCES

- [13] X. Wang, Y. Koç, R. E. Kooij, and P. Van Mieghem, arXiv:1505.06312 (2015).
- [14] M. E. J. Newman, Phys. Rev. E **66**, 016128 (2002).
- [15] Y. Moreno, M. Nekovee, and A. F. Pacheco, Phys. Rev. E **69**, 066130 (2004).
- [16] D. S. Lee, Phys. Rev. E **72**, 026208 (2005).
- [17] R. Pastor-Satorras, C. Castellano, P. Van Mieghem, and A. Vespignani, Rev. Mod. Phys. **87**, 925 (2015).
- [18] M. Faccin, P. Migdał, T. H. Johnson, V. Bergholm, J. D. Biamonte, Phys. Rev. X **4**, 041012 (2014).
- [19] G. D. Paparo, M. Müller, F. Comellas and M. A. Martin-Delgado, Scientific Reports **3**, 2773 (2013).
- [20] G. Bianconi, Europhysics Letters **111** (5), 56001 (2015).
- [21] J. Biamonte, M. Faccin, and M. D. Domenico, Comm. Phys. **2**, 53 (2019).
- [22] M. Pant, H. Krovi, D. Towsley, L. Tassiulas, L. Jiang, P. Basu, D. Englund, and S. Guha, npj Quantum Information **5**, 25 (2019).
- [23] D. N. Biggerstaff, R. Heilmann, A. A. Zecevik, M. Gräfe, M. A. Broome, A. Fedrizzi, S. Nolte, A. Szameit, A. G. White, and I. Kassal, Nature Communications **7**, 11282 (2016).
- [24] V. M. Bastidas, B. Renoust, K. Nemoto, and W. J. Munro, Phys. Rev. B **98**, 224307 (2018).
- [25] M. Mohseni, P. Rebentrost, S. Lloyd, and A. Aspuru-Guzik, Journal of Chemical Physics **129**, 174106 (2008).
- [26] A. M. Childs and J. Goldstone, Phys. Rev. A **70**, 022314 (2004).
- [27] M. Bukov, L. D'Alessio, and A. Polkovnikov, Advances in Physics, **64**, 2, 139-226 (2015).
- [28] S. Reich, J. Maultzsch, C. Thomsen, and P. Ordejón, Phys. Rev. B **66**, 035412 (2002).

REFERENCES

- [29] S. Roy, J. T. Chalker, and D. E. Logan, *Phys. Rev. B* **99**, 104206 (2019).
- [30] E. N. Gilbert, *The Annals of Mathematical Statistics* **30**, 1141-1144 (1959).
- [31] A. L. Barabási and R. Albert, *Science* **286**, 509-511 (1999).
- [32] R. Cohen and S. Havlin, *Phys. Rev. Lett.* **90**, 058701 (2003).
- [33] L. K. Grover, *Phys. Rev. Lett.* **79**, 325 (1997).
- [34] P. Benioff, in *Quantum Computation and Information*, Contemporary Mathematics Series. AMS, edited by S. J. Lomonaco and H. E. Brandt (2002).
- [35] S. Aaronson and A. Ambainis, *Proc. 44th IEEE Symposium on Foundations of Computer Science*, 200 (2003).
- [36] A. Ambainis, J. Kempe, and A. Rivosh, in *Proceedings of the Sixteenth Annual ACM-SIAM Symposium on Discrete Algorithms*, SODA, 1099 (2005).
- [37] A. Tulsi, *Phys. Rev. A* **78**, 012310 (2008).
- [38] A. M. Childs and J. Goldstone, *Phys. Rev. A* **70**, 042312 (2004).
- [39] I. Foulger, S. Gnutzmann, and G. Tanner, *Phys. Rev. Lett.* **112**, 070504 (2014).
- [40] A. M. Childs and Y. Ge, *Phys. Rev. A* **89**, 052337 (2014).
- [41] J. Janmark, D. A. Meyer, and T. G. Wong, *Phys. Rev. Lett.* **112**, 210502 (2014).
- [42] L. Novo, S. Chakraborty, M. Mohseni, H. Neven, and Y. Omar, *Scientific Reports* **5**, 13304 (2015).
- [43] D. A. Meyer and T. G. Wong, *Phys. Rev. Lett.* **114**, 110503 (2015).
- [44] S. Chakraborty, L. Novo, A. Ambainis, and Y. Omar, *Phys. Rev. Lett.* **116**, 100501 (2016).
- [45] E. Agliari, A. Blumen and O. Mülken, *Phys. Rev. A* **82**, 012305 (2010).
- [46] S. D. Berry and J. B. Wang, *Phys. Rev. A* **82**, 042333 (2010).
- [47] P. Philipp, L. Tarrataca and S. Boettcher, *Phys. Rev. A* **93**, 032305 (2016).

REFERENCES

- [48] A. Glos, R. Kukulski, A. Krawiec and Z. Puchal, *Quantum Information Processing* **17**, 81 (2018).
- [49] L. S. Schulman, *J. Phys. A* **16**, 17, L639 - L641 (1983).
- [50] C. M. Newman, L. S. Schulman, *Communication Mathematical Physics* **104**, 547 - 571 (1986).
- [51] D. Coppersmith, D. Gamarnik, and M. Sviridenko, *Rand. Struct. and Alg.* **21**, 1, 1 (2002).
- [52] B. Bollobás and O. M. Riordan, *Combinatorica*, **24** (1), 5–34 (2004).
- [53] B. Bollobás, in *Handbook of Graphs and Networks*, edited by S. Bornholdt and H. G. Schuster (Wiley-VCH GmbH & Co., Weinheim, 2003), p. 1 (2003).
- [54] Cleve Moler and Charles Van Loan, *SIAM Rev.* **45** (1), 3–49 (2003).
- [55] J. M. Kleinberg, *Nature* **406**, 845 (2000).
- [56] P. Deprez, R. S. Hazra, and M. V. Wüthrich, *Risks* **3** (1) (2015).
- [57] M. Biskup, *Rand. Struct. and Alg.* **39**, 2, 210–227 (2011).
- [58] S. N. Dorogovtsev, J. F. F. Mendes, and A. N. Samukhin, *Phys. Rev. Lett.* **85**, 4633 (2000).
- [59] K. I. Goh, B. Kahng, D. Kim, *Phys. Rev. E* **64**, 051903 (2001).
- [60] P. Bonacich, *American Journal of Sociology* **92** (5), 1170–1182 (1986).
- [61] L. C. Freeman, *Social networks*, **1** (3), 215–239 (1979).
- [62] L. C. Freeman, *Sociometry* **40**, 35–41 (1977).
- [63] S. White and P. Smyth, in *Proceedings of the ninth ACM SIGKDD international conference on Knowledge discovery and data mining* (Washington, D.C. 2003), 266 (2003).
- [64] M. E. J. Newman, *Social Networks*, **27** (1), 39–54 (2005).
- [65] J. D. Noh and H. Rieger, *Phys. Rev. Lett.* **92**, 118701 (2004).

REFERENCES

- [66] C. Godfrin, A. Ferhat, R. Ballou, S. Klyatskaya, M. Ruben, W. Wernsdorfer and F. Balestro, *Phys. Rev. Lett.* **119**, 187702 (2017).
- [67] J. L. O'Brien, A. Furusawa, and J. Vučković, *Nature Photonics* **3**, 687 (2009).
- [68] J. C. F. Matthews, A. Politi, A. Stefanov, and J. L. O'Brien, *Nature Photonics* **3**, 346 (2009).
- [69] A. Peruzzo, M. Lobino, J. C. F. Matthews, N. Matsuda, A. Politi, K. Poulios, X. Zhou, Y. Lahini, N. Ismail, K. Wörhoff, Y. Bromberg, Y. Silberberg, M. G. Thompson, and J. L. O'Brien, *Science* **329** (5998), 1500 (2010).
- [70] J. O. Owens, M. A. Broome, D. N. Biggerstaff, M. E. Goggin, A. Fedrizzi, T. Linjordet, M. Ams, G. D. Marshall, J. Twamley, M. J. Withford, and A. G. White, *New J. Phys.* **13**, 7, 075003 (2011).
- [71] K. Poulios, R. Keil, D. Fry, J. D. A. Meinecke, J. C. F. Matthews, A. Politi, M. Lobino, M. Gräfe, M. Heinrich, S. Nolte, A. Szameit, and J. L. O'Brien, *Phys. Rev. Lett.* **112**, 143604 (2014).
- [72] A. Gómez-León and G. Platero, *Phys. Rev. Lett.* **110**, 200403 (2013).
- [73] S. G. Kobourov, arXiv:1201.3011 (2012).
- [74] F. Steinlechner, M. Gilaberte, M. Jofre, T. Scheidl, J. P. Torres, V. Pruneri, and R. Ursin, *J. Opt. Soc. Am. B* **31**, 2068–2076 (2014).
- [75] C K. Hong, Z. Y. Ou, and L. Mandel, *Phys. Rev. Lett.* **59**, 2044 (1987).
- [76] J. Zhang, P. W. Hess, A. Kyprianidis, P. Becker, A. Lee, J. Smith, G. Pagano, I.-D. Potirniche, A. C. Potter, A. Vishwanath, N. Y. Yao, and C. Monroe, *Nature* **543**, 217 (2017).